Titre: Title:	Segmentation and Characterization of Small Retinal Vessels in Fundus Images Using the Tensor Voting Approach
Auteur: Author:	Argyrios Christodoulidis
Date:	2017
Type:	Mémoire ou thèse / Dissertation or Thesis
Référence: Citation:	Christodoulidis, A. (2017). Segmentation and Characterization of Small Retinal Vessels in Fundus Images Using the Tensor Voting Approach [Thèse de doctorat, École Polytechnique de Montréal]. PolyPublie. https://publications.polymtl.ca/2578/

URL de PolyPublie: PolyPublie URL:	https://publications.polymtl.ca/2578/
Directeurs de recherche: Advisors:	Farida Cheriet, & Thomas Hurtut
Programme: Program:	Génie informatique

UNIVERSITÉ DE MONTRÉAL

SEGMENTATION AND CHARACTERIZATION OF SMALL RETINAL VESSELS IN FUNDUS IMAGES USING THE TENSOR VOTING APPROACH

ARGYRIOS CHRISTODOULIDIS
DÉPARTEMENT DE GÉNIE INFORMATIQUE ET GÉNIE LOGICIEL
ÉCOLE POLYTECHNIQUE DE MONTRÉAL

THÈSE PRÉSENTÉE EN VUE DE L'OBTENTION
DU DIPLÔME DE PHILOSOPHIÆ DOCTOR
(GÉNIE INFORMATIQUE)
MAI 2017

UNIVERSITÉ DE MONTRÉAL

ÉCOLE POLYTECHNIQUE DE MONTRÉAL

Cette thèse intitulée :

SEGMENTATION AND CHARACTERIZATION OF SMALL RETINAL VESSELS IN FUNDUS IMAGES USING THE TENSOR VOTING APPROACH

présentée par : CHRISTODOULIDIS Argyrios
en vue de l'obtention du diplôme de : Philosophiæ Doctor
a été dûment acceptée par le jury d'examen constitué de :

M. PESANT Gilles, Ph. D., président
Mme CHERIET Farida, Ph. D., membre et directrice de recherche
M. HURTUT Thomas, Ph. D., membre et codirecteur de recherche
M. FAUCON Timothée, Doctorat, membre
M. DAI BUI Tien, Ph. D., membre externe

DEDICATION

To my family, friends, and teachers

Oculus animus index
(The eyes are the window of the soul)
-Latin proverb

ACKNOWLEDGMENTS

I could not finish this thesis without acknowledging the help and support of several people. First of all, I would like to thank the members of my doctoral committee, Professor Giles Pesant, Professor Tien Dai Bui, and Timothée Faucon (Ph.D.), for taking the time to read and evaluate this thesis.

I would like to thank my advisors for trusting me and letting me pursue this exciting project. I am grateful to my main supervisor Professor Farida Cheriet for her guidance at all the phases of this project, for her patience, motivation, as well as her immense knowledge. For the last four years, she inspired me and helped me to navigate through new intellectual avenues and challenges. Additionally, I want to thank Professor Thomas Hurtut for his cosupervision throughout my doctoral studies. His scientific inquiries were always on point helping me to turn my thoughts and ideas into concrete results ; the challenging questions incented me to think my research from different perspectives. Besides my advisors, I want to thank the chair of the department, Professor Pierre Langlois.

The research carried out in this thesis was funded in part by Diagnos Inc. and NSERC. I would like to thank the former and the current members of Diagnos team that helped me to facilitate important aspects of this project. Dr. Hadi Chakor for his help regarding the medical and clinical features of this thesis, Houssen Ben Tahar, Lama Seoud (Ph.D.), and Qifeng Gan (Ph.D.) for the feedback and technical support on various stages of the project.

I would also like to thank the following former and current members of the Laboratory of Imaging and Vision 4D. Among them are Philippe Debanné, Sébastien Grenier, Cosmin Luduşan (Ph.D.), Mahnaz Fasih, Cédric Meurée, Mickaël Garnier (Ph.D.), Maya Alsheh-Ali (Ph.D.), Jérémy Chambon, Hamza Bendaoudi (Ph.D.), Kondo Claude Assi (Ph.D.), Nesrine Zaglam (Ph.D.), Pascale Béliveau (Ph.D.), Rola Harmouche (Ph.D.), Fantin Girard, Mitchel Benovoy (Ph.D.), Pierre-André Brousseau, Thanh-Vân Phan, Mathieu Tournier, Florian Berton, Bilal Khomri, Rana Farah (Ph.D.), Ahmed Abdelsalam, Ola Ahmad (Ph.D.), and Maxime Schmitt.

I would like to close these acknowledgments by expressing gratitude to my parents, friends, and teachers. My parents for supporting me from distant, and letting me pursue my goals, dreams, and interests. My friends in Greece and here in Montréal for the endless discussions on the various matters of this project, on my life, on my experiences, and my discoveries. Finally, the teachers at all stages of my education that had sparked my interest in research.

RÉSUMÉ

La rétine permet de visualiser facilement une partie du réseau vasculaire humain. Elle offre ainsi un aperçu direct sur le développement et le résultat de certaines maladies liées au réseau vasculaire dans son entier. Chaque complication visible sur la rétine peut avoir un impact sur la capacité visuelle du patient. Les plus petits vaisseaux sanguins sont parmi les premières structures anatomiques affectées par la progression d'une maladie, être capable de les analyser est donc crucial. Les changements dans l'état, l'aspect, la morphologie, la fonctionnalité, ou même la croissance des petits vaisseaux indiquent la gravité des maladies.

Le diabète est une maladie métabolique qui affecte des millions de personnes autour du monde. Cette maladie affecte le taux de glucose dans le sang et cause des changements pathologiques dans différents organes du corps humain. La rétinopathie diabétique décrit l'ensemble des conditions et conséquences du diabète au niveau de la rétine. Les petits vaisseaux jouent un rôle dans le déclenchement, le développement et les conséquences de la rétinopathie. Dans les dernières étapes de cette maladie, la croissance des nouveaux petits vaisseaux, appelée néovascularisation, présente un risque important de provoquer la cécité. Il est donc crucial de détecter tous les changements qui ont lieu dans les petits vaisseaux de la rétine dans le but de caractériser les vaisseaux sains et les vaisseaux anormaux. La caractérisation en elle-même peut faciliter la détection locale d'une rétinopathie spécifique.

La segmentation automatique des structures anatomiques comme le réseau vasculaire est une étape cruciale. Ces informations peuvent être fournies à un médecin pour qu'elles soient considérées lors de son diagnostic. Dans les systèmes automatiques d'aide au diagnostic, le rôle des petits vaisseaux est significatif. Ne pas réussir à les détecter automatiquement peut conduire à une sur-segmentation du taux de faux positifs des lésions rouges dans les étapes ultérieures. Les efforts de recherche se sont concentrés jusqu'à présent sur la localisation précise des vaisseaux de taille moyenne. Les modèles existants ont beaucoup plus de difficultés à extraire les petits vaisseaux sanguins. Les modèles existants ne sont pas robustes à la grande variance d'apparence des vaisseaux ainsi qu'à l'interférence avec l'arrière-plan. Les modèles de la littérature existante supposent une forme générale qui n'est pas suffisante pour s'adapter à la largeur étroite et la courbure qui caractérisent les petits vaisseaux sanguins. De plus, le contraste avec l'arrière-plan dans les régions des petits vaisseaux est très faible. Les méthodes de segmentation ou de suivi produisent des résultats fragmentés ou discontinus. Par ailleurs, la segmentation des petits vaisseaux est généralement faite aux dépends de l'amplification du bruit. Les modèles déformables sont inadéquats pour segmenter les petits vaisseaux. Les forces utilisées ne sont pas assez flexibles pour compenser le faible contraste, la largeur, et

la variance des vaisseaux. Enfin, les approches de type apprentissage machine nécessitent un entraînement avec une base de données étiquetée. Il est très difficile d'obtenir ces bases de données dans le cas des petits vaisseaux.

Cette thèse étend les travaux de recherche antérieurs en fournissant une nouvelle méthode de segmentation des petits vaisseaux rétiniens. La détection de ligne à échelles multiples (MSLD) est une méthode récente qui démontre une bonne performance de segmentation dans les images de la rétine, tandis que le vote tensoriel est une méthode proposée pour reconnecter les pixels. Une approche combinant un algorithme de détection de ligne et de vote tensoriel est proposée. L'application des détecteurs de lignes a prouvé son efficacité à segmenter les vaisseaux de tailles moyennes. De plus, les approches d'organisation perceptuelle comme le vote tensoriel ont démontré une meilleure robustesse en combinant les informations voisines d'une manière hiérarchique. La méthode de vote tensoriel est plus proche de la perception humain que d'autres modèles standards. Comme démontré dans ce manuscrit, c'est un outil pour segmenter les petits vaisseaux plus puissant que les méthodes existantes. Cette combinaison spécifique nous permet de surmonter les défis de fragmentation éprouvés par les méthodes de type modèle déformable au niveau des petits vaisseaux. Nous proposons également d'utiliser un seuil adaptatif sur la réponse de l'algorithme de détection de ligne pour être plus robuste aux images non-uniformes. Nous illustrons également comment une combinaison des deux méthodes individuelles, à plusieurs échelles, est capable de reconnecter les vaisseaux sur des distances variables. Un algorithme de reconstruction des vaisseaux est également proposé. Cette dernière étape est nécessaire car l'information géométrique complète est requise pour pouvoir utiliser la segmentation dans un système d'aide au diagnostic.

La segmentation a été validée sur une base de données d'images de fond d'oeil à haute résolution. Cette base contient des images manifestant une rétinopathie diabétique. La segmentation emploie des mesures de désaccord standards et aussi des mesures basées sur la perception. En considérant juste les petits vaisseaux dans les images de la base de données, l'amélioration dans le taux de sensibilité que notre méthode apporte par rapport à la méthode standard de détection multi-niveaux de lignes est de 6.47%. En utilisant les mesures basées sur la perception, l'amélioration est de 7.8%.

Dans une seconde partie du manuscrit, nous proposons également une méthode pour caractériser les rétines saines ou anormales. Certaines images contiennent de la néovascularisation. La caractérisation des vaisseaux en bonne santé ou anormale constitue une étape essentielle pour le développement d'un système d'aide au diagnostic. En plus des défis que posent les petits vaisseaux sains, les néovaisseaux démontrent eux un degré de complexité encore plus élevé. Ceux-ci forment en effet des réseaux de vaisseaux à la morphologie complexe et inhabituelle, souvent minces et à fortes courbures. Les travaux existants se limitent

à l'utilisation de caractéristiques de premier ordre extraites des petits vaisseaux segmentés. Notre contribution est d'utiliser le vote tensoriel pour isoler les jonctions vasculaires et d'utiliser ces jonctions comme points d'intérêts. Nous utilisons ensuite une statistique spatiale de second ordre calculée sur les jonctions pour caractériser les vaisseaux comme étant sains ou pathologiques. Notre méthode améliore la sensibilité de la caractérisation de 9.09% par rapport à une méthode de l'état de l'art.

La méthode développée s'est révélée efficace pour la segmentation des vaisseaux rétiniens. Des tenseurs d'ordre supérieur ainsi que la mise en œuvre d'un vote par tenseur via un filtrage orientable pourraient être étudiés pour réduire davantage le temps d'exécution et résoudre les défis encore présents au niveau des jonctions vasculaires. De plus, la caractérisation pourrait être améliorée pour la détection de la rétinopathie proliférative en utilisant un apprentissage supervisé incluant des cas de rétinopathie diabétique non proliférative ou d'autres pathologies. Finalement, l'incorporation des méthodes proposées dans des systèmes d'aide au diagnostic pourrait favoriser le dépistage régulier pour une détection précoce des rétinopathies et d'autres pathologies oculaires dans le but de réduire la cessité au sein de la population.

ABSTRACT

As an easily accessible site for the direct observation of the circulation system, human retina can offer a unique insight into diseases development or outcome. Retinal vessels are representative of the general condition of the whole systematic circulation, and thus can act as a "window" to the status of the vascular network in the whole body. Each complication on the retina can have an adverse impact on the patient's sight. In this direction, small vessels' relevance is very high as they are among the first anatomical structures that get affected as diseases progress. Moreover, changes in the small vessels' state, appearance, morphology, functionality, or even growth indicate the severity of the diseases.

This thesis will focus on the retinal lesions due to diabetes, a serious metabolic disease affecting millions of people around the world. This disorder disturbs the natural blood glucose levels causing various pathophysiological changes in different systems across the human body. Diabetic retinopathy is the medical term that describes the condition when the fundus and the retinal vessels are affected by diabetes. As in other diseases, small vessels play a crucial role in the onset, the development, and the outcome of the retinopathy. More importantly, at the latest stage, new small vessels, or neovascularizations, growth constitutes a factor of significant risk for blindness. Therefore, there is a need to detect all the changes that occur in the small retinal vessels with the aim of characterizing the vessels to healthy or abnormal. The characterization, in turn, can facilitate the detection of a specific retinopathy locally, like the sight-threatening proliferative diabetic retinopathy.

Segmentation techniques can automatically isolate important anatomical structures like the vessels, and provide this information to the physician to assist him in the final decision. In comprehensive systems for the automatization of DR detection, small vessels role is significant as missing them early in a CAD pipeline might lead to an increase in the false positive rate of red lesions in subsequent steps. So far, the efforts have been concentrated mostly on the accurate localization of the medium range vessels. In contrast, the existing models are weak in case of the small vessels. The required generalization to adapt an existing model does not allow the approaches to be flexible, yet robust to compensate for the increased variability in the appearance as well as the interference with the background. So far, the current template models (matched filtering, line detection, and morphological processing) assume a general shape for the vessels that is not enough to approximate the narrow, curved, characteristics of the small vessels. Additionally, due to the weak contrast in the small vessel regions, the current segmentation and the tracking methods produce fragmented or discontinued results. Alternatively, the small vessel segmentation can be accomplished at the expense of

background noise magnification, in the case of using thresholding or the image derivatives methods. Furthermore, the proposed deformable models are not able to propagate a contour to the full extent of the vasculature in order to enclose all the small vessels. The deformable model external forces are ineffective to compensate for the low contrast, the low width, the high variability in the small vessel appearance, as well as the discontinuities. Internal forces, also, are not able to impose a global shape constraint to the contour that could be able to approximate the variability in the appearance of the vasculature in different categories of vessels. Finally, machine learning approaches require the training of a classifier on a labelled set. Those sets are difficult to be obtained, especially in the case of the smallest vessels. In the case of the unsupervised methods, the user has to predefine the number of clusters and perform an effective initialization of the cluster centers in order to converge to the global minimum.

This dissertation expanded the previous research work and provides a new segmentation method for the smallest retinal vessels. Multi-scale line detection (MSLD) is a recent method that demonstrates good segmentation performance in the retinal images, while tensor voting is a method first proposed for reconnecting pixels. For the first time, we combined the line detection with the tensor voting framework. The application of the line detectors has been proved an effective way to segment medium-sized vessels. Additionally, perceptual organization approaches like tensor voting, demonstrate increased robustness by combining information coming from the neighborhood in a hierarchical way. Tensor voting is closer than standard models to the way human perception functions. As we show, it is a more powerful tool to segment small vessels than the existing methods. This specific combination allows us to overcome the apparent fragmentation challenge of the template methods at the smallest vessels. Moreover, we thresholded the line detection response adaptively to compensate for non-uniform images. We also combined the two individual methods in a multi-scale scheme in order to reconnect vessels at variable distances. Finally, we reconstructed the vessels from their extracted centerlines based on pixel painting as complete geometric information is required to be able to utilize the segmentation in a CAD system.

The segmentation was validated on a high-resolution fundus image database that includes diabetic retinopathy images of varying stages, using standard discrepancy as well as perceptual-based measures. When only the smallest vessels are considered, the improvements in the sensitivity rate for the database against the standard multi-scale line detection method is 6.47%. For the perceptual-based measure, the improvement is 7.8% against the basic method.

The second objective of the thesis was to implement a method for the characterization of isolated retinal areas into healthy or abnormal cases. Some of the original images, from which

these patches are extracted, contain neovascularizations. Investigation of image features for the vessels characterization to healthy or abnormal constitutes an essential step in the direction of developing CAD system for the automatization of DR screening. Given that the amount of data will significantly increase under CAD systems, the focus on this category of vessels can facilitate the referral of sight-threatening cases to early treatment. In addition to the challenges that small healthy vessels pose, neovessels demonstrate an even higher degree of complexity as they form networks of convolved, twisted, looped thin vessels. The existing work is limited to the use of first-order characteristics extracted from the small segmented vessels that limits the study of patterns. Our contribution is in using the tensor voting framework to isolate the retinal vascular junctions and in turn using those junctions as points of interests. Second, we exploited second-order statistics computed on the junction spatial distribution to characterize the vessels as healthy or neovascularizations. In fact, the second-order spatial statistics extracted from the junction distribution are combined with widely used features to improve the characterization sensitivity by 9.09% over the state of art.

The developed method proved effective for the segmentation of the retinal vessels. Higher order tensors along with the implementation of tensor voting via steerable filtering could be employed to further reduce the execution time, and resolve the challenges at vascular junctions. Moreover, the characterization could be advanced to the detection of proliferative retinopathy by extending the supervised learning to include non-proliferative diabetic retinopathy cases or other pathologies. Ultimately, the incorporation of the methods into CAD systems could facilitate screening for the effective reduction of the vision-threatening diabetic retinopathy rates, or the early detection of other than ocular pathologies.

TABLE OF CONTENTS

LIST OF TABLES

LIST OF FIGURES

LIST OF ACRONYMS AND ABBREVIATIONS

DR	Diabetic Retinopathy
PDR	Proliferative Diabetic Retinopathy
NPDR	Non-Proliferative Diabetic Retinopathy
CAD	Computer Aided Detection
WHO	World Health Organization
MA	Microaneurysm
FOV	Field Of View
RPE	Retinal Pigment Epithelium
OCT	Optical Coherence Tomography
RNFL	Retinal Nerve Fiber Layer
GCL	Ganglion Cell Layer
IPL	Inner Plexiform Layer
INL	Inner Nuclear Layer
ONL	Outer Nuclear Layer
IS	Inner Segments
T	Temporal side
N	Nasal side
IRMA	Intra-Retinal Microvascular Anomalies
NV	Neovascularization
NVD	Neovascularization on the optic Disc
NVE	Neovascularization Elsewhere
VEGF	Vascular Endothelial Growing Factor
ETDRS	Early Treatment Diabetic Retinopathy Study
SVL	Severe Visual Loss
UK	United Kingdom
COS	Canadian Ophthalmological Society
2D	2-Dimensional
3D	3-Dimensional
MSLD	Multi-Scale Line Detector
GVF	Gradient Vector Flow
VFC	Vector Field Convolution
OOF	Optimally Oriented Flux
T-snake	Topology snakes

MHT	Multiple Hypothesis Testing
CT	Computed Tomography
ANN	Artificial Neural Network
K-NN	K-Nearest Neighbor
GMM	Gaussian Mixture Model
SVM	Support Vector Machine
EM	Expectation-Maximization
GA	Genetic Algorithm
FCM	Fuzzy C-Means
SOM	Self-Organizing Map
CNN	Convolutional Neural Network
TVF	Tensor Voting Framework
GLCM	Gray-Level Co-Occurence Matrix
HOS	Higher Order Spectra
STAPLE	Simultaneous Truth And Performance Level Estimation
MTVF	Multi-Scale Tensor Voting Framework
DT-CWT	Dual-Tree Complex Wavelet Transform
DWT	Discrete Wavelet Transform
CAL	Connectivity Area Length
Sens.	Sensitivity
Specif.	Specificity
H	Healthy
G	Glaucomatous
M	Mean
SD	Standard Deviation
VMR	Variance Mean Ratio
RBF	Radial Base Function
Kth-NN	Kth-order Nearest Neighbor
MRI	Magnetic Resonance Imaging

CHAPTER 1 INTRODUCTION

This chapter will motivate the reader about the segmentation and characterization problem on the small retinal vessels. To do so, we will introduce the necessary details about the impact of diabetic retinopathy on the society and the patient's vision. Moreover, the importance of small vessels in the diagnosis, and the progress of the disease into sight-threatening retinopathy. The scientific challenges for the existing methods will also be introduced. Additionally, we will provide the general context of the fundus imaging field and its challenges. Finally, we will give the objectives along with the general outline of the thesis.

1.1 Motivation

Vision is one of the five fundamental senses of the human body and probably the most important. The majority of the information that is received daily is visual cues from the outside world. Possible complications in the vision, therefore, can lead to incapacity for normal everyday function. Consequently, there is a fundamental need to study and eliminate the factors that might have an adverse impact on vision.

One important factor is diabetes. This disease affects the eyes indirectly, and it can lead to blindness if it is neglected. The diabetic eye disease or diabetic retinopathy, which is preventable, is the result of changes in the microvascular circulation system of the eye. According to the world health organization (WHO) [1] diabetic retinopathy is a significant cause of new-onset blindness cases in many developed countries. It was estimated that the prevalence of blindness, due to diabetic retinopathy, is 4.8% of 37 million cases throughout the world. The organization has also included it in VISION2020, a global initiative for the complete eradication of avoidable blindness by the year 2020.

The standard way to inspect the retina for detection is through the ophthalmoscope. Although ophthalmoscopy is considered a gold standard, digital fundus images along with imaging have been replacing the standard way of retina examination. In both cases, the physician searches for specific patterns of abnormalities in the small or large vessels as well as on the retina surface. The procedure is manually performed which is a very tedious work that takes time. Concurrently, the introduction of screening programs of the population will significantly increase the volume of data to be processed. Therefore, methods for computerized and precise quantification of the disease can be useful for the reduction of the invested resources.

An important tool that can be utilized in the computerized screening is the segmentation of the anatomical structures of the retina. Segmentation algorithms can highlight the most

important retinal structures like the vessels, or help the physicians to identify abnormal features that are related to the disease quickly. Due to the nature of the images, these algorithms need to perform under challenging imaging conditions. Furthermore, small vessels appear in the center or the periphery of the image varying in appearance with complex shape configurations and fade boundaries. Finally, pathology alters important image features.

1.2 The role of small retinal vessels in diabetic retinopathy

At a high-level, the classification of the disease is dichotomous indicating the presence or not of new vessels. This type of classification allows the separation of cases to diabetic retinopathy that is not sight-threatening against cases where there is very high probability of sight-threatening complications to the patients. At a more fundamental level, the disease alters the functionality of the small vessels that is reflected in changes in their appearance. Initially, vascular capillaries are occluded causing the appearance of microaneurysms (MAs), these mark the first stage of the disease. The more severe stages include the appearance of bright, or dark lesions caused by further complications at the small vessels level. Accumulated changes that occur as the disease progresses lead to the growth, or the proliferation, of new vessels that are similar in appearance to the small healthy vasculature. The presence of the new small vessels is critical for the outcome of the diagnosis as this category of vessels are prone to collapsing, hemorrhaging, and subsequently sight-threatening complications. In such cases, robust segmentation and subsequently characterization of the small vessels to neovessels or healthy becomes essential. The next step is the identification of the pathological regions that might directly indicate the presence of advanced diabetic retinopathy. Characterization of the regions to healthy or abnormal is the first step in the detection process.

1.3 Fundus imaging

The predecessor of today's fundus imaging devices was the direct ophthalmoscope which was first invented by Herman von Helmholtz in the 1850s [2]. Even though the eye is a semi-transparent organ, its optical properties do not allow inspecting it without direct external illumination. The working principle of ophthalmoscopy is based on the alignment of an illumination beam of light and an observing point. In order to achieve this, specially designed lens or mirrors are placed between the patient's and the physician's eye. If we substitute observer's eye with a digital photographic camera, we can have fundus imaging [3].

There is a standard acquisition protocol. The subject is seated in front of the camera, and then its head is positioned comfortably to the imaging apparatus. Under complete darkroom conditions, light is emitted by a flash lamp that is directed into the eye. Finally, the reflected

light is captured by the camera.

Different camera specifications can exist. The field of view (FOV) ranges from 35 to 60 degrees, which also depends if pupil dilation (mydriasis) is utilized. The latter is achieved by topical application of medication (tropicamide), and it is recommended when there is a need of inspecting the periphery areas of the retina. However, dilation can induce discomfort to the patient, and it is not disconnected from medical complications, so undilated inspection is usually preferred. The image resolution of a camera can range from low to high, e.g. 768x584 to 3504x2336 pixels. Higher resolution cameras are preferred as the vessels as well as other structures can appear in more detail. The next figure (Fig 1.1) shows a fundus camera along with a typically acquired image.

This imaging modality is of particular interest for our application. Fundus imaging is a widely accepted method for inspecting the retina and diagnosing diabetic retinopathy [4]. The advantages of using this modality are that it can produce digital images, which can be processed quantitatively. Furthermore, it is a non-invasive way to image the retina with minimal discomfort for the patient. It is also relatively cheap technology, which makes it attractive for screening programs. Finally, it is easy to transfer the data through a network to a data server.

Even though the acquisition protocol is standardized, the images suffer from artefacts that make the segmentation, and characterization of the small vessels challenging. In fact, the obtained images can suffer from non-uniform illumination problems. Vessels closer to the optic disc are more prominent, while vessels at the periphery more obscure. Due to the illumination, image contrast could substantially vary causing the smallest vessels to appear very faint relatively to the adjacent background region. Moreover, the quality of the images is not unrelated to the age of the subject, the coexistence of anterior or posterior retinal pathologies, and from the appearance of the retina.

1.4 Research contributions

The ultimate goal of the thesis is to propose new tools to facilitate the screening of diabetic retinopathy. Screening tries to sort cases to healthy, or cases deemed for further action. Moreover, according to the severity of the identified DR case, screening can refer the subject to the appropriate medical intervention. For example, an emergency treatment in case of a NV detection, or better management for a NPDR case. CAD could augment screening by using automatic methods for image analysis. In this context, small vessels play an important role as missing them could lead to increased false positive rates in dark lesion CAD systems or increased false negatives in sight-threatening CAD systems. As the number of available data scales up, computerized methods could be proved beneficial to exploit better the physician's

(a) (b)

Figure 1.1 Typical fundus image (a) and fundus camera (b)[1].

time. Furthermore, the new tools could be integrated into systems that would allow better screening access for a broader population. In that direction, the main objective of this thesis is to propose and validate a method that aims to segment the smallest retinal vessels. Given the segmentation, vessels will be characterized to healthy or abnormal based on new features. In turn, this could be used to detect the advanced stage of the disease directly. Accordingly, the following sub-problems were addressed in order to achieve the primary objective.

First, dealing with the problem of segmentation we developed a novel hybrid method that combines a line detector and the tensor voting framework. The developed method utilizes multiple scales for each individual approach. Furthermore, the multi-scale line detection response was adaptively thresholded to compensate for non-uniform images. Finally, small vessels were completely reconstructed from extracted centerlines based on pixel painting. Concerning with the problem of accurately assessing the segmentation on the smallest vessels, we separated the vessels in different categories according to the diameter of the vessel segment that they belong, and then we measured the performance on standard discrepancy metrics. Finally, based on the vascular information obtained by the segmentation as well as the junction information detected by the tensor voting framework, we introduced the spatial point analysis theory to extract new second-order features for region characterization to healthy or proliferative diabetic retinopathy.

1. Image courtesy of Topcon Canada

1.5 Thesis outline

This thesis proposes the segmentation of the small retinal vessels as well as their characterization to healthy or abnormal. This chapter gave the general motivation for the problem. To do so, we briefly introduced the different stages of the diabetic retinopathy, how these stages are related to the smallest retinal vessels, as well as how the fundus imaging is used in the clinical practice. We also presented the scientific challenges for both the segmentation of the smallest vessels and imaging of the retina using fundus cameras. Finally, the research goal and the research contributions were highlighted. The following chapter will present the necessary background and the literature review that will provide the state-of-the-art of segmentation techniques in healthy vessels. Additionally, the segmentation and characterization methods for the abnormal vasculature, as well as the evaluation metrics for assessing the performance of the methods are presented. Furthermore, Chapter 3 and Chapter 4 will present the proposed methodology for the segmentation and characterization of the vessels along with the results. Chapter 5 will provide a general discussion of the work together with the limitations, and possible future research developments. Finally, Chapter 6 will conclude the thesis by summarizing the work and providing possible future work.

CHAPTER 2 LITERATURE REVIEW

This chapter will begin by providing the necessary background about important concepts of the general anatomy and physiology of the retina under physiological, or under pathological diabetic retinopathy. Details will be provided on the diagnosis of the disease, the management, as well as how diabetic retinopathy is related to changes in the small vessels. This will be followed by the state-of-the-art of segmentation techniques in the healthy retinal vessels. Furthermore, this chapter will describe the available techniques for the abnormal retinal vessel segmentation and characterization problem. Moreover, different performance evaluation methods of the segmentation algorithms will be presented. Finally, a general discussion on the limits of the methods with respect to the problem of the smallest vessel will be provided. The chapter will close with the definition of the thesis objectives.

2.1 Background

Computerized techniques are becoming more prevalent in the retinal imaging field. Therefore, it is important to understand how the different methods, such as the segmentation and characterization of the small retinal vessel, could be used to facilitate the diagnosis and management of diabetic retinopathy. This section will describe the general anatomy of the structures that are affected by diabetic retinopathy : the eye, the retina, and the retinal vessels. How the disease is diagnosed and managed. Finally, the importance of neovascularization in the outcome of the retinopathy.

2.1.1 Eye anatomy

The eye consists of two compartments, as figure 2.1 shows, the anterior and the posterior chamber. The posterior chamber, or vitreous, which is located between the lens and the retina, is filled with a transparent non-renewable gel substance, the vitreous humor [5]. Additionally, two groups of fibrous layers can be found in the eye, the external and the internal. The external includes the sclera, the cornea, and the choroid, while the internal entails the retina. The latter, which is the most important for our application, is further divided into two layers, the posteromedial retina, which is the visual part where the light rays are concentrated, and the anterior, which is the non-visual part. Visual retina begins from the fovea centralis or macula and extends until the ora serrata.

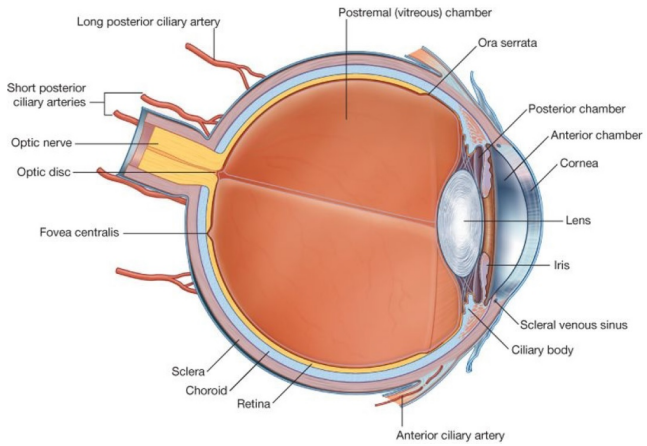

Figure 2.1 Sagittal slice of the eyeball[2].

2.1.2 Retina anatomy and physiology

Anatomically speaking, the retina is a thin sheet of tissue, approximately 100 to 250 μm thick, that lines the inside of the eye. It is located anterior to the choroid and posterior to the vitreous body. A thin acellular layer (2 to 4 μm), Bruch's membrane, separates it from the choroid layer [6].

Retina is considered part of the brain, both from developmental as well as functional point of view. As stated by D. Hubel [7], even though retina is separated from the brain early in the development process, it keeps the connection through the optic nerve. Additionally, the tissue that is made of is a part of the embryonic brain [8]. From the functional perspective, it involves the first two or four stages of the neural processing of vision [9]. Thus, developmental defects or functional damage anywhere on the retina can cause vision impairment.

Like other structures in the neural system, the retina is constructed, and organized in a hierarchical way. It consists of three layers of nerve cells separated by two layers containing synapses that interconnect the cells (Fig. 2.2(a)). The innermost layer is the retinal pigment epithelium (RPE). The cells of this structure contain melanin, a black pigment that helps in the absorption of the excess light. Retina's architecture is backward, having the light receptors at the back close to the pigment epithelium, and the neural cells that are responsible for processing and transferring the information to the front [7]. A closer look into the retina can reveal that there are ten distinct anatomical layers of cells (Fig. 2.2(b)). The various retinal layers can be visualized using a special imaging technique called Optical Coherence Tomography (OCT) [10] (Fig. 2.3).

The photoreceptor cells are separated into the rods and cones. These cells have different

2. This figure was published in R.L.Drake, A.Wayne, and A.W. Mitchell, Gray's anatomy for students, 3rd ed. Copyright Elsevier (2013).

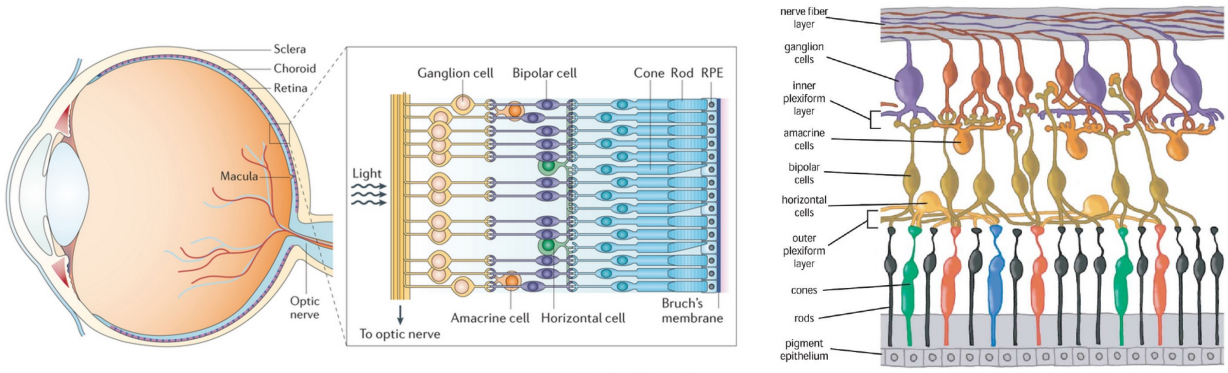

(a) (b)

Figure 2.2 The retinal layers at two different resolutions. (a) The front ganglion, the middle layer of the neural cells, and the back where photoreceptors are located[3]. (b) A sketch of the cellular retinal layers, at a more microscopic scale[4].

physiological characteristics. Rods are more sensitive in low light conditions (scotopic vision) than cones ; while cones, even though they are not very light sensitive (photopic vision), are responsible for our color recognition, and our ability to see fine details. The number of rods and cones vary significantly along the retina. Cones are concentrated at the fovea, where we can perceive the object with fine details. Rods, in contrary, are more scattered and they are absent in the fovea.

2.1.3 Retinal vessels

Retina blood supply comes from the central retinal artery, which is a branch of the ophthalmic artery. It enters the eye from the optic disc and follows a fairly standard pattern at the ganglion cell level. Just before entering the eye, it is divided into two secondary branches, the inferior and the superior. Each secondary branch is further divided to nasal and temporal arteries. The bifurcations continue through the periphery, where there is a gradual reduction in the vessels' diameter. This gradual change leads to the bifurcation of the large vessels into capillaries. Some temporal branches form arches around the fovea. The venous network also follows a similar pattern [12].

On the base, around the optic nerve, the major arteries measure approximately 100 μm in diameter having 18 μm thick walls. In higher order branches the diameter decreases until it ends up to only 15 μm [12]. The composition of the vessels also changes according to the vessel diameter. Large vessels are composed of five to seven muscle layers, while small

3. Adapted by permission from Macmillan Publisher Ltd : Nature Reviews Drug Discovery [11], copyright (2015)

4. Courtesy of American Scientist [8]

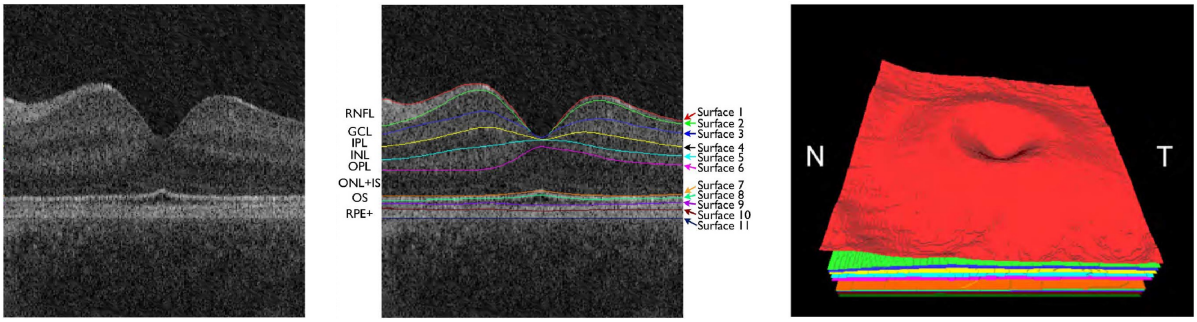

(a) (b) (c)

Figure 2.3 Illustration of the retinal layers in OCT. The first image (a) is the acquired OCT volume. The second image (b) is the segmentation result that reveals the different cellular layers, namely the retinal nerve fiber layer (RNFL), the ganglion cell layer (GCL), the inner plexiform layer (IPL), the inner nuclear layer (INL), the outer nuclear layer (ONL) + inner segments (IS), the outer segments (OS), and the retinal pigment epithelium (RPE+). The final image (c) is the segmented surfaces around the fovea (T : temporal side, N : nasal side) [14] (©[2010], IEEE).

arterioles include a single cell layer. The retinal vessel network does not communicate with any other network, so if there is any vessel obstruction, it can lead to impaired visual function [12, 13].

The vessel network is organized in such a way, to optimize the blood supply in all the critical areas of the retina. Furthermore, it has been observed that the normal vasculature is guided by pre-existing neuronal cells that act as scaffolds for the vessel growth [15]. The net effect is the appearance of the retinal vasculature as a tree-like structure (Fig. 2.4). However, there are two avascular regions, where vessels do not exist. Firstly, surface vessels cannot reach the fovea and a 0.5 mm circular region around it. Secondly, vessels cannot reside posterior to the boundary of the non-visual part of the retina called the ora seratta [12, 13].

2.1.4 Retinal vessel pathologies

Under diabetes, the glucose levels in the blood are higher than normal cases. This metabolic change has an adverse impact on the retinal circulation that triggers many pathophysiological changes [16, 17], of which the most important are related to the smallest vessels [18]. The previous changes lead to the disruption of the local blood flow in the retina tissue. In order to compensate for that, vessel growth factors are secreted causing angiogenesis and neovascularization [19]. These new vessels have poor prognostic value for vision because they grow at the vitreo-retinal interface, an interactive environment, that causes inflammation, and ultimately collapse of the fragile neovascularizations. Consequently, vitreous or preretinal

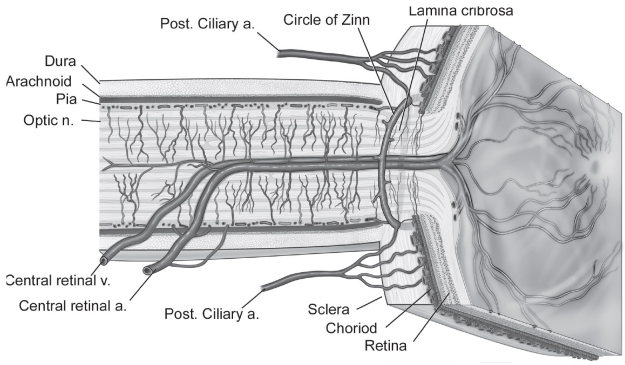

Figure 2.4 Graphical demonstration of the vessel network and supply in the retina. Retinal vessels belong to the central retinal artery/vein ; they cover the retina in a tree-line architecture, and they are superficial to the retina[5].

haemorrhages are induced followed by retinal detachment, and partial, or total vision loss [16].

2.1.5 Diabetic retinopathy diagnosis and screening

Diabetic retinopathy is a progressive disease that includes five main stages. The different stages document the severity of retinopathy based on the visible signs, observed by the retina specialists. Different distinguishable signs characterize the disease as it involves from the early to the later stages. The evolution of the retinopathy among the five stages, according to the Early Treatment Diabetic Retinopathy Study (ETDRS) [20], is :

1. No retinopathy : No sign is apparent that can indicate retinopathy.
2. Mild Non-Proliferative Diabetic Retinopathy(NPDR) : The first clinical sign is a limited number (>3) of microaneurysms (MAs). In this stage, only MAs can be observed.
3. Moderate to severe NPDR : Additional MAs are present on the eyes at these stages and other more complex manifestations lead to the appearance of noticeable dark or bright lesions. When a group of deep capillaries has been occluded, blot haemmorrhages appear in the retina. Another sign in the moderate NPDR is the emergence of hard exudates as well as the cotton wool spots. The former are lipid depositions leaked from the MAs ; while the latter are caused by the swollen neural axons on the nerve fiber layer. In parallel, intra-retinal microvascular anomalies (IRMAs) and venous beadings can be present in an extensive retinal area. As the disease progresses, extensive intra-vascular areas are occluded. Remodeling of the unobstructed vasculature thus takes

5. This figure was published in C.V.Network, Developmental anatomy of the retinal and choroidal vasculature, Copyright Elsevier (2011).

place, which leads to morphological as well as functional adaptations of the unaffected vessels. IRMAs are leaky tortuous capillaries in the areas of capillary occlusion ; while venous beadings are localized dilations of the venous wall, which represents the effort of the body to grow new vessels on the non-perfused tissue. As the disease advances, the appearance of lesions is more frequent.

4. PDR : At this point, vascular endothelial growing factors (VEGFs) are secreted that lead to the formation of new small, fragile vessels, the neovascularizations.

The five-level staging does not reflect visual function, but only the condition of the retina observed via ophthalmoscope or fundus photography. Maculopathy, the swelling of the macula, is another potential factor for visual complication thus for full range classification the presence or absence of maculopathy is reported separately from the retinopathy [21].

The disease can be unnoticed by the patient until its late stages, where the symptoms involve reduced visual acuity or even blindness. Thus, early cost-effective diagnosis and management are required. Diabetic retinopathy can be effectively assessed, based on the inspection of the retina through a direct or indirect ophthalmoscope as well as fundus imaging. Besides this, historically, prevention had been limited to the monitor, and tight control of the modifiable risk factors, like the blood glucose/lipid/pressure levels. The aforementioned established means of prevention together with the publishing of the ETDRS report about the effectiveness of laser therapy helped in the general reduction of the rates of progression to sight-threatening diabetic retinopathy [22].

As a second line of measure, screening was introduced to the public. According to WHO, [23] screening is defined as *"the presumptive identification of unrecognized disease or defect by the application of test, examinations or other procedures which can be applied rapidly. Screening tests sort out apparently well persons who probably have a disease from those who probably not. A screening test is not intended to be diagnostic. Persons with positive or suspicious findings must be referred to their physicians for diagnosis and necessary treatment"*. Screening for diabetic retinopathy is a broad public health practice, as it is highlighted in [21], that aims to identify patients with early signs of the disease, to provide effective management and treatment. Evidence for the effectiveness of screening for sight threatening diabetic retinopathy as part of national policies was given in [24].

In practice, screening programs designed on a national level have been proven adequate in further reducing visual complications. In parallel, the acceptance of fundus imaging as an equivalent to ophthalmoscopy [25] further facilitated the implementation of a range of national screening programs that ultimately helped diabetic patients. For example, Iceland had implemented a national screening program and achieved to reduce the blindness among diabetic patient from 2.4% in 1980 to 0.5% in 2005 [24]. Furthermore, in a metanalysis [22],

where a range of studies from two consecutive decades are examined, it was reported that after 10-years the incidence rate of proliferative diabetic retinopathy (PDR) and severe visual loss (SVL), has been reduced by 4.9% and 3.4%, respectively. In another cost-effectiveness study [26], conducted in isolated communities of Ontario in Canada, screening with fundus imaging was proved cost-effective versus no screening. Moreover, screening with fundus imaging was proved superior to ophthalmoscopy on site as the latter requires the manual inspection of the retina through a hand-held tool, as well as, more intensive employment of trained personnel.

Different screening schemes have been implemented around the world. These can be tailored to the specific needs of a country, in order to maximize the efficiency, and ultimately increase the coverage. In UK [21, 27] for example, fundus imaging is embedded in the secondary care level, with either centralized or decentralized grading by specialists in mobile units (technicians or trained physicians). Then the patients are referred to an ophthalmologist for further diagnosis or therapy if it is necessary. In a recent study published by a group in Australia [28], the burden of grading is proposed to be shifted towards the primary care ; in this way, there will be advantages in the impact and speed of the outcome. In Canada, Canadian Ophthalmological Society (COS) is responsible for publishing clinical practice guidelines for screening, and management of the diabetic retinopathy [29]. As can be seen, manual screening has been proven effective in reducing the progression rates of diabetic retinopathy. However, the screening rates are still lagging behind the expected influx of diabetic patients in the healthcare systems in the near future. Currently, in the US, 50% of type 2 diabetic patients do not have access to any type of eye examination [30]. While the corresponding non-attendance rates are 22% and 20-30% for Australia [28] and for the UK [30], respectively. The goal of the possible new policies would be to increase the screening coverage. These new policies will eventually lead to a dramatic increase in the size of processed data, and thus computerized approaches might play a major role. For example, RetinaCheck project [31] was launched which is a sino-dutch collaboration between an extensive network of hospitals and universities with the aim to screen the entire population of a Chinese province for sight threatening retinopathies, including diabetic. Accounting for approximately 24 million people, this large-scale retina screening program will be realized by CAD systems that will automatically analyze the retinal images. Additionally, it has been noticed that screening rates are analogous to the socioeconomic level. Hence, new means of access, like teleophthalmology, should be considered. In parallel, with the advent of new technologies, automatization of screening is cost-effective and in some cases, it is even encouraged [21]. In Scotland, for example, it has been estimated that the cost per patient for automated detection is approximate $0.25 [30], sufficiently low for subsidized programs. Finally, computerized-based screening is flexible, and it can be integrated into many models

for the effective management of the diabetic retinopathy.

2.1.6 Neovascularizations (NVs)

The appearance of a patient with proliferative diabetic retinopathy is considered an emergency and immediate therapy should be administrated, usually via lasers, VEGF inhibitors, or even vitrectomy [32]. Neovascularizations are particularly interesting for our project. In the comprehensive classification schemes, PDR stage is further divided in three subcategories : 1) mild, 2) moderate, and 3) severe. The following factors determine the severity. Firstly, the location of the neovascularizations, namely on the disc (NVD), or elsewhere on the retina (NVE). Secondly, the size of the neovascularizations area with respect to the area of the optic disc. Finally, the presence of vitreous or preretinal haemorrhages.

Neovascularizations, usually grow from the post-capillary venules in an abnormal pattern that does not obey the fractals' law properties of healthy vessel development. Neovessels lack a standard self-similar hierarchical pattern, branching in random directions. NVs can be mistaken with small healthy or IRMAs vessels, but not with other dark lesions like the microaneurysms. Neovascularizations demonstrate greater variability than the MAs both in shape as well as in size, and thus they pose extra challenges and requirements. Furthermore, NVs demonstrate special functional as well as morphological properties. New vessels lack the tight cellular junctions that are apparent in existing vessels, so they leak throughout their length. Additionally, neovascularizations occur along the border between healthy and ischemic retina, while IRMAs occur within areas of capillary occlusion. Individually, they are as tortuous as IRMAs, forming chaotic networks in groups that cover a large retinal area. They usually loop back to the optic disc (NVD) and have wider vessel diameter on the tip than the base. IRMAs on the other hand, never form loops. Furthermore, slightly different appearance regarding brightness and sharpness, of their edges, can be attributed to the fact that IRMAs grow deeper than neovascularizations. Figure 2.5 shows examples of isolated regions with neovascularizations on the optic disc and elsewhere from an image with PDR.

2.2 Healthy retinal vessel segmentation algorithms

Generally speaking, there has been a constant effort to classify the retinal vessel segmentation methods in a systematic way according to the methodology that is followed. Early segmentation methods were either categorized into contour-based or region-based approaches [33]. Since the establishment of the field of retinal vessel segmentation, several new methods have been presented that extend and utilize new knowledge, so several subcategories were started to emerge. Lately, scientists started combining algorithms together in hybrid schemes, and so blurred boundaries between the methods exist. A good point for someone to start is the

(a) (b) (c)

Figure 2.5 Example of the differences in the apperance of the vessels between a healthy and a PDR case. (a) Healthy retinal image, (b) PDR retinal image, (c) zoomed regions containing neovascularizations on the disc or elsewhere corresponding to the green, red, and blue inset in (b).

review of a series of surveys that have been published in the literature [34, 35, 36, 37].

The categorization that is followed in this thesis can be seen in the next figure (Fig. 2.6). To begin with, for each subcategory the working principles and the assumptions will be given. Then a critical analysis of the advantages and the disadvantages in the context of the retinal vessel segmentation will follow. Finally, similar work and contributions in other applications will be provided.

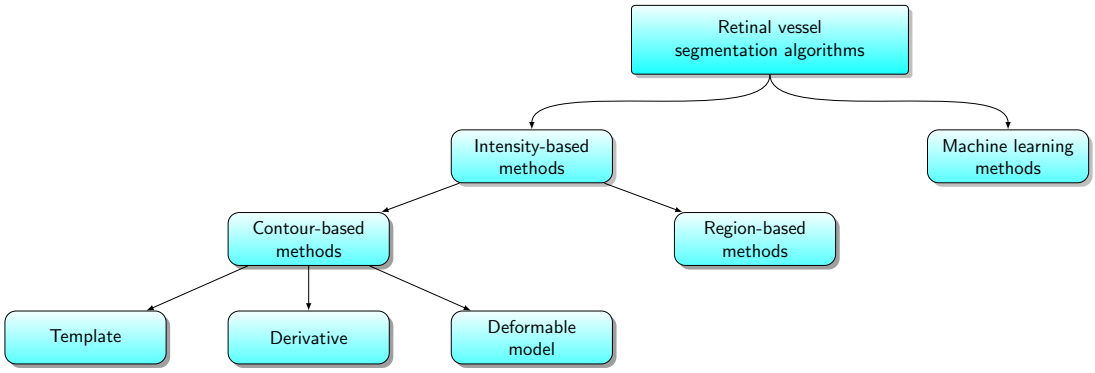

Figure 2.6 Categories of the retinal vessels segmentation methods.

2.2.1 Intensity-based methods

Intensity-based is the largest and broadest of all the categories of methods. The algorithms here segment the images by searching mainly for specific intensity patterns in the images. In turn, Intensity-based algorithms are divided between the region and the contour-based methods.

Contour-based methods are trying to include and group in the same contour, edge, or curve the pixels that satisfy a certain criterion that depends on an applied template. Pixels which are not separated by an edge are allocated to the same category. Additionally, in this category an initial curve can be defined that deforms according to some constraints or forces in order to fit a contour.

Region-based methods operate iteratively by grouping neighbor pixels which have similar intensity values into the same region or by splitting regions of pixels which have dissimilar values. A fundamental algorithm that applies the aforementioned principles is the region growing [38]. All subsequent methods in this category are an extension of the basic model. Additionally, representing the data using graphs facilitates the application of minimum-cost path approaches. Contour and Region-based methods are further separated in subcategories that we will analyze.

2.2.1.1 Matched filtering

One of the earliest introduced segmentation methods for retinal vessels was the matched filtering. This approach, which was first proposed in the 1980s, is based on template matching of a small representative vessel segment along the whole image in the spatial domain. Matched filtering has been widely used for retinal vessel segmentation [39] as well as for coronary arterial tree detection from X-ray angiography [40] and neuron tracing from 3D confocal biomicroscopy [41]. In the case of retinal vessels, the template is constructed as a 2D convolution kernel that filters the image and enhances the vessels. The design of the filter is based on four assumptions for the vasculature. Firstly, the large vessels demonstrate small curvatures so the filter can be approximated by a piecewise straight kernel. Secondly, the cross-sectional intensity profile of the vessels can be approximated by a Gaussian, so the profile of the filter should be a Gaussian too. Thirdly, vessels can appear in different orientations and scales, so the filter should be adapted accordingly. Finally, vessels are darker than their background so the sides of the filters should be at higher intensity level than the central region.

When matched filtering is applied, the effect is the enhancement of the vessels against their background. Subsequently, thresholding can take place as a final step in order to segment the vessels. Since the Gaussian is a very general representation, there are cases where it cannot approximate adequately vessels' shapes. For example, when the curvature is very high in short distance. Additionally, this method has a problem of over-segmenting irrelevant structures that resemble vessels. Indeed, physiological structures like the optic disc as well as pathologies such as microaneurysms and bright lesions can be falsely recognised as a vessel structure. For the smallest vessels in particular ($\sim$3 pixels in diameter), there may be not enough samples to model the profile with a Gaussian or any other model.

Efforts have been placed in the direction of improving several aspects of the basic matched filtering approach or introducing novel variations by applying more complex models. For example, multi-scale sensitivity can be achieved by varying the width of the kernel (Fig. 2.7) and then retaining the maximum response across all the scales [42]. A curved-support Gaussian model has recently been proposed to model non-straight structures [43]. Furthermore, in order to suppress the false positive detections some authors proposed the combination of matched filters with the first order derivative of the Gaussian [44] ; while others exploit features in the thresholding phase [45]. In another case [46], the authors used self-matched filtering, where the selected template is a 180° rotated version of the local neighborhood. In another study, the authors optimized exhaustively the Gaussian parameters before the application to the retinal images in order to reduce the computational time [47].

There have been efforts to include more information to cover all the available cases and overcome the possible limitation of the basic model. One problem is the central reflection that occurs on the large vessels and which appears as an elevation at the center of the Gaussian [48]. The central reflection can be modeled by utilizing a double Gaussian profile [49, 50], a difference of Gaussians [51], a Laplacian kernel [52], or a multiscale Hermite approximation [53]. The last model together with a method based on the superposition of Gaussian functions [54] in a local area, has been proposed to model the healthy vessel bifurcations. A more skewed model than the standard Gaussian was proposed in [55]. Some authors, moreover, introduced constrains to distinguish vessels from the pathologies. L. Zhang et al. [56], for example, reduced the false positives from non-line edges (Fig. 2.8) by incorporating a double-sided thresholding in the Gaussian matched filtering. This model reduces the probability of positive responses from non-vascular pathologies or the optic disc. Transforming the intensity profile in the frequency domain using phase congruency [57] offers a scale as well as intensity invariant representation of the vessel cross-section, that it can also compensate for the blurred boundaries. Finally, modeling of the dark or bright lesions was made possible using multi-concavity modeling [58] or by examining the divergence of the gradient vector field in the image [59]. This information was in turn incorporated into processes that distinguish vessels from pathologies on diabetic retinopathy images.

Detecting the object of interest by directly modeling it has been proved an effective, yet a straightforward way to filter most of the vasculature from the background. Besides matched filtering, other template-based methods have been proposed in the literature.

2.2.1.2 Morphological processing

A more general vessel representation that does not take into account the cross section information is the morphological processing. This category of algorithms tries to segment the

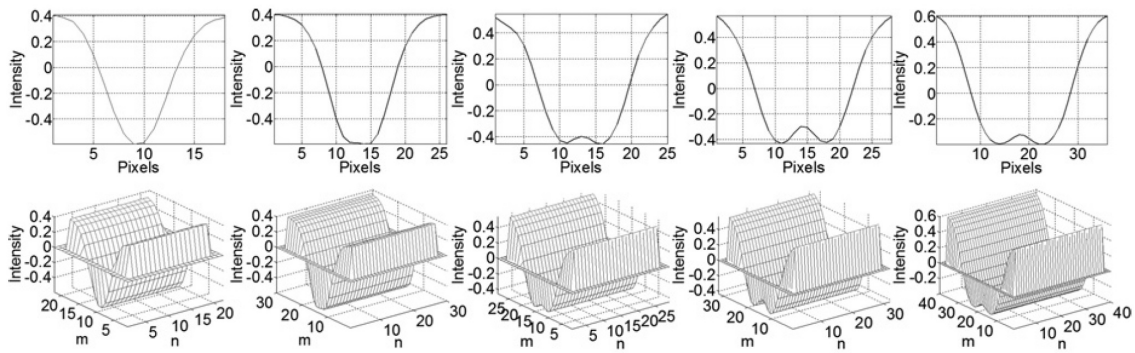

Figure 2.7 Example on the construction of kernels for multi-scale matched filtering. The intensity profiles (top row) are expanded both in length and in width to form the convolution kernels that will respond to vessels of different diameters, from the thinnest (left) to the broadest (right)[6].

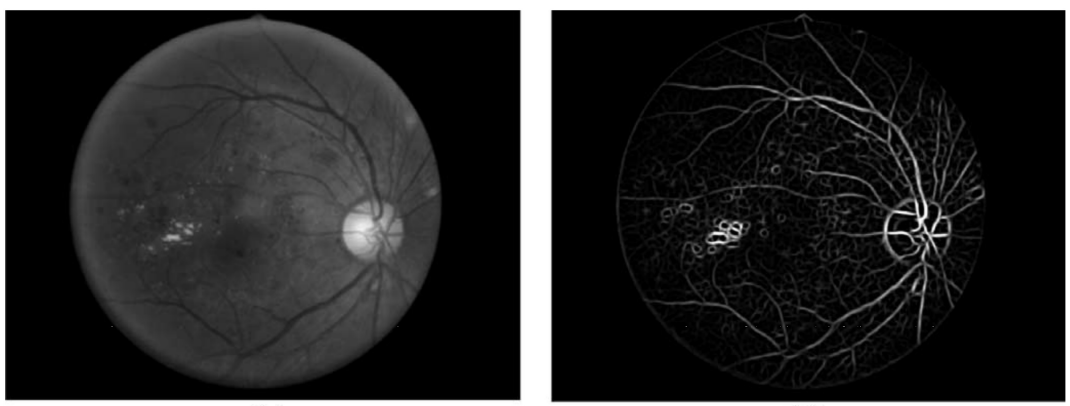

Figure 2.8 Application of standard matched filtering in a non-proliferative diabetic retinopathy image. Bright lesion as well as the optic disc boundary give high positive response when the filter is applied [56] (©[2009] IEEE).

vessels in the image by examining their local shape [60]. Morphological operators are employed, which are essentially ways of combining the image with a structural element that defines the shape that we are seeking. This category of methods are more mathematically formalized than matched filtering as their theoretical background rely on the mathematical morphology and the principles of the set theory [61, 62].

The two basic morphological operators that can be utilized are the dilation and erosion [38]. Dilation expands, removes holes, and connects separated close objects, depending on the shape of the structural element. On the other hand, erosion shrinks objects and clears

6. Reproduced by permission of the Institution of Engineering & Technology [63]

the image from isolated small island in the background, again based on the structural element. All subsequent advanced morphological operators, like opening, closing or top-hat are combinations of dilations or erosions in different orders.

The basic assumptions that are considered to segment the vessels include the fact that the vessels are piecewise, locally linear, elongated structures, thus similarly shaped structural elements can isolate them. Vessels, furthermore, can appear in different orientations and scales so the structural elements should be varied accordingly. Finally, vessels have uniform and higher grayscale intensity than the background.

The advantages of these algorithms against other available methods include their robustness to noise and reduced computational cost. Moreover, morphology has been utilized in pre/post-processing processes [64]. However, the basic algorithm does not employ the cross section information of the vessels. Additionally, morphological processing is inaccurate in term of localizing the vessels' boundary. The basic working principles, also, are not applicable in the thinnest or the most tortuous of the vessels ; and finally, over-segmentation is frequent from similar to vessel physiological structures. More particularly, for the narrow vessels, the size and shape of the structural element is inadequate to approximate the vessels, so there is low sensitivity in that cases.

Several studies exist that employ morphological processing either for enhancing or segmenting retinal vessels. In an early paper [65], vessels were enhanced by applying a multi-directional linear structural element ; while recently A.M. Mendoca et al. [66] employed multiscale circular structural elements in successive top-hat operations to enhance the vessels. Furthermore, M.S. Miri and A. Mahloojifar [67] proposed a new scheme where multi-structural elements of different orientations and scales are used in the same window area to segment the vessels. In another series of similar methods [68, 69, 70], the authors investigated the Gaussian cross-sectional profile of the vessels. Firstly, they computed the local curvature using Laplacian filtering, and after that, they isolated the vessels by applying an alternating filter with a linear structuring element and morphological reconstruction. The authors in [71] tried to overcome the problem of over-segmentation of the optic disc, by first employing morphology to localize the optic disc, and then a series of morphological processes for the retinal vessels. Lately, morphological definition of paths (see Fig. 2.9, 2.10) has been proposed that can reconnect vessel pixels to non-straight paths [72, 73]. In other applications, a recent advance includes the introduction of the spatially variant morphology [74], where Hessian based vesselness controls the size and orientation of the structural element.

Processing the images by means of morphology offers a more mathematically formalized way to detect the vasculature as all the operations are a combination of basic functions. An even simpler template-based method has been proposed to isolate the vessels.

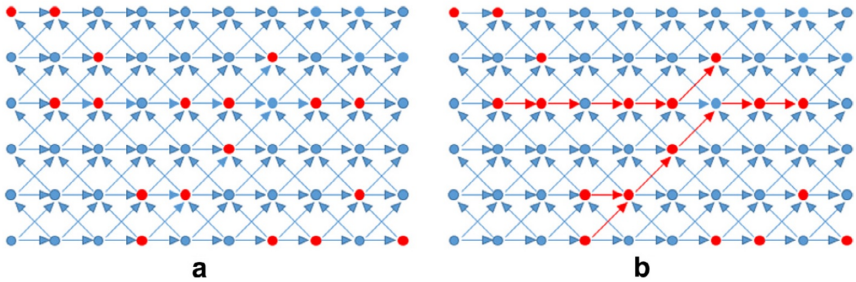

Figure 2.9 Schematic diagram of path opening. Given a specific binary adjacency relation, horizontal in (a) and the most prominent pixels (red), path opening connects neighbors to form three different paths (b)[7].

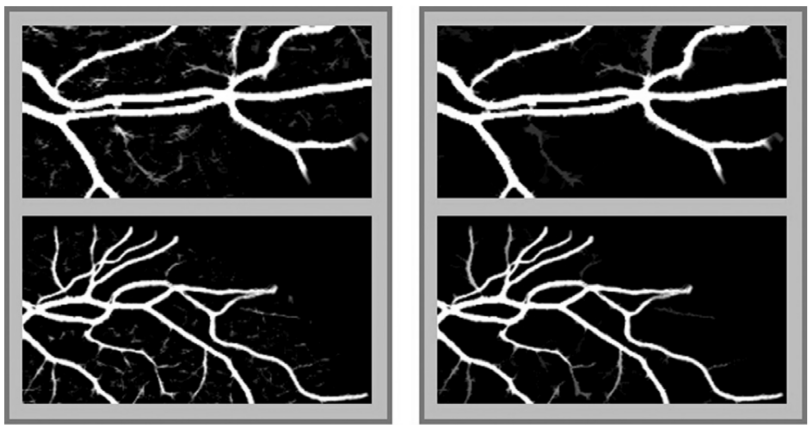

Figure 2.10 Example of path opening applied on a fundus image. Given the vessel enhanced image at the left column path opening reconnects the most prominent, with respect to the filter response, pixels to form paths at the right column[8].

2.2.1.3 Line detection

The simplest of all the template-based methods that do not include any width information is the line detection. The fundamental assumption that is being made in this subcategory of algorithms is that vessels are piecewise elongated line-like structures with lower intensity than the background. In the basic working scenario of a single-scale approach, a straight sampling line is utilized that computes the mean intensities along different orientations across the whole image in the spatial domain. When the line is parallel to the vessels, the mean response is maximum. The methodology here is closely related to the Radon and discrete Hough

7. Reprinted from B.Yin et al., Vessel extraction from nonfluorescein fundus images using orientation aware detector, vol. 26, Pages. 232-242, Copyright (2015), with permission from Elsevier [73].

8. Reprinted from B.Yin et al., Vessel extraction from nonfluorescein fundus images using orientation aware detector, vol. 26, Pages. 232-242, Copyright (2015), with permission from Elsevier [73].

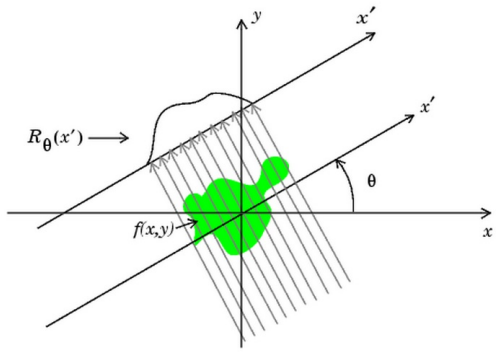

Figure 2.11 Radon transform [9].

transform [75], (see Fig. 2.11). Radon transform computes a series of parallel line integrals in different offsets from the center of the object that are projected in a certain distance in an another projection line (x'). The projection line, in turn, is rotated to accommodate different angles (θ). The final value that is registered, in another parametric space, is the sum of all the projections. Equally, the basic line detector is a special case of this transform. This is true if we substitute the basic integral functional with the computation of the mean value ; if we only allow the central line to be projected ; and if we finally assume that the response is the maximum along the available orientations.

This method was first utilized to identify linear structures in mammographic [77] as well as ultrasound [78] data. However, it was recently being applied to retinal images [79] (Fig. 2.12). Lately, it was adapted to multi-scale schemes to cover all the available vessels' diameters by varying the length of the sampling line [80]. Additionally, line-based approaches are computationally inexpensive, embarrassingly parallel, and can be combined in hybrid schemes [73]. One drawback of the basic line detector is that it produces high responses in pathologies like microaneurysms and bright lesions because these structures have similar characteristics to the vessels. The former has been effectively tackled by examining more carefully the results derived by the line detectors. More precisely, it could be assumed that in case of the vessel there will be a peak in the response of the filter in a specific direction, parallel to the direction of the vessel, while in small microaneurysms the response will be high in all the examined directions [81, 82]. Another limitation is in the detection of the vessels' bifurcations. This problem was tried to be solved by representing the local image around the examined central point into polar coordinates [83] ; another possible way is to use the analysis of the orientation space [84] to identify multiple response peaks that indicate the existence of a junction or a crossing. Based on the line detectors other authors extended the method to be

9. Courtesy of Mathworks : [76]

applied in the optic disc localization [85]. A different configuration of multiple parallel lines, or measuring the contrast instead of the intensity, was implemented in order to facilitate the detection of the smallest vessels [86, 87, 88]. Finally, local orientation selection by the application of the Hessian followed by line detection was proposed for X-ray angiography, as well as for retinal images, in [89].

The previous template-based methods try to detect the vessels in the spatial domain. Instead, we can investigate the vascular properties differently by examining the images in another space, the variational domain.

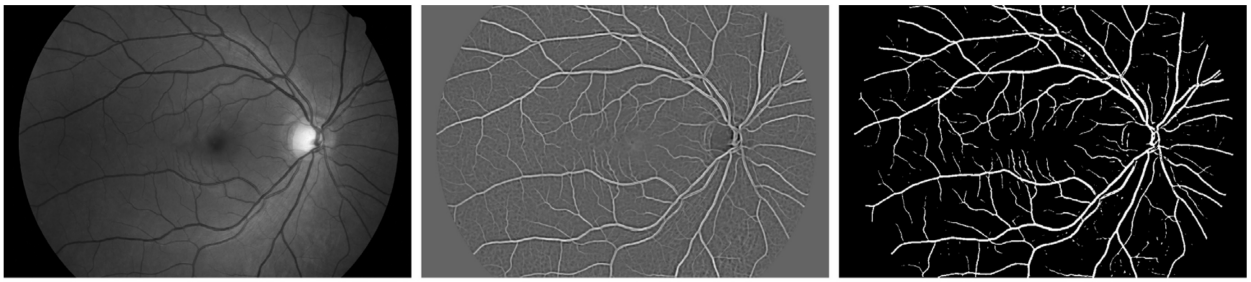

(a) (b) (c)

Figure 2.12 Example of the multi-scale line (MSLD) detection approach applied on a high resolution retinal image. (a) input image, (b) MSLD response, and (c) segmented vessels based on thresholding.

2.2.1.4 Derivative methods

In this category of algorithms it is assumed that the images are two-dimensional functions $f(x, y)$ where the vessels appear as local maxima or minima [90]. The vessel detection is then performed by examining the image derivatives properties.

One of the earliest adopted methods for vessel segmentation was edge detection via first-order derivatives or gradients. Gradient-based edge detectors (Sobel, Prewitt, Robert, Canny) had been utilized in many studies [91, 92, 93]. The process is based on low level primitives, and the implementation requires less computation. The method tries to identify the local gradient direction together with its response. However, the kernels cannot easily handle non-straight vessels, fragmenting the result. Secondly, the kernels are of single-scale and thus they do not take into account any information about the intensity variation. Thirdly, the method can only detect the boundary of the large vessels ; while its response is low if the line deviates from an ideal step edge.

A methodological extension is the combination of the local gradient into a matrix, the structural tensor. By decomposing the tensor, neighbor information can be considered impro-

ving the response of the vessels against other irrelevant structures. This approach has been effectively implemented in [94] for differentiating vessels, from bifurcations, and nodules in chest computed tomography (CT).

Different groups tried to tackle some problems related to the gradient-based methods by taking into account the fact that vessels' cross-sectional profile is a Gaussian. To do so, they utilized the first-order derivative of the Gaussian function [66, 95]. The first-order improves the performance of the basic gradient-based edge detectors ; however, it only extracts fragmented centerlines. Post-processing hence is required to connect the fragmented detected centerlines. Additionally, the convolution with a Gaussian filter is equivalent to the application of filtering in all the image directions (isotropic diffusion) [96] ; where the direction of the gradient determines the orientation of the filtering. When isotropic filtering is applied to images it removes the excess background noise ; however at the expense of filtering the vessel boundary, merging close vessels, and filtering out small vessels. Anisotropic diffusion was proposed to overcome the problem by filtering the image in an orthogonal direction to the detected gradient [97, 98, 99]. For the problem of merging close vessels, alternative methods that have been proposed utilize the gradient vector flow (GVF) [100] or the optimally oriented flux (OOF) [101].

An extension to the previous methodology is the exploitation of the second-order derivative properties. Similarly to tensor, the higher order representation offers additional information from the neighborhood, like the curvature, which has different values depending if the object is tubular or blob-like. One appealing implementation is the Hessian matrix computation in every pixel I_s of the image (2.1) :

$$Hessian(I_s) = \begin{pmatrix} \frac{\partial^2 I_s}{\partial x^2} & \frac{\partial^2 I_s}{\partial xy} \\ \frac{\partial^2 I_s}{\partial yx} & \frac{\partial^2 I_s}{\partial y^2} \end{pmatrix} \tag{2.1}$$

The image derivatives can be approximated numerically by convolving the image with the partial second-order Gaussian derivatives. This is a practical way also for scale space representation of the image because by varying the width of the Gaussian function we can examine vessels of different diameters. Eigen decomposition of the Hessian matrix follows, where the principal directions of the underlying structure are computed. The extracted principal directions are very important features because the vessels are parallel to the eigenvector that corresponds to the maximum eigenvalue [90]. The vessel enhancement is then performed by combining the eigenvalues in appropriate quantities or models. Examples include : Lorenz's [102], Sato's [103], and Frangi's [104] vesselness models. Vascular centerlines can also be detected by decomposing the Hessian matrix as it was presented in C. Steger paper [90].

Since Gaussians are used to approximate the derivatives, Hessian matrix representation

also suffers from the same problems as the isotropic diffusion filtering. In this case, the situation is even worse because the second derivatives' effects are magnified. Additionally, the method is insensitive to noise, which is connected to the detected vessels. Also, the method is insensitive to inhomogeneous regions, and the approach has a problem at bifurcations. Nevertheless, it has been extensively utilized in many contemporary applications [105, 106]. In [107] T. Linderberg introduced γ variable to weight the scale response. To further improve the method in another study, a vessel diameter depending on an equalization factor d was used to weight retina vessels of different diameters [108]. For the problem of merging close vessels, a new second-order derivative was proposed in [109] that is based on a bi-Gaussian operator. M. Sofka et al. [110], in another study, proposed a hybrid scheme where the responses from matched filtering and Hessian matrix were combined to better detect the retinal vessels. In a similar fashion, a general multi-scale method for centerlines detection was proposed that combines the second and the first-order derivatives together on a dimensionless ratio, overcoming their disadvantages [111]. In two very recent studies, the response of Frangi's model is improved by redefining the contribution of each eigenvalue in the final vesselness measure [112] (Fig. 2.13), or by applying the model in another parametric space, the orientation score domain [113].

Derivative-based methods are a category that has received considerable attention from the community. Derivative methods have been also incorporated in more sophisticated and

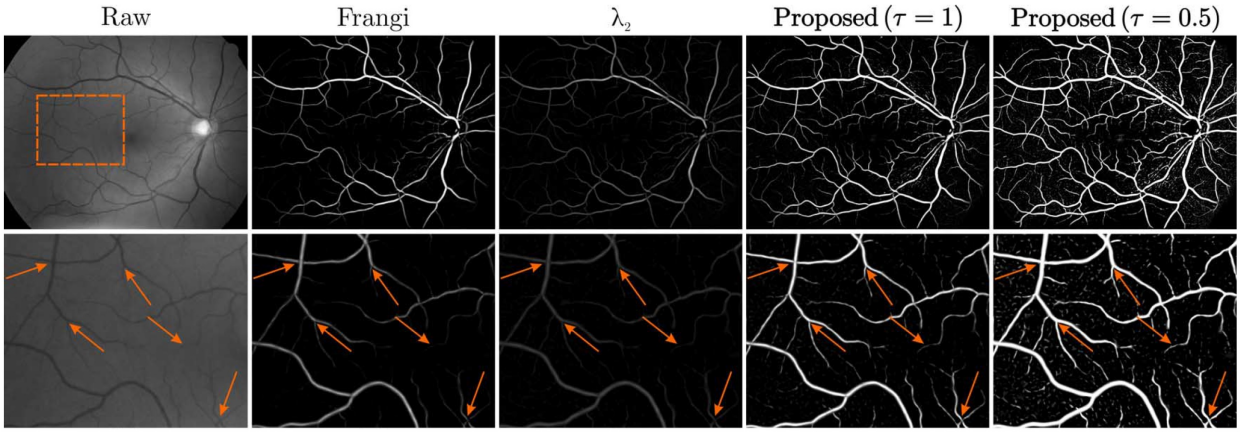

Figure 2.13 Example of the application of the new vesselness measure proposed by T. Jerman et al. [112] on a high resolution fundus image. The figures along the columns show the input image, the response of the standard Frangi filter, the second eigenvalue of the decomposed Hessian matrix, and the simple thresholded response of the new vesselness measure, respectively. The second row shows the responses and segmentation corresponding to the orange inset in the first figure. Finally, the arrows point to bifurcations and small vessels that are faint in Frangi's method (©[2016] IEEE).

complex models that try to reach a global solution by minimizing an energy asscociated with the location of a contour with respect to the vessel.

2.2.1.5 Active contours

Active contours or snakes, which were first proposed by Kass et al. [114], are part of the deformable models methodology. Along with level sets, another framework that we will present in the next subsection, these methods track the evolution of a contour with time by modifying an initial curve according to some constraints or forces.

Active contours define the position of the model parametrically as $v(s) = (x(s), y(s))$ with $s \in [0, 1]$ and try to minimize the energy associated with its shape constraints (internal), and its distance with respect to the features of interest (external) as the next equation shows (Eq. 2.2) :

$$E_{snake} = \frac{1}{2}\int_0^1 \left[\left(\alpha\left|\frac{\partial^2 v}{\partial s^2}\right| + \beta\left|\frac{\partial^4 v}{\partial s^4}\right|\right) + E_{external}\right]\partial s \tag{2.2}$$

In this equation, the first two terms control the stretching and bending of the snake, while the third attracts the snake to the target position. In the original case this was the image gradient : $E_{external} = -\left|\nabla I\left(x, y\right)\right|$ [114].

The advantages of using this family of algorithms in vessel segmentation are their computational efficiency, at least for the 2D case, the ability to track their evolution in "real-time", and their interactivity. For example, the user can place some high-level constraints or points that the snake will be forced to converge to or avoid. Additionally, the snake can be represented with splines which allow for sub-pixel accuracy and smoothness [115]. Finally, active contours demonstrate robustness to sparse or incomplete boundary information. On the other hand, due to the contour parametrization good initialization close to the features is a prerequisite. If this does not happen the snake can be trapped easily in local minima or attracted by features similar to the target one in the vicinity. The inability to change topology is another weakness of the snakes, even though there are efforts to overcome this limitation.

Active contours have been applied extensively in many 2D/3D vessel segmentation applications. Many directions of research were investigated for possible improvements. In the case of the external forces, the original static metric was not robust enough when concavities were encountered and it had to be initialized very close to the boundary of the object of interest. Breakthroughs that have been proposed include a dynamic inflating, like a balloon force [116] ; while gradient vector flow (GVF) [117], and vector field convolution (VFC) [118] are considered state of the art. In the context of vessel segmentation, a novel advancement

is the eigen-snake proposed by R. Toledo et al. [119]. The external force, here, learns to recognise, by classification, the vessels features by filtering the image at multiple scales in the direction of the principal eigenvector of the structural tensor.

Higher-order geometrical constraints are utilized in the ribbon snakes [120, 121]. It is assumed that elongated linear structures, like the vessels, consist of two parallel edges with a varying diameter. Thus, two parallel snakes can be fitted on the boundary of the lines. Similarly, Bashir Al-Diri et al. [122] utilized the ribbon snake approach for the segmentation, but to facilitate the initialization of the model they firstly identified the centerlines by tramline filtering.

Another drawback of the original active contour methodology is the inability to change its topology, namely to split and merge during its evolution. This problem has been addressed by topology adaptive t-snakes [123] and more recently by the extended topological active nets [124]. Figure 2.14 shows an example of T-snakes applied on the retinal image. Multiple T-snakes are initialized across the vessels that merge to segment the vessels.

Active contours represent the deformable model explicitly on the image plane. A methodological extension is to represent the evolving model implicitly, as the interface between an hyper-surface and the image plane.

2.2.1.6 Level sets

Level sets, which were first proposed by S. Osher and J.A. Sethian [125], define the problem one dimension higher than the dimensionality of the data. Thus, for the 2D segmentation case, it is assumed that the model is embedded in a 3-dimensional surface, usually initialized as a signed distance function. In this scheme, the model is defined as the zero level-set of the 3D function ($z = 0$). Formally, if $\Psi : \Re^2 \rightarrow \Re$ is the level-set function, the segmentation contour is given by the following equation :

$$C = \left\{ p \in \Re^2 | \Psi\left(p\right) = 0 \right\} \tag{2.3}$$

The evolution phase now concerns the motion of the hypersurface and not the 2D model itself. In the original work [125, 126], the evolution of the surface over time t is the solution to the next equation :

$$\frac{\partial \Psi}{\partial t} + v \left\| \nabla \Psi \right\| = 0 \tag{2.4}$$

where v is a velocity term normal to the contour direction that guarantees convergence. The incorporation of different external forces can drive the level-set closer to the boundary of the object of interest. Figure 2.15 demonstrates the principle of hyper-surface evolution as a function of time in level sets. The final contour is the intersection between the image plane

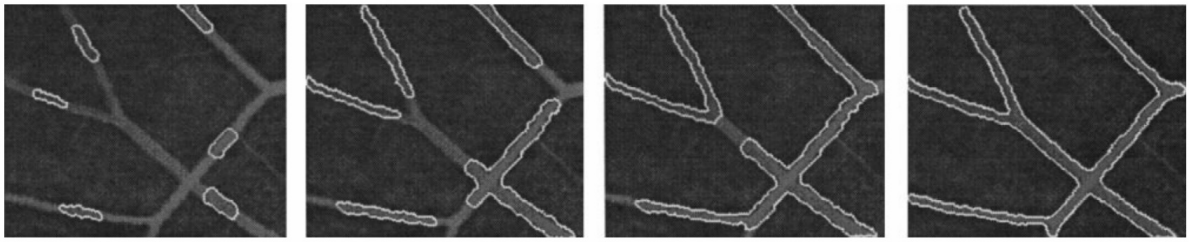

Figure 2.14 Example of T-snake vessel segmentation. Several active contours are initialized on the vessels that subsequently merge into a single contour as the algorithm iterates[10].

and the specific instance of the hyper-surface at time t.

The basic advantages of the level sets are that they do not suffer from the parametrization issues of the snakes. Additionally, the topology can change very easily ; so the zero level-set can break into more than one contours during its evolution to capture multiple objects. One drawback of the level-sets is their increased computational cost.

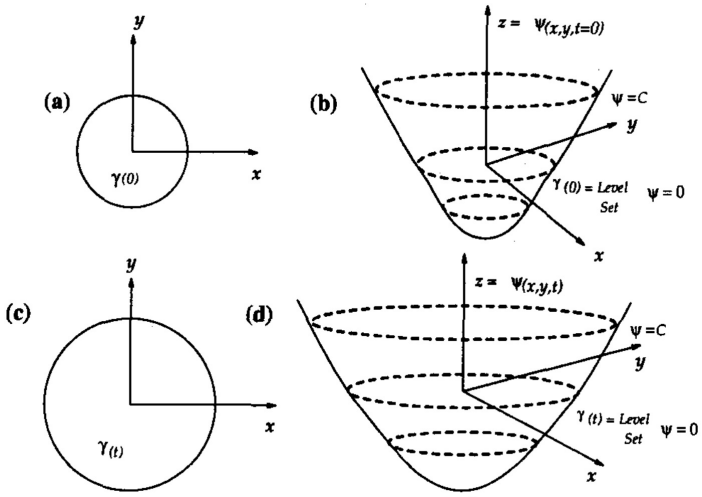

Figure 2.15 Example of the evolution of level sets. The first row shows the initialization of the curve (a) and hyper-surface (b) at $t = 0$, while the second row shows the evolution of the curve (c) and its corresponding hyper-surface (d) at time t [127] (©[2002] IEEE).

Extension to the original framework is the implicit geometric active contour proposed by M. Malladi et al. [127]. An internal curvature-based force together with a ballon-like external force guides the level-set towards the object boundary. Other available external forces are the mean curvature motion [128], and the gradient vector flow [129] applied on a geodesic

10. Reprinted from T. McInernry and D. Terzopoulos, T-snakes : Topology adaptive snakes, vol. 4, no. 2, Pages. 73-91, Copyright (2000), with permission from Elsevier [123]

active contour. In [130] a flux-based external force was constructed based on the Hessian vesselness measure. Similarly, Y. Zhao et al. [131] incorporated the vesselness into an infinite perimeter active contour model in order to improve the propagation of the curve at the thin and elongated vessels. T. Chan and L. Vese [132], moreover, modified the external force to demonstrate no dependency on the image gradient but only on the regional information ; which is an extension to the original D. Mumford and J. Shah method [133]. Although the method can be trapped into local minima, its multi-scale and noise robustness made it appealing for vessel segmentation applications [134]. A new method was proposed in [135] that accelerates the minimization of the Mumford-Shah model. The new method was combined with Gabor wavelets to overcome the non-uniform illumination problem. In the context of small vessel segmentation, Chan Vese model [136] is outperformed by a newer method, the Sobolev active contours [137] (Fig 2.16). This can be accounted to the fact that Sobolev-based method contains a length increasing term that is better suited for approximating elongated structures like the vessels. Other algorithms that utilize prior shape information include the one proposed in [138]. Here, the method allows fitting a ball measure during the level-set evolution, which can constrain the contour expansion to approximate the tubular shape, penalizing possible leakage phenomena. Furthermore, P. Yan and A.A. Kassim [139] were inspired by the capillary force associated with thin tubes to propose a new model. In their algorithm, the small diameter of a tube can facilitate the level-set to evolve deeper into the very narrow vessels.

Level sets, as well as the previous subcategories represent the most diverse group of the intensity-based approaches. The second major category of methods is the region-based methods which consists of tracking and minimum-cost techniques.

2.2.1.7 Tracking

One major drawback of the basic region growing method is that it does not constrain the growth of the region to a specific shape locally, which leads to leakage phenomena in low contrast areas. We can overcome this limitation by assuming that the region growing should include a shape constraint. Under that consideration, tracking is an iterative process, where a vessel model is compared to a local image segment to get the vessel's parameters of centerline and width. This is followed by the prediction of the direction from the current position via optimization.

The advantages of tracking over other methods include the low computational burden since the image is processed locally. Connectivity is also preserved because the method is based on a region growing algorithm. Furthermore, the use of an explicit model can extract the local information of centerline position and diameter. On the other hand, limitations

Figure 2.16 Example of the application of Sobolev active contour for vessel segmentation. The figures from left to right demonstrate how the initialized contour of the level set expands to segment the vessels[11].

of the method include the inadequacy to continue the tracking process when challenging areas are encountered. In our context, the challenging regions are those that demonstrate reduction on the vessel/background contrast and diameter, bifurcations, vessel crossings, or encountered adjacent vessels.

Several numbers of vessel models descriptions exist in the literature. For example, it can be assumed that the boundary of the vessels coincides with the ridges computed by the gradient magnitude [140] or the Hessian matrix [141] in a preprocessing step. Template matching is another option [142]. Finally, a cross-sectional model compared or fitted locally to the corresponding perpendicular vessel profile has been proposed [143, 144] ; the model can be similar to the searching pattern namely, a double Gaussian, or a more general ellipsoid cross-section [145]. Tubular tracking, as proposed in [144] that utilizes a generalized circular cross-section template for localizing the vessel, is considered more appropriate for our application. Since it is a general vessel representation, it can approximate not only medium to large scale vessels, but also small vessels that have a different, more circular cross-sectional profile. Independent of the considered application, other models or methods that have been proposed are the spheres [146] and the flexible super-ellipsoids [147].

The optimization step tries to find the possible location or direction of the vessel in the next step. The correct prediction of the local direction can be achieved by looking in the direction indicated in a previously tracking step. Then in the next iteration, the model is recentered by employing different measures. Fuzzy C-mean clustering [148], Kalman filtering [149, 150], particle filtering [151, 152], and Bayesian-based tracking [153, Fig. 2.17] have been employed. Fuzzy C-mean clustering is an unsupervised classification approach. Kalman filtering identifies the possible direction by taking into account all the previous predictions in a

11. New possibilities with Sobolev active contours, International Journal of Computer Vision, vol. 84, no. 2, pp. 113-129, G. Sundaramoorthi et al., With permission of Springer [137]

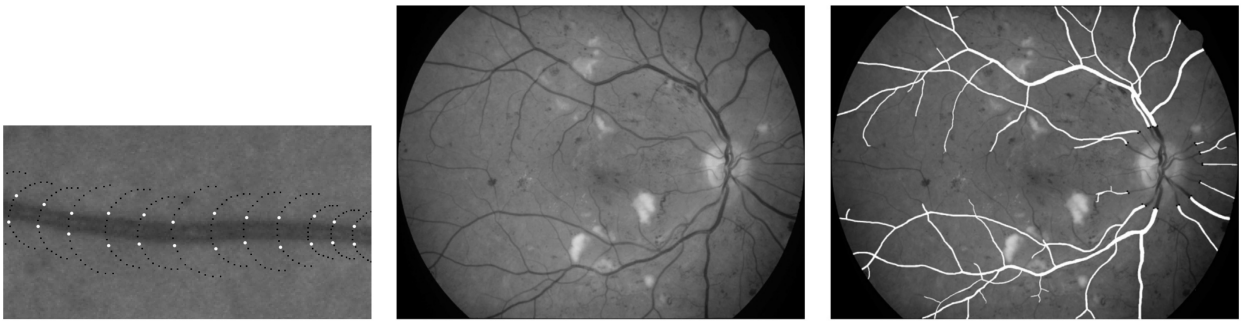

(a) (b)

Figure 2.17 Example of tracking. (a) tracking iterations along a straight vessel. (b) tracking result on a high resolution fundus image[12].

probabilistic way ; however, it is a single hypothesis method that does not take into account alternative paths in low contrast or branching cases. An extension to the former methodology is the particle filtering, a multiple hypothesis approach, which employs a number of particles each one representing an alternative state. The net effect is to overcome the previous limitations at the expense of increased computational cost, at least for three-dimensional problems. Optimization based on maximizing the a posteriori criterion of Bayes theory in order to identify the vessel edges has been also proposed. In a purely deterministic way, multiple hypothesis testing (MHT) [144], which has been applied only on 3D applications, finds the best direction by testing all the available branching options up to a predefined depth in the searching space. This allows the method to decide about the local vessel direction using information from subsequent steps overcoming challenging areas. Another approach that has been proposed, is the prediction based on the geometrical image moments, that was applied to a CT angiography application [154].

Bifurcations are taken into account in the vessel modeling level, or dealt by seeking actively in a depth first search fashion ; namely, after a single branch has been detected the tracking process is reinitialized in the first identified candidate. Tracking has been combined with deformable models to augment the process [155, 156]. Automatic initialization, also, has been achieved by employing a preprocessing step where probable vessel points are identified by applying filtering (vesselness [90, 157], simple Gaussian [158]), or by considering the ending points of pre-identified large vessels as the tracking seeds in hybrid schemes.

Region-based methods are further subdivided to algorithms according to the used data representation. Tracking methods are directly applied on the image space while representing

12. Reprinted from J.Zhang et al., A retinal vessel boundary tracking method based on bayesian theory and multi-scale line detection, vol. 38, no. 6, Pages. 517-525, Copyright (2014), with permission from Elsevier [153]

the images as graphs allow us to use minimum-cost techniques.

2.2.1.8 Minimum-cost path

In the semi-automatic case, given a starting and an ending point inside a vessel, we can utilize a minimum-cost approach to identify the centerline. Generally speaking, minimum-cost methods try to minimize a cost function associated with the path that connects two points. Representing the data as a weighted undirected graph with vertices as the image pixels and edge weights as the intensities can help in the direction of applying the shortest path method proposed by Dijkstra [159]. Fast marching [160] is another numerical optimization scheme, related to the level set approach, which tries to find the shortest path by solving the Eikonal equation.

The method is robust against possible discontinuities or low contrast areas [161] ; however, the second point is required, and only a single centerline is defined between two points at a time. Another potential problem is that there are cases of local minima paths extracted by the algorithm that are shortcuts, especially in low contrast areas. This can be solved by selecting an appropriate cost, the cost aggregation rule, and a penalizing term for deviating away from the desired course. For example, in [162] the authors used the Hessian vesselness instead of the grayscale intensity to increase the probability of constraining the path into the vessel. In [163] also, the authors penalized the great changes in the mean intensity level around a neighborhood that might denote the jumping of the path to an adjacent close vessel (shortcut). Additionally, they penalised differently the diagonal from the vertical or horizontal transitions. A curvature regularization term independent of the vessel length was introduced that deals with the problem of shortcuts in retinal images [164]. Lately, the combination of curvature penalization and a new metric defined on the orientation space was proposed to deal with the same problem [165]. However, it has only been applied for closed contour detection in natural images.

Furthermore, the extraction of a single centerline requires the exhaustive exploration of the searching space greatly increasing the computational time. Methods that have been proposed to speed up the searching process includes, the bidirectional propagation [166], where the searching is initiated from both the source and the target point. Eventually, the search trees that begin from the two points meet in an image pixel, and the optimal path is extracted. In another approach, a freezing scheme is introduced that acts as a stopping criterion for further searching branches with very high costs [167].

Minimum-cost path techniques' aim is to extract centerlines ; however, we might be interested in extracting whole vessels. One way to overcome this problem is to incorporate an additional dimension that corresponds to the vessel width. In [168], the authors modified

the fast marching algorithm to include the aforementioned characteristic, and applied it to several applications, including to images coming from ophthalmological data.

Finally, the algorithms require the user intervention ; however, recently an exploratory approach has been proposed to overcome the problem. R. Estrada et al. [169] developed an algorithm based on forest representation, which applies an iterative procedure until convergence is achieved and the whole retinal vessel network is segmented without user intervention. Lately, Da Chen et al. [170] used an anisotropic fast marching scheme applied on vessel keypoints detected by vesselness to extract the full retinal vasculature from a single retinal image. Figure 2.18 gives an example.

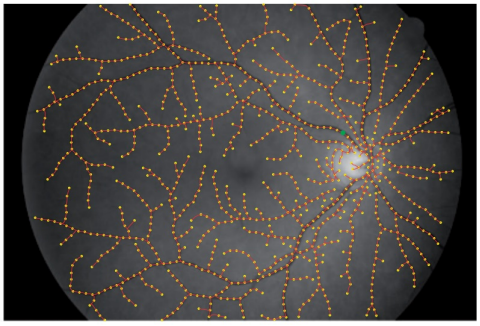

Figure 2.18 Example of the application of anisotropic fast marching proposed by Da Chen et al. [170] for full retinal vessel segmentation ((c) D. Chen et al., 2016).

2.2.2 Machine learning algorithms

The algorithms based on machine learning techniques deal with the automatic determination of the class of a pixel that is examined. In our case we usually have a two class problem : 1) vessel and 2) non-vessel or background. The methods here are divided into two main subcategories : supervised and unsupervised. Lately, a third subcategory of methods started to emerge that try to model the way the human visual perception system functions at a fundamental or a more abstract level.

The learning process is performed after vessel descriptors are extracted. The descriptors are based on feature extraction. For that, a set of N-dimensional image feature of each pixel is required. A large variety of feature descriptors has been proposed in the literature spanning from the existing segmentation to filtering methods.

2.2.2.1 Supervised

Supervised algorithms usually consist of two stages, the designing stage and the application phase. The sequence of actions is the following : A special classifier is firstly employed, and

then a rule for vessel detection is statistically learned by employing a characteristic labeled training set. Usually, the latter is a subset of the available data that acts as a validation set for the classifier. Then, the trained classifier is applied to a new image, which belongs to the test set, in which case it categorises its pixels as vessels or non-vessels. The resulting categorization can be either hard, explicitly assigning the examined pixel in one of the available class or soft where the examined pixel is assigned a probability belonging to a specific class.

There are some advantages and disadvantages related to this category of algorithms. Firstly, the performance of the algorithms depends on the careful tuning of its components. The existence of a ground truth or a manually labeled set, additionally, is prerequisite since it is used to train the classifiers. This set should be representative of the test set that will be used to evaluate the algorithm. For the smallest vessels, more particularly, the labeling can be performed with little consensus on their exact position among experts leading to extra challenges for the classifier. The selection of the features, additionally, should be appropriate for the application and should give good discrimination power. Over-fitting can also be observed. Finally, the classifier should be robust enough to be able to handle the problem. Neovascularizations more particularly can demonstrate high variability on their shape and location ; these together with the fact that NVs are rare can make the construction of a representative training/feature set challenging. If the previous conditions are satisfied then supervised, methods are usually better than other available approaches. Another advantage is that they can be perceived as a black box ; hence after the training/testing phase the user simply inputs the image, without being concerned about tuning any parameters. The next section will present some examples where supervised algorithms were employed to segment the retinal vessel. The analysis will focus mostly on the analysis of the existence of different categories of classifiers.

Usually the methods are categorized according to the classifier that they utilize, so we can have the following methods based on : 1) Artificial neural networks (ANNs) [171, 172, 173, 174], 2) K-nearest classifiers (K-NNs) [175, 176], 3) Support vector machines (SVMs) [79, 177, 178, 83], 4) Statistical [179, 180, 181, 182], and 5) Ensemble techniques [183, 184, 185].

Inspired by the basic biological processing unit, or the neuron, ANNs were proposed. An artifical neuron is a mathematical representation, as a function, of the transformations that occur on an input in a biological neuron. Based on the fundamental unit, ANNs were proposed as an early effort to model the human visual perception system. The artificial system is a layered network of interconnected nodes, where the input is transformed according to a characteristic function and some adaptive weights. The input is the feature vector and the output is the decision about the input vector. The learning phase involves the adjustment of

the weight. ANNs is a non-linear classification method. D. Marín et al. [172], utilized ANN and a 7-D vector composed of gray-level and moment invariant-based features for vessel/non-vessel discrimination.

The general principle behind the second category, KNNs, is that the values in the feature space are similar for pixels that belong to the same class and so in a sense, they are clustered in a close distance. Thus, the goal is to find the decision boundary that separates the clusters [176]. In order to find this boundary, the training set is utilized. One special characteristic of this classifier is that it can produce soft classification, namely a probability for a pixel to belong to a certain class.

Similarly, SVMs, try to find a boundary that separates the features. The goal of this classifier is to find an hyperplane in the N-dimensional feature space that maximizes the functional margin, namely the distance between the hyperplane and the closest point of any class. Then in the testing phase, every input feature vector will be assigned in a class with respect to their position from the trained hyperplane function. There are different algorithms that have been proposed in the literature that use SVMs. For example, Ricci and R. Perfetti [79] proposed a scheme, where firstly a single-scale line detector is used to obtain the features and then SVM for pixel classification, the performance is very good in the public database.

Bayesian approaches are probabilistic methods. If we assume that $y = (y(s))_{s \in S}$ is the observed image and $y = (x(s))_{s \in S}$ the groundtruth where $x(s)$ denotes the true (unknown) segment or region which pixel s belongs to. The observed $y(s)$ is interpreted as a realization of a random variable whose parameter is a function of $x(s)$. The probability distribution of the observed image y has a density $f(y/x)$. This density describes the "forward problem" of image formation, including both the stochastic noise in observing y and the deterministic influence of x on y. Given a prior distribution $\pi(x)$ of x, the posterior distribution of x given y is

$$P\left(\frac{x}{y}\right) \propto f\left(\frac{y}{x}\right)\pi(x) \tag{2.5}$$

and the segmentation x is usually estimated by choosing an estimator that maximises the posterior probability [179].

A recent new approach is to combine different classifier to increase the discrimination power. This ensemble scheme is used to improve the classification by weighting the "opinion" of each individually employed classifier.

Additional supervised methods that have been proposed for segmenting vascular structures are the reinforcement learning and the regression. Reinforcement learning algorithms try to find the optimum solution by interacting with their environment. The concept of rewarding or punishment in the learning phase is introduced, where feedback is obtained through

a comparison of the result of an action with an ideal segmentation or measure [186]. In [187], the authors applied reinforcement learning to facilitate the automatic placement of a segmentation contour on the heart ventricles. Regression is a method of statistically fitting a function to the feature space [188] which in turn acts as the separating plane for the classes. Different types of regression exist that depend on the fitted function (linear, logistic, etc.). In the biomedical context this classifier has been utilized in [189] (see also Fig. 2.19) for centerline extraction of neurons and retinal vessel/dendrite detection in [190].

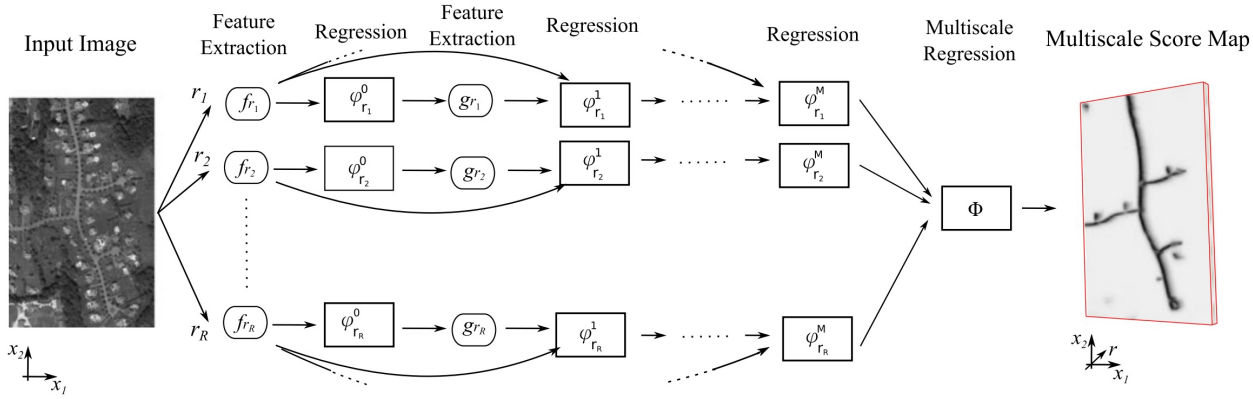

Figure 2.19 Example of the application of multi-scale regression for centerline detection [189] (©[2016] IEEE).

2.2.2.2 Unsupervised

As in the previous category, in the unsupervised learning, we try to recognize the underlying pattern of the vessels in a specially employed image feature space. In contrast with the supervised learning, a groundtruth label set is not required for training.

Among the different unsupervised methods, clustering is the most investigated approach. Clustering is a diverse category of algorithms that tries to group the feature vector in different clusters so as different groups have as much as dissimilar objects as possible. The algorithms consist of five components : 1) the model, 2) the dissimilarity function, 3) the feature selection process, 4) the number of clusters, and 5) the initialization step. The model defines the way the data are grouped into clusters. The dissimilarity functions measure the distance between the objects, while a subset of the existing features are chosen to be utilized in clustering. The number of clusters defines the number of objects of interest. In case of the healthy vessel segmentation problem, the application can be described as a binary clustering problem (vessel/non-vessel), so the number of the clusters that we will use is known a priori. However, for the neovessels problem, the task of defining the number of clusters is not trivial. Many

definitions of what cluster is, exist in the literature. Additionally, the use of different similarity functions gives rise to the total number of available algorithms [191, 192]. Initialization of the cluster centers in the feature space is also challenging in the small vessel segmentation problem as the optimization step does not guarantee the convergence of the cluster centers to the global minimum. To begin with, clustering can be distinguished into hard or soft/fuzzy. In the former case, the algorithm assigns the features as belonging to a single cluster ; while in the later case a function is utilized to show the likelihood of membership of the features in all the available clusters.

The simplest clustering algorithm is the K-means which aims to group the features into the clusters that are in the minimum distance. The process is iterative that includes the assignment step, where the features are assigned to the closest clusters, and the updating step where the clusters' location is recomputed. Examples of the previous are the K-NN [176, 193] and Fuzzy C-Means [194, 195]. Another approach is to assume that the features come from a Gaussian mixed distribution. In order to find the parameters of each distribution (mean, standard deviation, weight) expectation-maximization (EM) can be utilized [196]. This technique has also been applied outside of the context of clustering [197]. Another subcategory of algorithms is the hierarchical clustering. Here, a dendrogram is constructed that represents the grouping of the features in clusters and their corresponding similarity at every iteration. This method was applied in the following study [198] to find the best threshold in an image histogram, which was further utilized for vessel segmentation. Recently, evolutionary approaches were considered for clustering. The working principle is drawn from biological evolution, and so the notation is the same (mutation, gene, generation, parents, daughters, selection, crossover, etc.). Genetic algorithms perform global searching, in contrast to other algorithms so they can overcome local minimums. In [199] GA and FCM were combined in a hybrid scheme to segment the retinal vessels.

The unsupervised classification method equivalent to the ANNs is the self-organizing maps or SOMs. This technique, which was first proposed by T. Kohonen [200], is based on the neurobiological principles of visual perception and how the biosignal is processed early in the neural-retina using competitive learning [201]. In this technique, neurons are interconnected forming local clusters within the same layer. Later, in the training phase, the neurons compete in a given stimulus, which is a random sample of the training set. The winner is determined by the distance between the input and the output of the neurons modified by some preselected weights. The activity of the winning neuron then is spread in a short distance mutually reinforcing the weights of the neighbor cells. After many training cycles, testing takes place where SOMs are applied to a new set of images. SOMs and clustering have been combined to segment the retinal vessels in [202].

Insipired by the principles of human visual perception and relying on the ANNs new unsupervised learning methods have emerged. In parallel, there has been an effort to model original theories proposed by cognitive scientists about the visual perception into a common computational framework .

2.2.2.3 Deep learning

Deep learning has emerged as an alternative to the ANNs method for image analysis tasks giving very promising results [203]. Significant advances allowed deep learning to outperform traditional ANNs as well as other supervised methods [204]. These include the use of a simple characteristic function to speed up the training phase. The non-handcraft feature extraction step realized via convolving the input image with trainable kernels (CNN). Additionally, the introduction of deep architectures with many interconnected layers that are able to represent complex compositional hierarchies of features, namely high order features that rely on lower level features such as shapes constructed by lines. The use of max pooling and dropout to accelerate the training phase and increase the robustness to overfitting, respectively. Additionally, graphical processing units are used for the acceleration of training and testing.

However, deep architectures and more particularly CNNs require a lot of resources in order to be effectively applied. The basic parameters that are learned during the training phase are the weights of the convolution kernels. Depending on the size of the kernels and the depth of the architecture, the number of parameters that has to be learned is in the order of hundreds of millions. This can place a computational strain to the task of finding the optimal values. Furthermore, initialization of the weights is very important. Lately, initialization of the convolution weights with specially designed filters [43] has been proposed that can accelerate the training phase by approximately 82% [205]. Furthermore, the number of training samples play a crucial role in the effective training of a CNN. A large number of examples, together with their labels, should be provided in order for the network to construct the most representative features. In a recent work, for example, P. Liskowksi and K. Krawiec [206] trained their CNN (Fig. 2.20) on 400000 healthy vascular regions achieving high accuracy. However, this is inadequate in the neovascularization segmentation case. As it was showed that the vascular proliferations are rare among the screened population. On top of that, they demonstrate very high variability in their appearance, and pixel-level labeling by an expert is not provided.

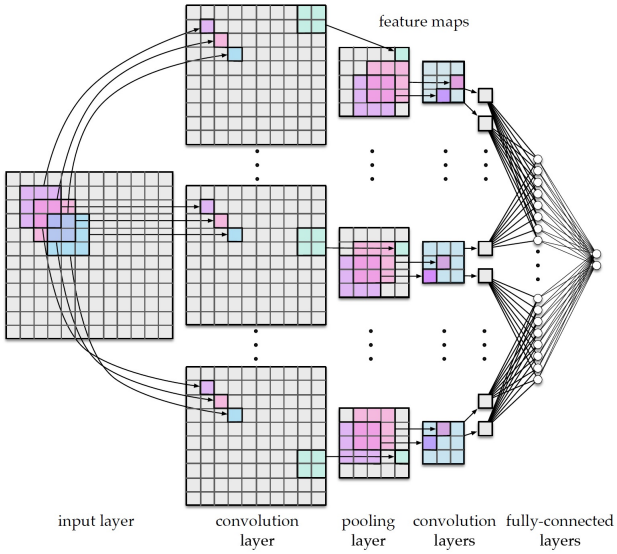

Figure 2.20 Example of a basic convolutional neural network (CNN) architecture. Three 3x3 convolutional, one 2x2 pooling with stride 2, and two fully connected layers are applied on the three channels (R,G,B) of an input image in this example [206] (©[2016] IEEE).

2.2.3 Tensor voting

Adopted from the field of computer vision, tensor voting framework (TVF) is another method for vessel segmentation. Tensor voting was developed by Medioni and Kang [207] and Medioni et al. [208]. This a bottom-up approach for organizing neighborhood information based on perceptual principles from Gestalt theory. Essentially, TVF is another approach to model the human visual perception system that can be used to segment thin fragmented structures. It formalizes the observation that high-level perceptual structures can be formed by grouping individual lower level structures. Tensor voting consists of two components, given as two criteria : (1) the proximity criterion, namely pixels belonging to the same structure are close to each other ; and (2) the continuity criterion, namely grouped structures have constant curvature. In order for the scheme to be applied, every image pixel is perceived as a token with an orientation, or a second order tensor. The process starts by initializing the directions of the structures via a method to estimate orientations, such as ball voting or gradients. Stick voting is then applied to refine the directions, propagate second-order structural information, reconnect the information between the structures, and finally compute the saliency. Saliency measures the certainty about the existence of a line in a particular location, and it demonstrates a local maximum along the principal direction of the structure. A scale parameter σ_{TVF} controls the range of influence of the voting. Figure 2.21 shows the basic components of tensor voting as well as the propagation process.

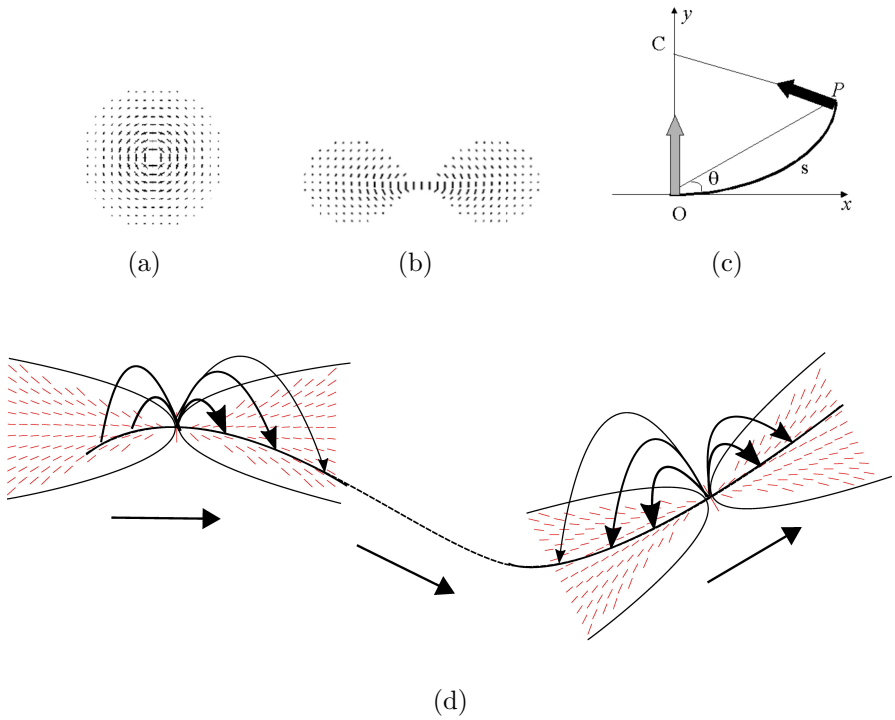

Figure 2.21 Components of tensor voting. (a) Ball voting field. (b) Stick voting field. (c) Second order vote cast on P by a stick tensor located on O along the osculating circle that ensures the satisfaction of continuity [13]. (d) Votes propagation along a line.

2.2.3.1 Tensor representation

Second order symmetric tensors are utilized to capture the information provided by points as well as curves. Tensors can be visualized as ellipses, where their shape encode the type of information (curve or point), while their size the saliency. For example, a point on a curve is represented as an elongated tensor (stick tensor) with a stretched principal direction that corresponds to its tangent. For an isolated point, on the other hand, there is no preferred direction and as such a blob-like tensor (ball tensor) is more appropriate (Fig. 2.22). More formally, tensors are expressed as symmetric, positive, semi-definite 2x2 matrices that are further decomposed into eigenvalues and eigenvectors as the following equation shows (Eq. 2.6) :

13. Medioni, Gerard ; Kand, Sing Bing, Emerging Topics in Computer Vision, 1st, ©2005. Reprinted by permission of Pearson Education, Inc., New York, New York.

$$
\begin{aligned}
\mathbf{T} &= \begin{bmatrix} a_{xx} & a_{xy} \\ a_{xy} & a_{yy} \end{bmatrix}, \\
&= \lambda_1 \widehat{\mathbf{e}}_1 \widehat{\mathbf{e}}_1^T + \lambda_2 \widehat{\mathbf{e}}_2 \widehat{\mathbf{e}}_2^T, \\
&= (\lambda_1 - \lambda_2)\, \widehat{\mathbf{e}}_1 \widehat{\mathbf{e}}_1^T + \lambda_2 \left(\widehat{\mathbf{e}}_1 \widehat{\mathbf{e}}_1^T + \widehat{\mathbf{e}}_2 \widehat{\mathbf{e}}_2^T \right),
\end{aligned} \tag{2.6}
$$

where λ_1 is the largest eigenvalue, λ_2 the smallest eigenvalue, and $\mathbf{e}_i$ the corresponding orthogonal eigenvectors. According to the previous, a point or ball tensor will have very similar eigenvalues $\lambda_1 \approx \lambda_2$, while a curve or stick tensor a predominant direction with $\lambda_1 > \lambda_2$ (Fig. 2.22). Subsequently, every tensor can be defined as a function of three parameters $\mathbf{T}(\beta, s, b)$ (Eq. 2.7), namely the ballness/stickness plus the orientation. After the tensor representation, sparse and dense voting is applied to determine the final saliency at every location.

$$
\begin{aligned}
\mathbf{T}(\beta) &= arccos\left(\widehat{e}_1 \widehat{e}_x^T \right), \\
\mathbf{T}(s) &= \lambda_1 - \lambda_2, \\
\mathbf{T}(b) &= \lambda_2
\end{aligned} \tag{2.7}
$$

2.2.3.2 Voting process

As it is mentioned in the original work, a vote describes the estimation of the existence of a geometric structure that passes from both the voter's and the receiver's location, and the associated certainty of the estimation is expressed with the saliency. Since vector information is propagated through voting, the estimated direction of the structure is also included. Then the "opinion" or votes of all the tensors are combined by adding the accumulated votes. There are two types of voting that are applied consecutively following the tensor encoding, sparse and dense voting. Sparse voting, involves the communication of votes between only tensors, while dense voting the communication of information at every possible location or pixel adjacent to the examined tensor. To facilitate the previous, a vote generation function is used.

Assuming an osculating circle [16] that passes from the voting token (O) to the receiving token (P) (Fig. 2.21(c)) the strength or magnitude of the vote depends on the arc length OP s, the curvature factor k, the degree of decay with curvature c, and the scale of voting σ : (Eq. 2.8) :

16. The osculating circle of a curve C at a given point O is the circle that has the same tangent as C at point O as well as the same curvature.

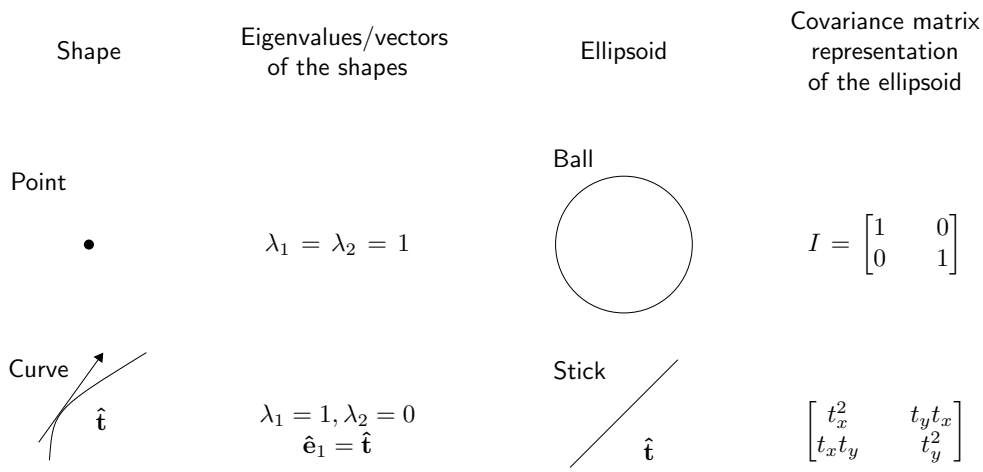

Figure 2.22 Encoding of point and line structures as tensors[15].

$$DF\left(s, \kappa, \sigma\right) = e^{-\frac{s^2 + ck^2}{\sigma^2}} \tag{2.8}$$

where $c = \frac{-16log(0.1)\times(\sigma-1)}{\pi^2}$, and σ is a modifiable scale parameter that controls the range of influence of the tokens.

A voting field centered and aligned with the principal direction of the voter can be used to compute the orientation and magnitude of the vote in the neighborhood of the voter. Two possible voting fields can exist : 1) stick (Fig. 2.21(b)) and 2) ball (Fig. 2.21(a)). Vote interpretation follows where at each pixel the sum of all votes is analyzed. This is performed by eigenvalue/vector decomposition of the accumulated votes in matrix T. Then, the saliency ($\mathbf{T}\left(s\right)$) and the orientation uncertainty ($\mathbf{T}\left(b\right)$) are returned by the eigenvalues of the final tensor.

$$\mathbf{T} = \begin{bmatrix} \widehat{\mathbf{e}}_1 & \widehat{\mathbf{e}}_2 \end{bmatrix} \begin{bmatrix} \lambda_1 & 0 \\ 0 & \lambda_2 \end{bmatrix} \begin{bmatrix} \widehat{\mathbf{e}}_1^T \\ \widehat{\mathbf{e}}_2^T \end{bmatrix} \tag{2.9}$$

The final algorithmic step is the extraction of a centerline, via non-maximal suppression, from the saliency map as the measure is locally maximum perpendicularly to the direction of the curve.

15. Reprint from G. Medioni et al., A computational framework for segmentation and grouping, Copyright (2000), with permission from Elsevier [208]

2.2.3.3 Tensor voting as an inference technique

Relying on dense voting, TVF demonstrates elements of an inference engine, a concept first proposed by cognitive scientists to explain how visual perception works. Inference methods are very useful as they try to predict the existence of information in locations that are missing. This kind of methods are a different kind of approaches than the existing, as they do not try to directly model the objects of interest. Instead they try to model the visual perception. Similarly, the framework can quantify the orientation uncertainty of the structures from the neighborhood. Thus it can infer the existence of junctions even if these are missing. In an example where a fragmented line is input into the framework, the effect is the reconnection of the fragments in a single line as can be seen in Fig 2.23. Additionally, the method can detect the center of a junction, in a more perceptual way, even if the individual branches are disconnected. The application of a standard morphological based method for junction detection would have failed in this case.

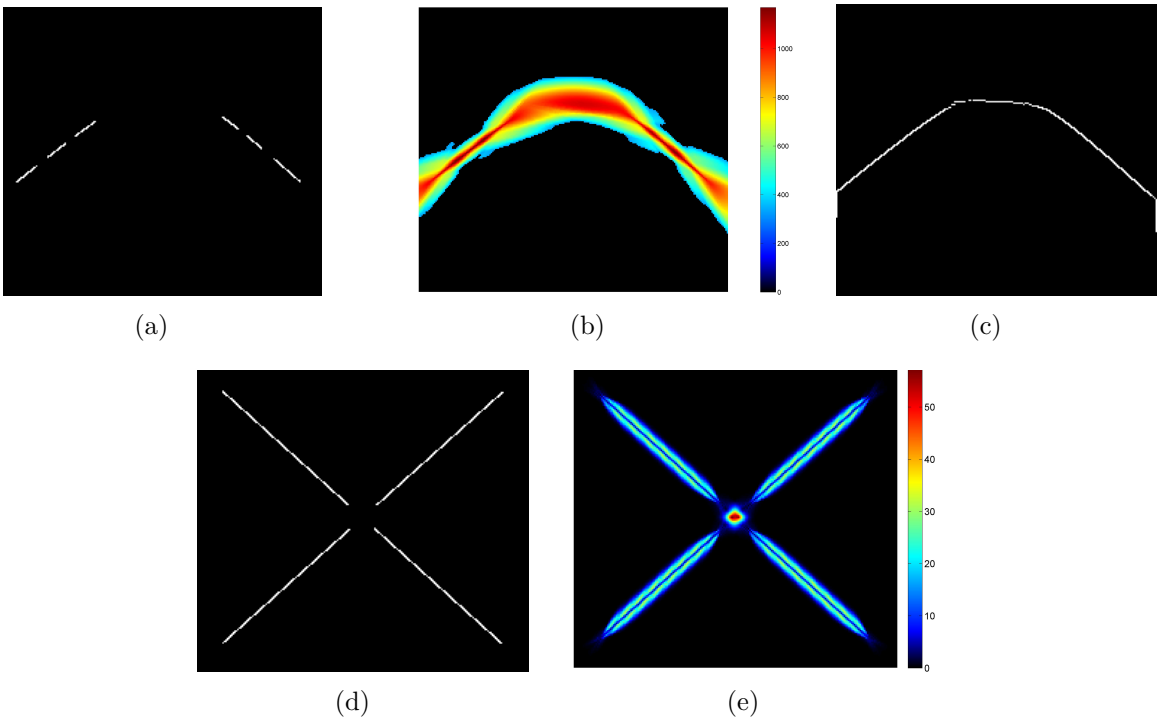

Figure 2.23 The result of the application of the tensor voting approach in a fragmented input line (a-c) and a fragmented junction (d-e). The method works by computing a dense curve saliency map (b, e) by applying the appropriate steps. Furthermore, the orientation uncertainty λ_2 can be extracted (e). As a result, it reconnects the fragments into a single line and infers the existence of the curve perceptually in locations that the information is missing (c). It can also identify the location of junctions perceptually (e).

2.2.3.4 Tensor voting applications and specifications

The method is closely related to the structural tensors, however in the latter case the tensors are constructed exclusively by using the image gradient information. The tensor voting framework, on the other hand, is flexible and there is no restriction on the type of information that it could be considered as a tensor. Another difference is that here a tensorial voting field is applied instead of a scalar field. In the original framework, also, the method was proposed to be applied only in binary images. This is a constraint posed by the algorithm, however this limitation can be overcome by assuming that the gray-scale responses are weights to the pixels as it was applied in [209]. Moreover, in contrast with other perceptual based approaches [210], it can work in open curves so it can directly be applied to vessel segmentation.

As it was explicitly mentioned in [211] there are many ways to generate the tensor field from the image : *"The way to generate is application specific. As an example, a tensor field could be obtained by creating features images of the orientation and stickness by applying any type of orientation-sensitive filter with 180°degrees symmetry on the image data and taking the orientation with the maximum filter response. The ballness could be obtained by any isotropic filter on the image data"*. Indeed, in the following paper [209], where tensor voting is applied for retinal vessel segmentation (centerline detection), image gradients are used to encode the direction information [209, Eq. 7]. Furthermore, in another study [212] the Hessian matrix is applied to obtain the tensor.

Finally, the approach is time consuming, having an asymptotic computational complexity of $O\left(s^2k^2\right)$ that depends on the image (s) and the voting kernel (k) size. The authors in [211], implemented a method based on steerable filters and managed to drop the complexity to a logarithmic scale $O\left(s^2 logs\right)$.

This method has been successfully applied to a range of biomedical imaging applications [213, 214, 215, 216, 217]. These include filling microvascular discontinuities [213] based on interpolating the width between reconnected segments, and detecting important cellular structures [214] by iterating a TVF along a range of scales. A variety of algorithmic improvements to the basic framework was proposed in the literature that were comprehensively reviewed by Maggiori et al. [217]. In the same context, R. Duits et al. [218] proposed a more generalized definition of the tensor voting as part of a formalized set theory, namely the Lie group using variational methods, where exponential curves fit in another parametric space, the roto-translational group $SE\left(d\right)$. In the $d = 2$ case, the osculating circles that define the tensor voting field are used for fitting in the new parametric space. The method was recently adopted in a hybrid scheme for retinal vessel segmentation [113].

In retinal imaging applications, single scale TVF has been applied to either extract full vessels [219] or segment centerlines [209]. No particular care was given to the problem

of full small vessel segmentation in either of these studies. The work in Park et al. [219] focused on identifying the optic disc as the converging point of the largest vessels and used a direct thresholding of the saliency map. In this manner, disconnected curvilinear structures belonging to lesions or irrelevant structures can get high saliency values, so thresholding is likely to remove small vessels without suppressing the false positives. The authors in Leng et al. [209] extracted the centerlines based on steerable tensor voting [211]. Rather than applying the framework for extracting the saliency of the structures globally, they used the method to link pre-identified edges. Moreover, in a preliminary phase, edge points were discarded based on the global length criterion. But the setting of a non-adaptive global length parameter is not effective for retaining the smallest vessels and causes a translation in the final centerline location.

2.3 Neovascularization segmentation and characterization

A recently identified problem is the precise segmentation and characterization of neovascularizations. As far as fundus imaging is concerned, some of the efforts have been placed towards the localization of the neovascularization within the the optic disc only (NVDs) [220, 221, 222, 223], while lately some of the studies shifted towards both NVE and NVD cases [56, 224, 225, 226, 227, 228, 229, 230, 231, 232, 233]. NVDs are well contrasted against the background owing to the fact that the optic disc is the brightest retinal structure. Moreover, the severity of the proliferative diabetic retinopathy can be directly determined by the location of the new vessels. Pathophysiologically speaking, neovascularizations first grow in locations away from the optic disk and then elsewhere. On the later stages, NVDs are classified as more severe since there is a higher impact in the retinal detachment following haemorrhages. Nevertheless, it is preferred to detect neovascularization early rather than in late stages at more critical locations. A patient with PDR requires immediate medical intervention, and hence we have to focus detecting the NVs in all possible locations.

2.3.1 Neovascularization segmentation

Some authors relied on pre-existing algorithms such as matched filtering to segment the vessels, while others further improved the segmentation process via pre-processing and enhancement before incorporating the characterization step. As we will show, some methods do not require the segmentation to initiate the neovascularization detection process.

Preprocessing and vessel enhancement of the retinal images was proposed as a mean of mitigating the effect of artifacts during the acquisition process and the influence of other structures or pathologies. The latter is reasonable because at the PDR stage several bright or dark lesions can coexist. For the preprocessing the operations that are utilized involve :

median filtering [226, 229], adaptive histogram equalization [226, 233], contrast enhancement [225, 229, 230], morphology [229], and wavelets [229, 230]. For the vessel enhancement step wavelets [227, 228], matched filtering [56, 225], Gabor filtering [231], vesselness based on Hessian [231], multi-scale line detection [230], morphology [225, 226], and non-linear diffusion [231] has been proposed.

Subsequently, segmentation on the preprocessed or vessel enhanced image is performed. To begin with, fuzzy clustering was proposed in [226]. Moreover, a heuristic approach was utilized in two studies [227, 228] that segments the image by applying multi-layered thresholding. Zhang et al. [56], also, designed a method based on matched filtering that can segment neovascularizations, by effectively suppressing false positives edges that originate from non-linear structures. However, they did not extend their research towards the vessels characterization. Welikala et al. [230] applied the same principles on MSLD [80] as well as thresholding [230], while Gupta et al. [231] isolated the thin vessels by thresholding the combination of different vesselness features. Finally, morphology [229] coupled with Gaussian matched filtering [225] was utilized in order to identify the vessels. Figure 2.24 shows an example of NV segmentation on the disc and elsewhere.

One problem with the existing studies is that the segmentation performance is not clearly reported. Besides the work of three research groups [56, 227, 228, 230] the methods do not provide clear evidence about the segmentation in the normal as well as abnormal cases. Apart from some limited cases, this can be accounted for the fact that manual neovascularization segmentation is not provided in the available databases. Subsequently, the characterization step is confined at the region level. Furthermore, the amount of available images with NVs is limited therefore very high success rate is reported, especially from the supervised approaches.

2.3.2 Neovascularization characterization

The next step is the characterization of the identified vessels [224, 225, 226, 227, 228, 229, 230, 231, 232, 233]. The majority of the previous work is based on the application of machine learning techniques, and more specifically supervised, to characterize the healthy from the abnormal small vessels based on some extracted features. These include grayscale as well as binary measurements on individual vessels' appearance, morphometry, geometry, and texture. In this work, we categorized the features (Figure 2.25) according to the measured quantity, as well as the study that they were introduced and applied.

The available features are either extracted from the grayscale region or based on measurements on the segmented vessels. The main advantage of the grayscale based features is that they do not rely on pre-segmenting the vessels, mitigating the impact of possible over-under segmentation performance on subsequent steps. Furthermore, second-order information is ta-

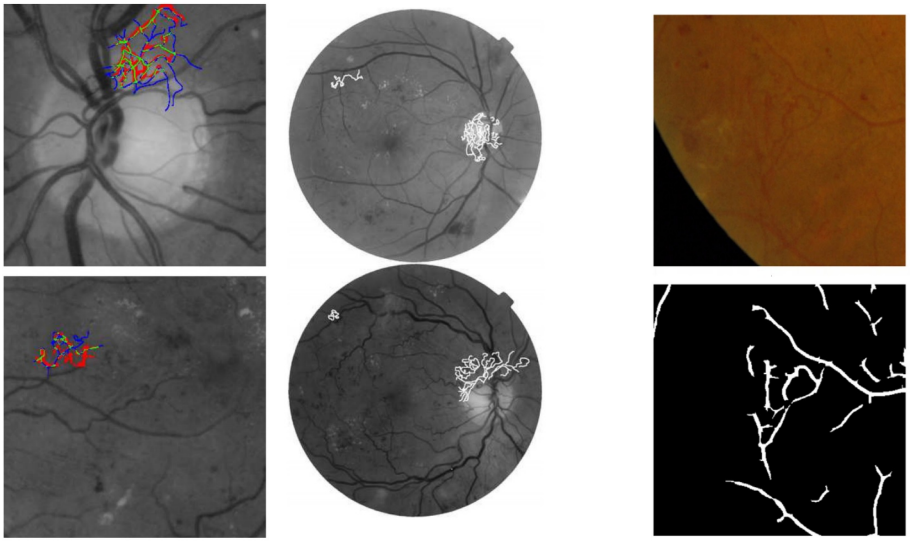

(a) (b)

Figure 2.24 Examples of segmentations of neovascularizations on the disk and elsewhere (NVE/D) using a) [228][17] and b) [230][18] methods. (a) The neovascularizations on the leftmost column are compared with a groundtruth segmentation and colored according to the class that they belong. Green vessels are the true positives ; red are the false positives ; while blue correspond to the false negatives. The central column illustrates how the system annotates the abnormal vessels on the retina. (b) neovascularizations segmentation using MSLD.

ken into account, when for example textures are used. However, the appearance or geometry of the vessels such as the tortuosity or orientation cannot be directly extracted from the grayscale region.

On the other hand, features extracted from binarized regions are straightforward to compute. Furthermore, they are based on quantities that have a more natural meaning. The last point is very important because it is easier to interpret the results. For example, it has been assumed that vascularization is denser at the proliferative stage [225], or that vessels grow in random directions at that stage [220, 230], we can easily study the previous assumptions using binary based features. However, in that family of features, the performance depends on the quality of the segmentation. Additionally, the existing work is limited to first-order statistics, such as counting the total number of junctions, and their density in an image, or the region. Therefore, the relative spatial arrangement of the segmented vessels is not taken into account.

17. Reprint from M. Usman Akram et al., Detection of neovascularization in retinal images using multivariate m-Mediods based classifier, Copyright (2013), with permission from Elsevier [228]

18. Reprint from R. Welikala et al., Genetic algorithm based feature selection combined with dual classification for the automated detection of proliferative diabetic retinopathy, Copyright (2015), with permission from Elsevier [230]

In another direction, a new classifier, the m-Mediods, was proposed by M.U. Akram et al. [228]. Without relying on specialized features, as the previous studies did, it achieves the highest performance against traditionally exploited classifiers (SVMs, kNNs, and GMMs). An example of the application of the algorithm can be seen in figure 2.24.

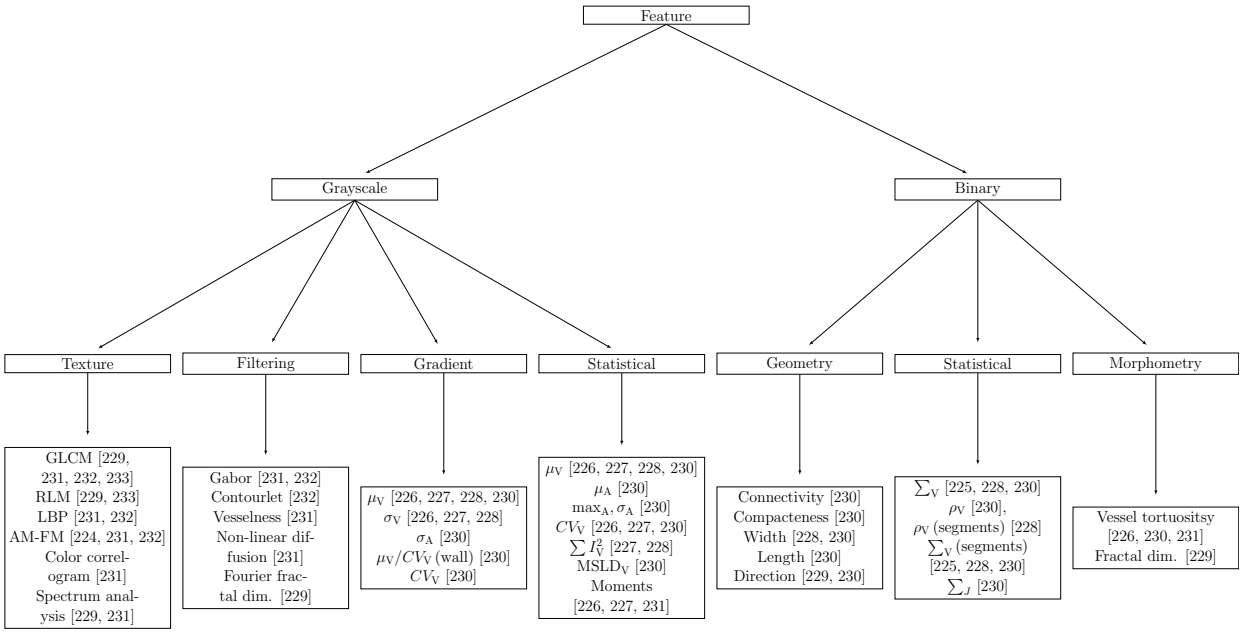

Figure 2.25 Categorization of available features for vessel characterization. In the different measures subscripts V and A denote the extraction of information at the vessel pixels or at the whole area, respectively.

Unsupervised algorithms were utilized to a limited degree in the context of NVs characterization. S.S.A. Hassan et al. [225] tackled the problem by applying simple morphological rules in a local window area on the pre-segmented image. The method is not automatic. Instead of detecting the abnormalities on the vessels' location the algorithm works on a local window ; while the parameters for the rules are empirically set. There are also false positives from other lesions (bright, dark) that are not suppressed during the segmentation process and they might contribute toward false positives.

Finally, in [229] an unsupervised statistical learning method is applied for the characterization of the vessels. The following features were selected : 1) statistical textures (GLCM and run-length matrix) ; 2) higher order spectra (HOS) analysis ; and 3) fractal analysis. Fractals have been extensively used for neovascularization characterization in diabetic retinopathy. Those features were extracted from the binary as well as directly from the grayscale image.

2.4 Retinal vessel segmentation metrics

Generally speaking, the lack of a segmentation algorithm that could perform equally good in all sorts of scenarios had raised the need of effectively evaluating the segmentation performance. For this reason, different evaluation metrics has been developed that assess and rank the performance of different algorithms applied to the same problem, namely the vessel segmentation.

Various schemes that classify the segmentation metrics in a range of categories has been proposed in the literature. According to Y.J. Zhang et al. [234], the segmentation evaluation methods can be divided into four categories : 1) the analytical methods, 2) the empirical goodness, 3) the empirical discrepancy and 4) the perceptual metrics. In another study [235], the empirical methods are further separated into standalone and relative methods. Finally, perceptual metrics were analyzed in [236].

Quantitative evaluation of empirical approaches is much elaborated and can extract an objective metric about the applied segmentation algorithm. The decision is made independent of the human factor and based only on the relative comparison with a reference manual segmentation, in the empirical discrepancy case. Alternatively, the a priori knowledge about a good segmentation can be utilized to infer about the performance, as it is applied in the empirical goodness case.

First, we will analyze the discrepancy measures that are commonly utilized for the performance evaluation of the retinal vessels segmentation algorithms. After that, we will continue with a new category of measures, the perceptual measures.

2.4.1 Discrepancy measures

A very well documented family of measures is based on the discrepancy metrics that count the number of miss-segmented pixels between the estimated and groundtruth segmentation. The confusion matrix (Table 2.1) as well as the derived measures (see Eq. 2.10, 2.11, 2.12) [237] are considered as very reliable for assessing the segmentation performance on the healthy and diseased retinal vessels. Usually, a percentage is computed for all three metrics for each selected image. Higher values are preferred. For example, 100% sensitivity demonstrates that the algorithm can perfectly recognize as vessels pixels that are truly vessels pixels from the reference image. Specificity, moreover, works on the non-vessels class, while accuracy reports about both categories.

$$\text{Sensitivity} = \frac{\text{number of True Positives}}{\text{number of True Positives} + \text{number of False Negatives}} \tag{2.10}$$

$$\text{Specificity} = \frac{\text{number of True Negatives}}{\text{number of True Negatives} + \text{number of False Positivies}} \tag{2.11}$$

$$\text{Accuracy} = \frac{\text{number of True Positives} + \text{number of True Negatives}}{\text{number of Positives} + \text{number of Negatives}} \tag{2.12}$$

Table 2.1 Confusion matrix together with the standard discrepancy metrics

	Groundtruth		
Estimated (Algorithm)		Vessel	No vessel
	Vessel	True Positive	False Positve
	No vessel	False Negative	True Negative
		↓ Sensitivity	↓ Specificity

Despite their extensive use, as the next studies show [108, 79, 151, 122, 229], there are several disadvantages related to these metrics that we will analyze. First and foremost, the discrepancy methods require a manual segmentation from an expert in order to work. This is very tedious work and sometimes the result is subjective ; general public repositories of retinal images were introduced to the community to address the problem.

Examples of these databases are the DRIVE, STARE, MESSIDOR, DIARETDB and more recently HRF. Some of the databases include one or more manual segmentation from an expert of the vascular tree, while others only the diagnosis about the examined image. The segmentation algorithms, depending on the popularity of the database, can be tested across a range of methodologies. Sometimes around 20 different algorithms can be assessed at the same time, and get a comprehensive opinion about their performance. However, these databases are general, and apart from some cases, they do not include delineations of abnormal vessels such as neovascularizations ; thus in occurrences of a special problem either an ophthalmologist has to spend some of his valuable time to segment the regions or validate a segmentation produced by trained staff.

Furthermore, these metrics work on a pixel-by-pixel basis comparing corresponding pixels between the estimated and the manual segmentation. This is a particularly undesirable feature since the measures cannot account for slight variations on vessel detections. Especially for the smallest vessels, the centerline, the bifurcations, and the vessels' boundary the probability of locating the positives away from their true location is very high reducing the

performance rates. Some efforts have been placed in the direction of penalizing the distance between the detected and true vessels [238], while more recently a measure has been proposed that among other things tolerates for possible deviations by morphologically dilating the segmentation result [239].

Additionally, as has already been pointed out by M.Niemeijer et al. [175] the global binary classification metrics do not take into account the heterogeneity of the pixel population of segments of the vasculature with a different diameter. In fact, the smallest vessels represent approximately 10% of the total surface area of the vessel network, while the whole vasculature covers 10% of the available field of view. Applying the aforementioned metrics give high success rates even when the narrow vessels are missed. Finally, they do not correlate well with the human perception of a good segmentation.

2.4.2 Perceptual metrics

The ultimate goal of the metrics is to objectively simulate the evaluation that a human observer or expert would perform if he was asked to assess the quality of segmentation on an image [235]. To achieve this, one proposed way is to incorporate the information about how different errors in the segmentation are perceived by the human. Since different kinds of errors are not visually equally important, up to some degree, weighting according to the human perception can be applied to facilitate the process. This can be achieved by incorporating subjective experiments [240]. The subjective evaluation offers a way to study and characterize the different categories of artifacts that can exist and weight according to the human or a more expert opinion. Then perceptually driven objective metrics can be derived by finding the mathematical relation or psychometric function [236], between the perceptual as well as a predefined objective metric. Alternatively, discrepancy metrics can be statistically correlated directly with the subjective quality evaluation results to indicate their degree of similarity [239].

Perceptual metrics offer a better way to evaluate the segmentation methods than simple discrepancy measures. They produce results that are consistent with the human opinion about a good segmentation as the next studies have shown [240, 239]. Additionally, they can effectively model complex artifacts that under discrepancy measures are difficult to deal. For example, the "annoyance" of false positive ranges perceptually with its location, size, shape and so weighting should be applied that depends on these factors. Moreover, artifacts can be perceived differently according to the context or their importance. Finally, subjective experiments allow the perceptual metric to be tailored for a specific application, for example, the identification of the small healthy or unhealthy retinal vessels.

Several studies have been published for the subjective evaluation step for images [239,

241, 242] and video applications [240, 243, 244]. Besides the next study [236], where a comprehensive designing scheme is presented, the task is informal, and there is no standardized way to study and characterize the impact of different kind of artifacts. Moreover, it requires much-elaborated designing from the researcher side and the experiments are not easily replicable. Usually, non-expert subjects participate in the study under conditions that are fixed by the researcher. Some of the studies [235, 245] have utilized empirical weighting for the artifact which is not adequate to characterize the metric as perceptual. Finally, like other discrepancy methods, they still require a groundtruth in order to be able to apply the objective metric not only in the designing but also in the application phase. In a different direction, when there is a lack of a single representative reference this can be estimated by comparing several manual segmentations on the same data using various techniques [246] amongst of which STAPLES is the most popular [247].

As far as the retinal vessels are concerned, in [239] individual metrics that characterize important vasculature features were utilized to build a new metric. Then the authors combined the individual quantities with subjective experiments and statistically concluded [248] that their approach correlates better than other examined discrepancy metrics with the human perception. However, in their study, the authors did not examine the performance on diseased retinas. Additionally, they assumed equal weights for all the individual metrics without first considering the effect that each quantity measured by the individual metric has on the human perception. Finally, even though the proposed metric can tolerate for deviations in the detection of the vessel pixels by including morphological dilation and erosion, this is done at the expense of invariance on the diameter detection.

2.5 General discussion on the limits of the existing methods

The preceding sections presented the state-of-the-art of algorithms for the segmentation of the retinal vessels, and the characterization of neovascularizations. This section will discuss the limitations of the existing methods for our problem.

2.5.1 Vessel segmentation methods

The current literature is limited to the problem of segmenting the medium-to-large retinal vessels. The authors of the existing work were mainly focused on the scope of demonstrating that the various proposed methods were sufficient to tackle the problem of global retinal vessel segmentation using standard discrepancy measures. The different methods were evaluated on the segmentation task using all the available vessels calibers which are not suitable as fundus images contain predominantly medium-to-large vessels. Subsequently, algorithmic improvements of the methods against already existing one were carried out with respect to

the problem of general retinal vessel segmentation. One reason might be that CAD systems along with the automatization of screening were not prevalent enough to justify the investment of resources into the problem of small retinal vessels segmentation. Furthermore, small vessels demonstrate challenges that make it a difficult problem to be addressed. As new developments require comprehensive CAD systems with several steps that could be able to assist and detect all the possible stages of the sight-threatening diabetic retinopathy, small vessels importance is becoming more relevant.

The existing methods are limited by challenges posed by the small vessels. Machine learning techniques require the existence of an already established model, in the form of a descriptor, to be effectively applied. The work is done on a highly abstract level where one or multiple algorithms can be combined forming a feature vector. Additionally, training on a labeled set containing the small vessels is a prerequisite. This set is difficult to be isolated from existing databases, or extracted by an expert. Additionally, unsupervised methods require the correct initialization of a predefined number of clusters to avoid the trapping of the cluster center into a local minimum, or the assignment of pixels coming from irrelevant structures into the wrong class.

In the intensity-based approaches, on the other hand, the work is done on a more fundamental level. Here, a model should be constructed that based on some assumptions it will approximate the problem. Scientifically speaking, this kind of approaches are more appropriate since new knowledge can be acquired that can improve our understanding of the general nature of the problem. Subsequently, if the model is adequate, it can be incorporated in a descriptor as part of a machine learning approach.

However, the construction of a model is not a trivial issue, and this can be the subject of our work. For the model to be sufficiently robust, assumptions must be formulated that will hold under different cases. As has been seen in the previous review, a variety of methods have been presented but their assumptions are weak for the small vessels. Template-based methods, for example, assume a very general representation that is not flexible enough to accommodate the curvature variability in the small vessels, resulting in the fragmentation of the result. Furthermore, derivatives are usually approximated using Gaussians, so there is certainly filtering of important information. This causes the derivative-based method not to be sensitive enough to the presence of small vessels at low contrasted areas, magnifying or even reconnecting the background noise to the vessel. Moreover, deformable models have to be initialized close to the fade boundary of the small vessels, and even if level-sets are used their external forces are not sensitive enough to get attracted to the full extent of the retinal vessels. The areas around the small vessels demonstrate increased intensity inhomogeneity, background noise, lower contrast, and at the same time, the appearance of the vessels is

thin, variable, and curved. Region-based methods are either semi-automatic, or they are not able to merge small vessels into a single region with the medium-to-large vessels as they can stop their evolution at the first encountered difficulty. In addition to the previous challenges, the contrast of the fine vessels against the background is so low that essentially the small vessels can appear as disconnected. Eventually, tracking can stop at the first fragmentation. Finally, the application of tensor voting in retinal field is limited as it was only used for retinal centerline detection. It does not produce a fully reconstructed vasculature, and it was applied on a single scale only, namely it considers a particular distance between structures for perceptual reconnection. Therefore, to tackle the problem of small vessel segmentation we have to propose a new method.

2.5.2 Neovascularization segmentation and characterization methods

Limited work has been done on the domain of effective segmentation and characterization of neovascularizations. This can be attributed to the fact that this kind of dark lesion is rare among the total screening population. Epidemiologically speaking, during the preceding years with the increased awareness about the impact of diabetic retinopathy, the prevalence of PDR has been reduced. Additionally, accurate segmentation and characterization of the NVs are not trivial, so the efforts are limited only to the healthy blood vessels. Nevertheless, their detection is crucial, because it is the predominant sign of proliferative diabetic retinopathy, and possible missing can immediately lead to visual impairment.

Intensity-based methods, as well as machine learning, coupled with preprocessing, have been proposed to isolate the neovascularizations. These methods include template, derivative, as well as unsupervised methods. The aim is to detect as many abnormal vessels as possible and then perform characterization, at the region level, in order to identify case with abnormal vessels. However, this is achieved at the expense of missing vascular junctions that are not easily recoverable.

Features that measure first or second order characteristics are computed directly from the grayscale version of the selected regions, while only first order information are computed from the binarized version of the selected region. Second order information can be extracted from the grayscale regions via textures. However, the extracted quantities are not easily interpreteable and require several steps of further processing. At the same time, the current methods cannot extract second order information from the segmented vessels of the regions as it is not trivial to incorporate the distance information between the vessels, without first defining a relevant anatomical landmark. Thus, for the binary case, only first order information is currently used.

Many methods depend on the number of available data, especially the supervised me-

thods. Another problem is the shortage of images with neovascularizations on the available datasets. For example, the authors in [220] covering approximately 30.000 people with diabetes managed only to obtain and examine 38 cases of PDR, while the freely available databases, combined, do not offer more than that. Table 2.2 illustrates the number of neovasculariazation cases per database across the various studies. As a result, the algorithms are not rigorously tested or trained in many examples. Consequently, in the testing phase, in case of a new previously difficult unencountered configuration, the algorithm might produce an error. Our aim is to apply our system for screening in a range of populations, which means that the algorithm should be tested in a wide range of images. In this direction, the lack of data was tried to be addressed in the literature by developing algorithms for computer simulated neovascularizations on the retina based on fractal modeling [249].

Table 2.2 Cases of images with neovascularizations in different studies

Type of PDR	Study	Num. of images/total	Type of PDR	Study	Num. of images/total
NVD only :	[56]	4/35	NVD & NVE :	[224]	20 (regions)/120
	[220]	38/109		[225]	11/313
	[221]	27/57		[226]	20/50
	[222]	9/23		[227]	1097(segments)
	[223]	100/300		[228]	52/1440
				[229]	27/110
				[230]	20/60
				[231]	100/779
				[232]	31/43
				[233]	50/180

2.6 Thesis objectives

An important tool that can facilitate the computerized detection of diabetic retinopathy is the segmentation of retinal vessels. Segmentation algorithms can highlight the most important retinal structures like the healthy vessels, or help the physicians to quickly identify abnormal features that are related to the disease. Due to the nature of the images, these algorithms need to perform under challenging conditions. Small vessels appear in the center or the periphery of the image varying in appearance with complex shape configurations and fade boundaries. Also, the disease may alter the appearance of the vessels or lead to the growth of lesions that

Table 2.3 Images with PDR per database [228]

Database	No. of Images	Normal	With PDR	NVD	NVE
DRIVE [175]	40	19	3	0	3
STARE [45]	81	30	5	3	4
DIARETDB [250]	89	5	7	3	5
MESSIDOR [251]	1200	397	37	27	18
HRF [63]	45	30	7	-	-

are similar to the small vasculature. In such cases, robust segmentation and subsequently characterization become essential.

As it was presented in this chapter, several algorithms have been proposed to isolate the vasculature. However, they are incapable of correctly identifying the smallest vessels, or they are not tested in datasets containing the smallest vessels exclusively. Therefore, the first objective of the thesis is the vessel segmentation.

Given the small retinal vessel segmentation, the next step is the identification of the pathological regions that might directly indicate the presence of proliferative diabetic retinopathy. Characterization of the regions to healthy or abnormal is the first step in the detection process. Several supervised approaches have been proposed to characterize regions to healthy or abnormal. However, they use a standard set of features based on the various measurement on the already segmented vasculature. Therefore, the second objective of the thesis is the vessel characterization.

This thesis will try to address the previous two objectives by proposing new methods for the segmentation of the smallest retinal vessels as well as the characterization of regions to healthy or abnormal. Achieving the previous would help in the direction of constructing CAD systems that could be used for the early detection of sight-threatening diabetic retinopathy. For both tasks, we propose methods that examine how the retinal structures are perceptually or spatially organized using the neighborhood information. To assess the segmentation performance on the smallest vessels, we will separate the vasculature in different categories according to their caliber. Then we will apply standard discrepancy measures. The next section will analyze the proposed methodology that was used to achieve the objectives.

CHAPTER 3 SMALL RETINAL VESSEL SEGMENTATION

This chapter will analyze the developed method for the segmentation of the smallest vessels. The method is applied on high resolution fundus images that are publicly available. Additionally, in this chapter we provide the experimental results for the evaluation of vessel segmentation performance.

3.1 Methodology

The diagram in Figure 3.1 demonstrates the proposed pipeline for retinal vessel segmentation. Images are first preprocessed, then vessels are segmented by the application of MSLD. Adaptive thresholding is then applied to extract the large and medium-sized vessels. Next, the multi-scale tensor voting framework (MTVF) is applied to the segmented image in order to identify and reconnect the smallest vessels. Moreover, starting from the largest vessels, a local tracking procedure merges the information from different scales. In parallel, the smallest vessels are reconstructed to their whole extent. Finally, the images are postprocessed to suppress the background noise.

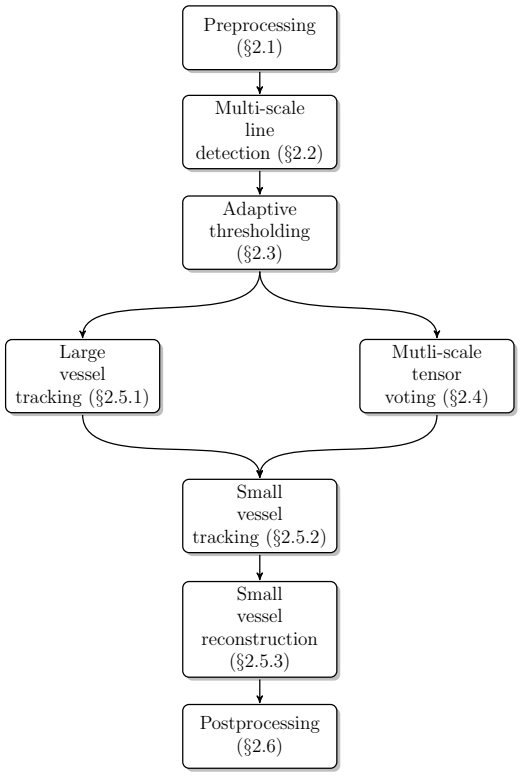

Figure 3.1 Block diagram of the proposed pipeline for retinal vessel segmentation.

3.1.1 Preprocessing

The retinal images are preprocessed to correct for non-uniform lighting, to normalize the image contrast, and to suppress the background noise. Even though the full color range is used by a human observer to recognize the vessels, simultaneously processing the three image channels require significant computational resources. Instead, we use a single channel for preprocessing. The green channel of the input image I_{green} is used as it provides the highest contrast between the vessels and the background.

Several approaches have been proposed for contrast enhancement and illumination correction, however each one focuses on a specific task. Locally adaptive contrast ehnancement is a standard method achieving good results, but illumination variations are not corrected. Conversely, illumination correction methods like high-pass filtering, large sized median filtering, or mathematical approximation do not improve the contrast. M. Foracchia *et al.* have achieved simultaneous local illumination and contrast correction [252]. This method was specifically designed for retinal images. In our work, the method is applied on the images to get $I_{enhanced}$.

Moreover, the dual-tree complex wavelet transform (DT-CWT) [253] is applied to $I_{enhanced}$ in order to filter out the background noise. The applied DT-CWT, which is an extension of the discrete wavelet transform (DWT), is widely used in retinal images. The applied method is multi-scale, it approximates shift-invariance, and it increases the directional sensitivity of the discrete wavelets. Although other wavelet families (Gabor, ridgelets, curvelets, or contourlets) are more directionally sensitive and thus more tailored for vessel enhancement than background noise suppression, they are more computationally expensive. Since the focus of our work was to filter out the background impulse noise, we considered DT-CWT for filtering. Filtering is applied [254] with the parameter t experimentally selected as described in Section 3.2.2 to suppress the background noise without distorting the information on the smallest vessels. High values not only can remove the noise, but they can also filter out the smallest vessels. For example, Figure 3.2 shows the effect of filtering on the final segmentation result using three different filtering levels $t = 0$, $t = 0.015$ and $t = 2$. In this example, the region is first preprocessed, MSLD is then applied to enhance the vessels, and simple thresholding isolates the vessels from the background. The preprocessing step allows us to remove most of the background noise ; however, the filtering parameters must be carefully selected to avoid removing the smallest vessels.

3.1.2 Large to medium caliber vessel segmentation

Following the preprocessing step, we aim to isolate the large to medium caliber vessels, and at the same time detect fragmented the smallest caliber vessels. Since the prerequisite is

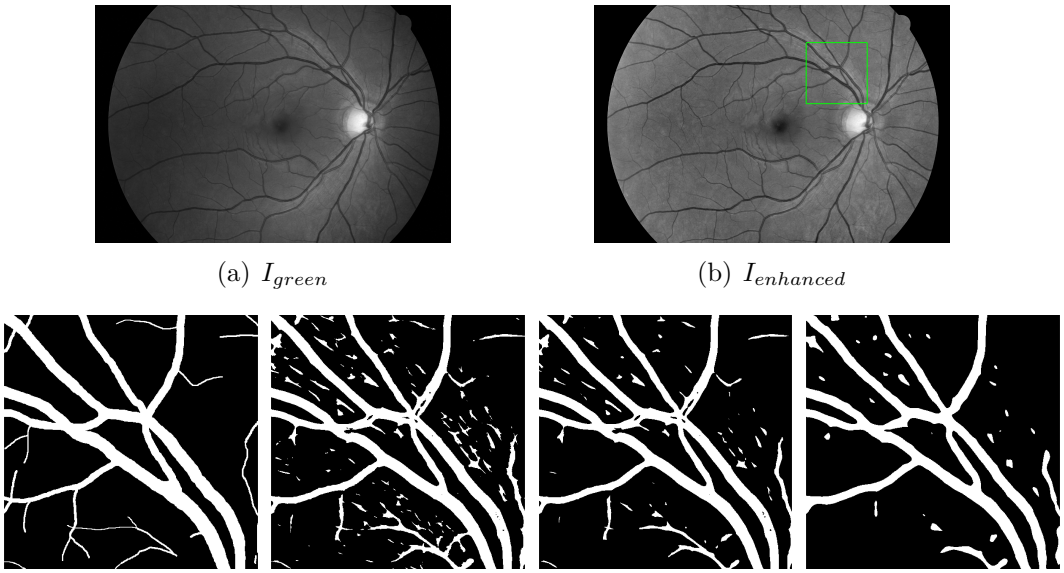

(a) I_{green} (b) $I_{enhanced}$

(c) Groundtruth (d) $t = 0$ (e) $t = 0.015$ (f) $t = 2$

Figure 3.2 Effect of the preprocessing steps on the final segmentation result in Image_01_h. (a) input image I_{green}, (b) lighting-corrected and contrast-enhanced image $I_{enhanced}$, (c) groundtruth segmentation corresponding to the green square inset in (b), and (d)-(f) effect of wavelet filtering on the final segmentation result at three different levels : $t = 0$, $t = 0.015$, $t = 2$.

to detect small vessel fragments, multi-scale vesselness or tracking pipelines are inadequate. Multi-scale vesselsness methods, approximate the Hessian matrix by Gaussian filtering that has the effect of filtering out the small vessels, magnifying the background noise or even reconnecting it to the detected vessels. Moreover, tracking methods, halt in the first encountered fragmentation. For this reason, MSLD is applied to the images as proposed in [80]. In contrast to matched filtering and morphological processing, MSLD eliminates the width parameter from the model. Therefore, the model is simpler, depends on a single modifiable parameter, and it can better approximate vessels of smaller caliber. Moreover, the approach is simple to implement, fast, achieving similar segmentation performance to matched filtering in the large to medium sized vessels. MSLD was proposed as an extension to the single-scale line detector and is contemporary to other standard template-based approaches. The length of the rotating line W, which implements the multi-scale component of the approach, varies from a minimum to a maximum value and the unweighted average response across the scales is computed in order to enhance the vessels. The response is thresholded to distinguish the vessels from the background. In our case, we adjust parameter W according to the vessel resolution (Section 3.2.2). Figure 2.12 shows an example of applying the original MSLD method on an image.

3.1.3 Adaptive thresholding

The resulting line response is then fed into an adaptive thresholding step to isolate the vessels. In the original MSLD approach, simple thresholding with a fixed value for all the images in the database was proposed [80]. But since there is variability in the acquisition process, the background of the retinal images does not show a uniform distribution across our database. Thus, the choice of a single fixed threshold is inadequate when the whole database is processed. Figure 3.3 shows an example where simple thresholding with a fixed value ($T = 120$) is used to segment two healthy images in the database. The given global threshold only partially segments the vessels in the second case (Figure 3.3(d)). Therefore, we apply adaptive thresholding in order to extract the vessels more reliably. The proposed step is faster than if a more locally adaptive thresholding method has been used.

The histogram of the MSLD responses has a specific form, resembling a normal distribution with a distinguishable peak corresponding to the largest anatomical structure, namely the fundus background (Figure 3.3(a), 3.3(c)). In addition, there is an elevated region or a valley to the right of the peak which corresponds to the foreground. In order to choose an optimal global threshold we can follow the rule of thumb proposed in [255]. This work suggests finding the central location of the background distribution, i.e. its mean, and adding to that the full width of the background at half height. In order to apply this, we fit a simple Gaussian to the histogram. To obtain the adaptive thresholding value, we modify the rule of thumb slightly by varying the distance from the mean ($\mu_{Gaussian}$). Thus, the threshold value (T) is given by Equation 3.1 :

$$T = \lfloor \mu_{Gaussian} \rfloor + \alpha \lfloor \sigma_{Gaussian} \rfloor, \tag{3.1}$$

where $\mu_{Gaussian}$ and $\sigma_{Gaussian}$ are the mean and standard deviation of the fitted Gaussian, respectively. The value for weighting factor α is experimentally determined as in Section 3.2.2. Figures 3.3(e) and 3.3(f) demonstrate the adaptive thresholding result for the two healthy images. For the second image, the method is much more effective at segmenting the vessels than non-adaptive thresholding.

3.1.4 Small vessel centerline extraction

Following the thresholding step, many smaller vessels remain fragmented, and a MTVF is used to reconnect them. Besides deep learning, tensor voting is an interesting method as it is closer to the way human visual perception functions than other existing models. As an inference engine, it propagates rich information in the gaps between the small vessels that are useful for subsequent steps of our algorithm. The existence of a curve, the direction, as

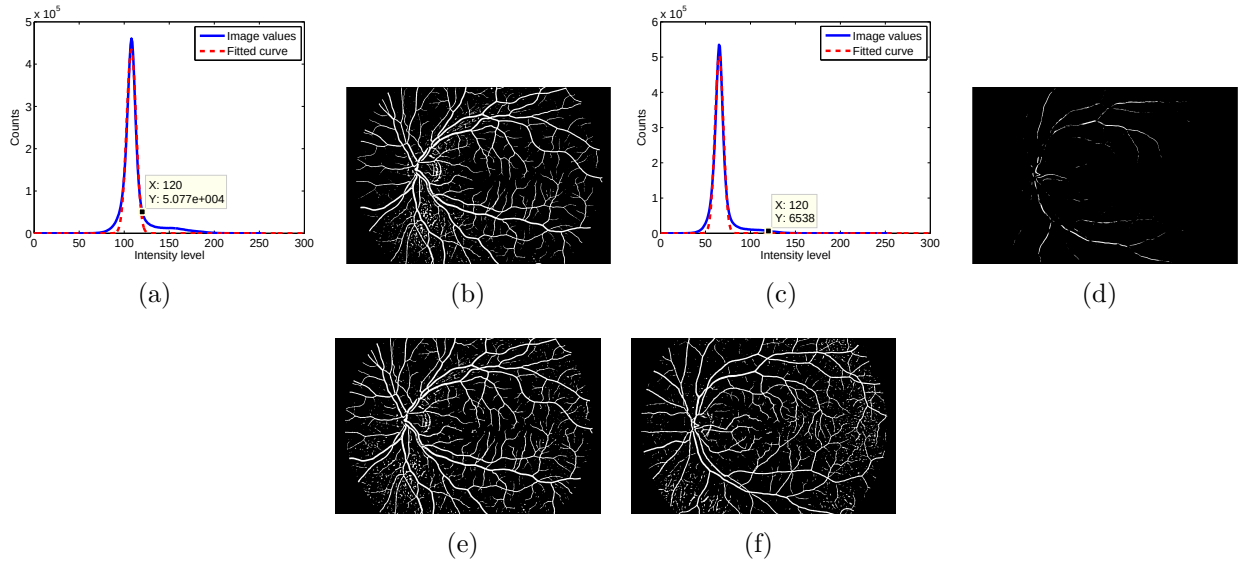

Figure 3.3 Example of applying fixed thresholding versus adaptive thresholding in two images of healthy subjects from HRF database. (a) histogram of the normalized line response values (X-axis) against the number of counts (Y-axis) of the 2nd healthy subject (blue line) together with the fitted Gaussian (red dashed line), (b) segmentation result of the 2nd healthy subject using a fixed threshold value at $T = 120$, (c) histogram of the normalized line response values of the 10th healthy subject (blue line) together with the fitted Gaussian (red dashed line), (d) segmentation result of the 10th healthy subject using a fixed threshold value at $T = 120$, and (e)-(f) segmentation result of the 2nd and 10th healthy subjects using adaptive thresholding.

well as the orientation uncertainty can be extracted from TVF. Morphological processing, on the other hand can only reconnect aligned fragments that are not very distant from each other.

The basic component of single scale tensor voting, namely the second order symmetric tensor, is used to capture the information provided by points as well as curves according to the following expression :

$$\mathbf{T} = \begin{bmatrix} a_{xx} & a_{xy} \\ a_{yx} & a_{yy} \end{bmatrix} = \lambda_1 \widehat{\mathbf{e}}_1 \widehat{\mathbf{e}}_1^T + \lambda_2 \widehat{\mathbf{e}}_2 \widehat{\mathbf{e}}_2^T = (\lambda_1 - \lambda_2)\, \widehat{\mathbf{e}}_1 \widehat{\mathbf{e}}_1^T + \lambda_2 \left(\widehat{\mathbf{e}}_1 \widehat{\mathbf{e}}_1^T + \widehat{\mathbf{e}}_2 \widehat{\mathbf{e}}_2^T \right), \tag{3.2}$$

where entries a represent the a priori information about the orientation of the tensor. In our case, we do not assume any specific direction thus we initialize the tensor with the identity matrix. Additionally, λ_1 (resp. λ_2) is the largest (resp. smallest) eigenvalue, and $\mathbf{e_1}$ (resp. $\mathbf{e_2}$) is the corresponding eigenvector that is normal (resp. parallel) to the local structure. If we set $\lambda_2 = 0$ and $\lambda_1 = \lambda_2$ we get the measures of saliency and ballness, respectively. Ball voting is used to initialize the direction of the structures among the tensors. Since the orientation information is not available for the ball voting step, the points are encoded with

the second order identity tensor $\mathbf{T}$. Stick voting follows, where a symmetric fan-shaped voting field centered and aligned with the principal direction of the voter propagates information to every neighboring pixel around the tensor. The voting distance depends on the scale factor σ_{TVF} according to the following equation [207, Eq. 5.2] :

$$c = \frac{-16log\,(0.1)\,(\sigma_{TVF} - 1)}{\pi^2}, \tag{3.3}$$

Interpretation follows voting ; at each pixel, the sum of all votes is analyzed by eigen-decomposition of matrix $\mathbf{T}$. The saliency measure gives a maximum perpendicular to the local stickness direction, so centerlines can be extracted by non-maximum suppression.

We use MTVF to group the fragmented smallest vessels into single longer vessels. This is justifiable if we consider that the gap between the vessels can vary, that higher voting scales can capture neighborhood information at a greater distance, while smaller scale can capture neighborhood information at a smaller distance. The tensor voting scale σ_{TVF} is varied between a maximum and a minimum value with a predefined step which is determined experimentally (Section 3.2.2). The same adaptive thresholded image is used as input across all the scales. Here we apply the voting separately for each scale, and then we fuse the information by computing the union of the centerlines across all the scales during tracking. Iterative voting [214], where the output centerline under a given scale is the input to a higher scale has been proposed, however we wanted to keep the centerlines from all the scales for tracking as multiple centerlines can better support the existence of a curve at a given location.

The framework is applied without saliency thresholding [219] or vote weighting [209]. Indeed, directly thresholding the saliency map can lead to suppression of important information from the small vessels. Therefore, we instead extract the local maximum from the saliency map without thresholding. Moreover, the grayscale contrast as well as the MSLD response between the smallest vessels and the background is very low. Additionally, there are cases where the background has a higher response than the structure of interest, so weighting the votes can lead to amplifying the saliency on the false positives.

The framework as it was originally proposed by G. Medioni *et al.* [207, 208] is applied here. In this framework, ball voting takes into account directional information at a greater distance than local gradient [209], and the extent of influence is directly determined by the selected scale in the framework. Even though the implementation based on steerable filtering is superior, in terms of computational time, it is an approximation to the original framework [217]. Figure 3.4 shows an example of how the method is applied at scales $\sigma_{MTVF} = 5 : 50$ to reconnect small fragmented vessels in a challenging isolated image region, in the periphery. The same adaptive thresholded input image (Figure 3.4(a)) is used for each voting scale.

Non-maximum suppression on the saliency map (Figure 3.4(b), 3.4(c), 3.4(d)) extracts the centerlines that, combined into a single map, are used at the reconstruction phase (Figure 3.4(h)). In this example, higher voting scales manage to reconnect the fragmented vessels (Figure 3.4(e), 3.4(f), 3.4(g)).

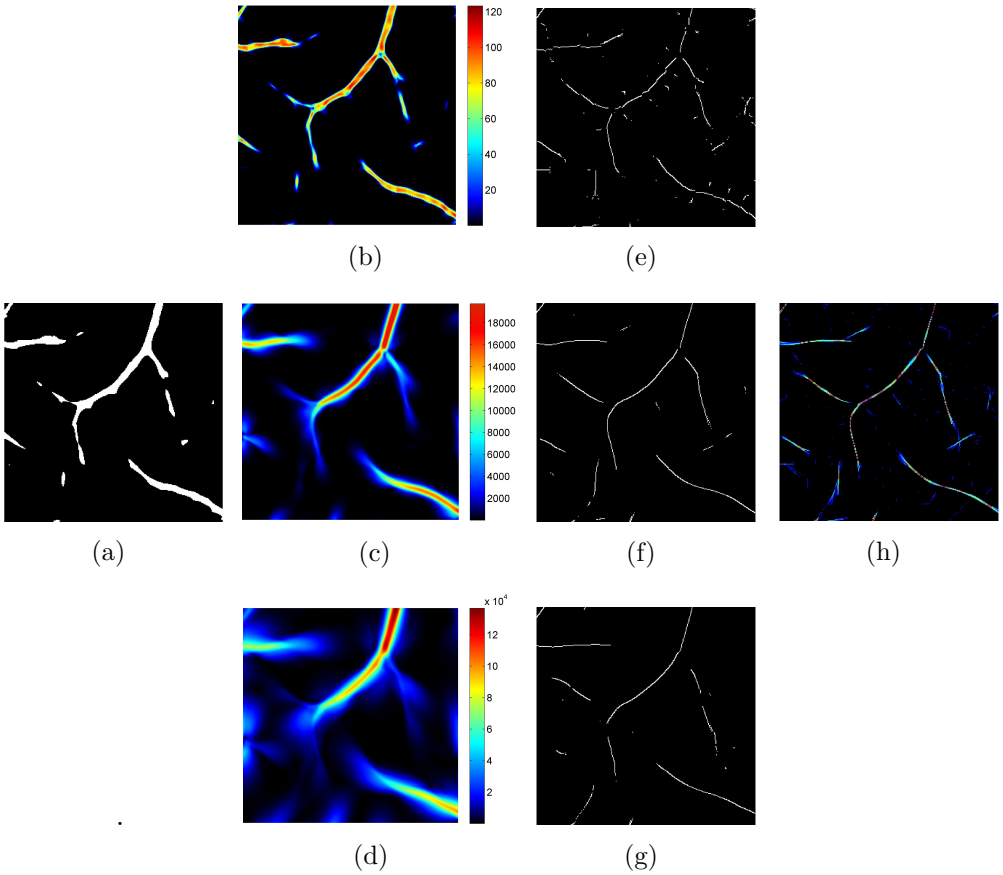

Figure 3.4 Small vessel reconnection example. (a) input image, (b)-(d) saliency maps obtained by small ($\sigma_{TVF} = 5$), medium ($\sigma_{TVF} = 25$) and large ($\sigma_{TVF} = 50$) voting scales, (e)-(g) centerline maps corresponding to each tensor voting scale, and (h) centerlines union across $\sigma_{TVF} = 5 : 50$ where each color represents a different voting scale.

3.1.5 Small vessel reconstruction

The result of the previous step includes the reconnection of the small vessels into single centerlines, and in turn their connection to the larger caliber vessels. Still, the small vessels do not have full width, multiple centerlines represent the location of a single vessel, and background noise is present. We choose a tracking approach to combine the previously segmented large vessels with the small vessel centerlines obtained by the MTVF. The advantage of this approach is that we can examine individual vessels as we proceed and obtain useful informa-

tion that can facilitate their reconstruction. Furthermore, as we track the smallest vessels, we can combine the fused multi-scale centerlines to reconstruct single centerlines. Methods based on morphology, on the other hand, would be inadequate as they do not fully utilize the rich information that TVF can provide, namely the direction and the connection of small vessel centerlines to the large vessels. Unless a more complicated morphological method is implemented, they are global as they apply the same operator everywhere, vessels and background. The proposed method uses two centerline maps : (1) the skeletonized image of the large vessels (Section 3.1.3), and (2) the fused small vessels centerline map (Section 3.1.4).

3.1.5.1 Large vessel tracking

The process is initialized by identifying vascular seed points around the optic disc. Vessels are highly interconnected there, forming a tree-like structure that emerges from the optic disc. Therefore, the chance of missing a larger vessel by following all the branches from their root is low. If for example we start the tracking from a distant large vessel that is fragmented, we will stop when we reach a gap, thus stopping the process before reaching any other vessels. On the other hand, by starting at the optic disc we are able to continue tracking by selecting a large vessel that is next to the one that we stopped tracking. Furthermore, initiating tracking from the optic disc allows us to only keep small vessel centerlines and not reconnect background noise. The seeds are the intersection points between a circle with a center at coordinates $C\,(x, y)$ and radius R with the skeletonized image of the large vessels. The circle parameters are directly dependent on the optic disc size and location ; they were manually identified by an expert for all the images in the database.

A depth first based tracking approach is applied on the large vessel skeleton where individual vessels are tracked down to their terminal points. In this way, tracking prioritizes reaching the vascular terminal points, and subsequent initiation of the small vessel tracking, over exploring distant branched vessels. Sequential thinning is applied to obtain the skeleton, thereby suppressing small and noisy branched vessels caused by incomplete and noisy segmentation at the vessel tip.

From there, the next step is the local searching around the endpoints reached by tracking, in a 3-by-3 neighborhood A, for a small vessel seed that corresponds to a TVF centerline point. This centerline point will initiate the small vessel tracking process. In that way, we confine our analysis to areas of interest around the large vessel end-points without trying to reconnect background noise. The neighborhood size is crucial for the initialization of the second tracking phase, because it links the large and small vessel segmentation processes. A search neighborhood larger than three pixels risks tracking disconnected noise.

3.1.5.2 Small vessel tracking

We proceed to the small vessel tracking from the combined TVF centerlines across all the available scales. This is an iterative process that loops between three steps : (1) the *searching step*, (2) the *estimation step*, and (3) the *refinement step*. Tracking advances by one pixel at each iteration, and terminates when no new centerline is returned. The search direction $\mathbf{V_{dir}}$ at a given iteration is computed based on the local TVF eigenvector $\mathbf{e_2}$. Figure 3.5 shows a small vessel tracking example. More specifically :

1. *Searching step :* Centerlines (blue stars, Figure 3.5(a)) are searched along a line that is placed one step from the previous iteration and oriented perpendicularly to $\mathbf{V_{dir}}$ (red arrow, Figure 3.5(a)).
2. *Estimation step :* Starting from the center of the perpendicular line, the first centerline point that is found is the estimation of the final centerline position (blue star, Figure 3.5(b)).
3. *Refinement step :* We can have multiple centerlines slightly shifted from each other (by 1-2 pixels) that correspond to the same vessel. To merge the multi-scale information into a single centerline point we use the local TVF eigenvector $\mathbf{e_1}$ to obtain perpendicular profile P (yellow line, Figure 3.5(c)). The position that minimizes the sum of squared distances between itself and all the other centerlines along the profile is kept as the refined centerline position (green star, Figure 3.5(c)).

   Direction $\mathbf{V_{dir}}$ (red arrow, Figure 3.5(a), 3.5(d)) is computed by averaging of the $\mathbf{e_2}$ centerlines along P. Since the directions represent angles, circular averaging is used [256]. The resulting directions from eigenvector decomposition can be flipped. If $\mathbf{e_2}$ points in the wrong direction it can guide tracking backwards, thus we compare it with the direction at the previous step and correct for this ambiguity when needed.

3.1.5.3 Small vessel reconstruction

The previous work in the literature has focused on the extraction of centerlines, while in our context we are interested in obtaining full vessels. In parallel to tracking, full vessel reconstruction is applied by pixel painting along the length of the profile P. Alternatively, Gaussian fitting on the saliency map can be performed to extract the diameter, however at the expense of high computational time. In our case, the direction, as well as the center of P are determined during the refinement stage of the small vessel tracking process (Section 3.1.5.2). The large vessels' diameters are tracked over the whole skeleton of the larger vessels by minimizing the length of a rotating line, similarly to [80]. Then, the reconstructed diameter D_{small} of a small vessel is equal to the tracked diameter $\mu_{diameter}\,(large\ vessels)$ of

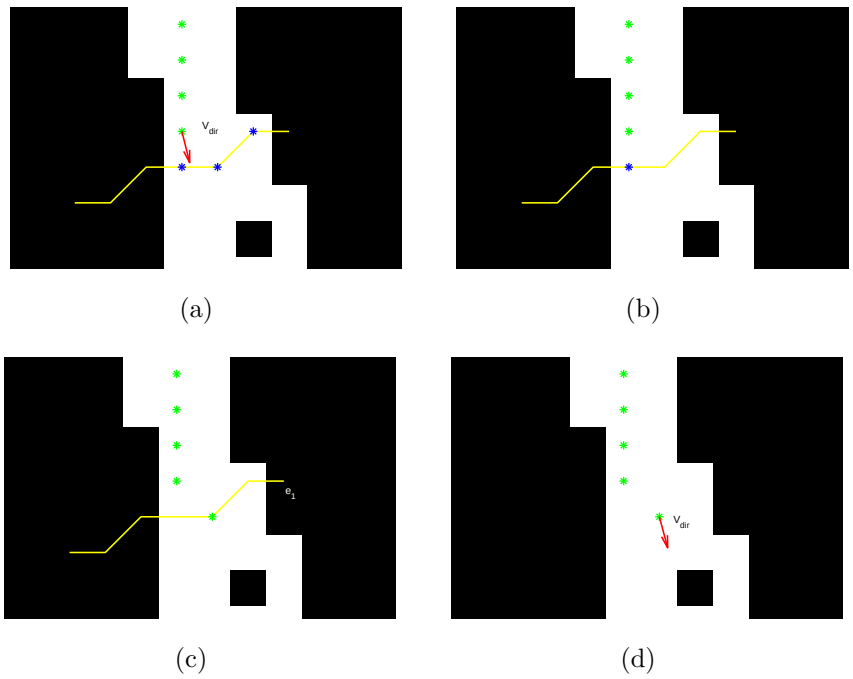

Figure 3.5 Small vessel tracking example. (a) Searching of centerlines (blue stars) perpendicularly to $\mathbf{V_{dir}}$ (red arrow), (b) estimation of the final centerline position (blue star), (c) refinement of the final centerline position (green star) by searching along profile P (yellow line), and (d) $\mathbf{V_{dir}}$ search direction for next tracking iteration.

the preceding large vessel, averaged over several skeleton points at the end of that vessel. Averaging of the diameter is necessary because the large vessel gradually narrows towards its tip, so we have to normalize $\mu_{diameter}\,(large\ vessels)$ by considering a number N of preceding points, N being experimentally determined (Section 3.2.2). The reconstruction process is restricted to the smallest vessels, i.e. those of diameter $D < 8$ pixels (see section 3.2.1). As a final step, morphological closing with a small circular element is applied to fill holes in the reconstructed vessel caused by the inpainting of curved vessels along straight lines. Figure provides an example of small vessel reconstruction.

3.1.6 Postprocessing

The MSLD response is sensitive to background lesions and artifacts, so non-vascular disconnected components remain after the adaptive thresholding stage. Additionally, branched vessels may remain disconnected after tracking. Junctions are high order morphological features that represent the separation of a main vessel into smaller branches. Both MSLD and TVF are inadequate to approximate the bifurcation pattern when it comes to enhancing or segmenting vascular regions at less prominent junctions. MSLD applies a straight line tem-

plate, while there is a high degree of directional uncertainty that cannot be estimated by second order tensors in the TVF.

The final step in our pipeline is the morphological cleaning of background artifacts from the image, together with the inclusion of disconnected vessels. The choice of morphology was based on the algorithimic and computational requirements of the step. According to our method, all the connected components (CC) that are disconnected from the main vasculature are sequentially analyzed. If they are larger than a specific size ($Area_{CC} > Area_{value}$), elongated enough ($Elongation_{CC} > X$) and not very solid ($Solidity_{CC} < X$), then they belong to vessels and thus they are retained from the thresholded image. Elongation or eccentricity of an ellipse (ε) is defined as :

$$\varepsilon = 2\frac{\sqrt{\left(\frac{Length_{MajorAxis}}{2}\right)^2 - \left(\frac{Length_{MinorAxis}}{2}\right)^2}}{Length_{MinorAxis}}, \tag{3.4}$$

where $Length_{MajorAxis}$ and $Length_{MinorAxis}$ are the major and minor axis lengths of an ellipse, respectively [257]. Solidity is defined as the ratio of the area over the convex hull area. Conservative values for the parameters used at this step were experimentally determined as described in Section 3.2.2. This allowed us to clean the images while retaining important vascular structures. Figure 3.7 shows an example where the postprocessing step for background noise suppression is applied in a highlighted area of an image.

3.2 Experiments

3.2.1 Image database

Our approach was evaluated on high resolution fundus images from the HRF database [63]. The database contains three categories of images : healthy subjects (H), diabetic retinopathy patients (DR),and glaucomatous patients (G). Each category comprises 15 images acquired

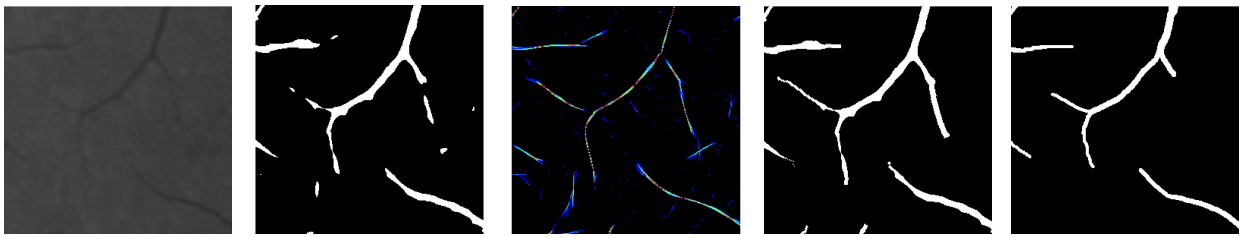

(a) (b) (c) (d) (e)

Figure 3.6 Small vessel reconstruction example. (a) Input grayscale image, (b) simple thresholded image, (c) centerline union, (d) reconstructed vessels, and (r) reference.

using a CANON CF-60UVi camera [258] with fixed resolution of 3504 x 2336 pixels and pixel size of 6.05 x 6.46 μm. Manual segmentations of the vessels are provided for the whole database. In this study, all the vessels of small width were considered as small vessels. This definition of size is invariant to location and branching order, however it depends on the acquisition process, the field of view and the image resolution. For this particular high resolution database, we qualitatively selected the vessel diameter value that isolates most of the terminal, non-fragmented vessels, without including vessels that might belong to the larger vascular structures, such as the major arcades. Everything below 8 pixels in diameter was thus considered as a small vessel. This value yielded a good compromise between the aims of identifying complete terminal vessels and excluding larger vessels. The rest of the vasculature, with diameter above the 8-pixel threshold, was considered as belonging to the large and medium-sized categories of vessels.

3.2.2 Parameter setting

The vessel segmentation performance was evaluated at two levels : (1) using the full vasculature, and (2) restricting the analysis to the smallest vessels. The glaucomatous cases in our database were not severe, so they show deterioration on the optic disc but none for the

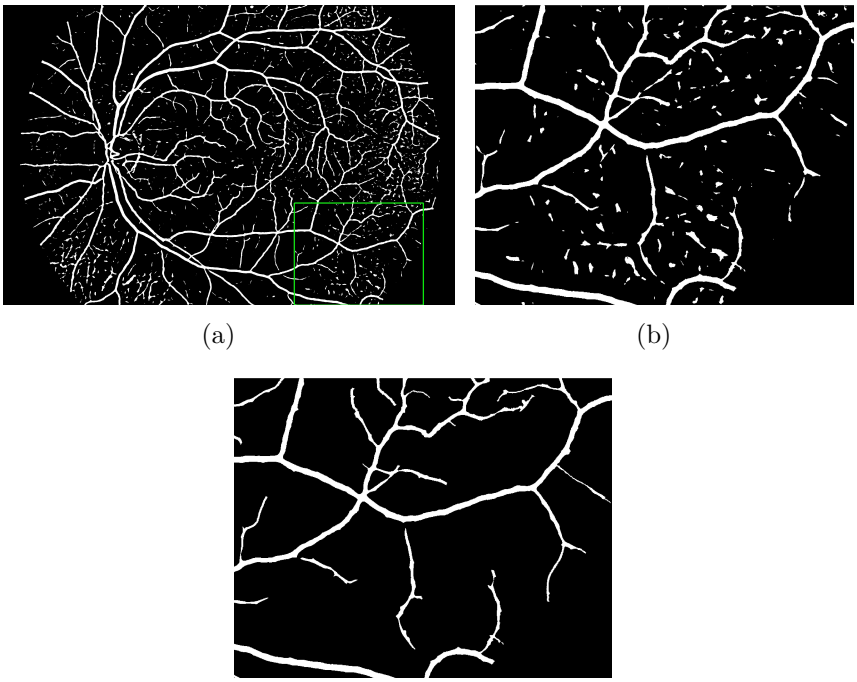

Figure 3.7 Postprocessing example. (a) Adaptive thresholded input image, (b) zoomed area corresponding to inset in (a), and (c) same image area after postprocessing (cleaning).

vascular network. Hence, this group of images was used as a training set to tune the method's parameters, while the rest of the database was used for validation purposes. We also compared our vasculature segmentation results to recent methods published in the literature. Before proceeding to the evaluation stage, we examined different parameters values and how their values affected the segmentation performance in the training set. Table 3.1 lists the method's main parameters.

In order to examine which value t from the wavelet filtering step was most appropriate for our method, we varied this parameter between several representative values : $t = 0, 0.015, 0.03, 0.06, 0.12, 0.5$, and 2. The filtering value that gave the highest improvement in the sensitivity rate against the original MSLD method [80], at the same noise level, as chosen as the optimum filtering value. The changes in sensitivity rate for the above t values were respectively 1.13%, 1.15%, 0.76%, -0.66%, -2.90%, -7.28% and -8.02%. Therefore, we choose $t = 0.015$ for subsequent experimentation as it gave the highest increase.

For the MSLD step, we considered a maximum available line length of $W = 40$ pixels, which was twice the diameter of an average vessel in the images. Moreover, we determined the adaptive thresholding factor α by testing different values in a range and evaluating the result using the CAL metric (Section 3.3.1). Given the observed mixed distributions of the MSLD responses in Figure 3.3, we had to try high sigma values ($\alpha < 3$) to investigate the response of the segmentation at these levels. Even though the maximum was achieved at $\alpha = 2.2$, this value was not optimal because, together with the background noise, small vessels were removed from the result. Retaining the fragmented small vessels, which is necessary for vessel reconnection, was more important than cleaning the background, thus we select a value in the middle of the range, namely $\alpha = 1.55$, as the optimum for segmentation purposes. Figure 3.9(c) shows the effect of varying factor α on the CAL metric.

Next, the effect of using single-scale tensor voting instead of MTVF on the small vessel reconstruction was evaluated. We tried different values for the scale parameter in the range $\sigma_{TVF} = 5 : 50$, and measured the sensitivity (Figure 3.9(a)) and specificity (Figure 3.9(b)) rates across the training set. As we increased the MTVF scale range, more vessels were included in the final result. The inclusion of high voting scales can help in the direction of letting the algorithm to reconnect fragments in a greater distance than if only smaller voting scales are used, however at the expense of a reduction in the specificity rate. Beyond a certain point, though, the inclusion of larger scales not only fails to improve the segmentation performance, but in fact causes more noise to be reconnected to the vessel network. Since we want to segment as many vessels as possible, we used the range of values from the smallest scale to the scale where there is stabilization in the variation of the sensitivity rate ($\sigma_{TVF} = 5 : 50$). Also, it is clear from Figure 3.9(a) and Figure 3.9(b) that MTVF had better performance

measures than single scale TVF.

We then evaluated the small vessel reconstruction parameter N to determine the value giving the best improvement in sensitivity rate against the original MSLD method [80] at the same noise level. The changes in sensitivity rate, as we increased N from 1 to 8 (by steps of 1), were respectively 1.13%, 1.14%, 1.14%, 1.15%, 1.12%, 1.13%, 1.12%, and 1.12%. Therefore, we choose $N = 4$ for the rest of the experiments. Finally, the postprocessing parameter values were selected by examining the CAL performance metric. As described in section 3.1.6, these parameters establish the morphological limits between real vessel segments (to be reconnected) and artifacts (to be removed). We varied $Area_{value}$ from 200 to 600 and X from 0.2 to 0.9. Values of $Area_{value} = 500$, or 10 times the largest vessel diameter, and $X = 0.5$, gave the maximum perceptual response (Figure 3.9(d)). Table 3.1 summarizes the results of the parameter setting process. The computational time across the different scales in MTVF for a typical image is given in Figure 3.8.

Table 3.1 Parameters of the proposed approach and the selected values

Parameter (Section)	Function	Selected value
t (§3.1)	Wavelet filtering	$t = 0.015$
W (§3.2)	MSLD (80)	$W = 40$
α (§3.3)	Adaptive thresholding factor	$\alpha = 1.55$
σ_{TVF} (§3.4)	Multi-scale tensor voting range	$\sigma_{TVF} = 5 : 5 : 50$
N (§3.5)	Large vessel skeleton pixels for reconstruction	$N = 4$
$Area_{value}, X$ (§3.6)	Postprocessing	$Area_{value} > 500, X = 0.5$

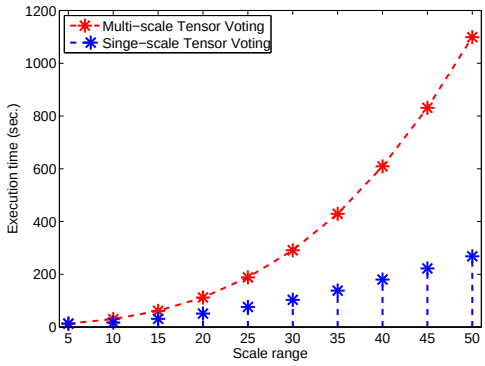

Figure 3.8 Single (blue line) and multi (red line) scale tensor voting execution time for a typical retinal image across scales $\sigma_{TVF} = 5 : 5 : 50$.

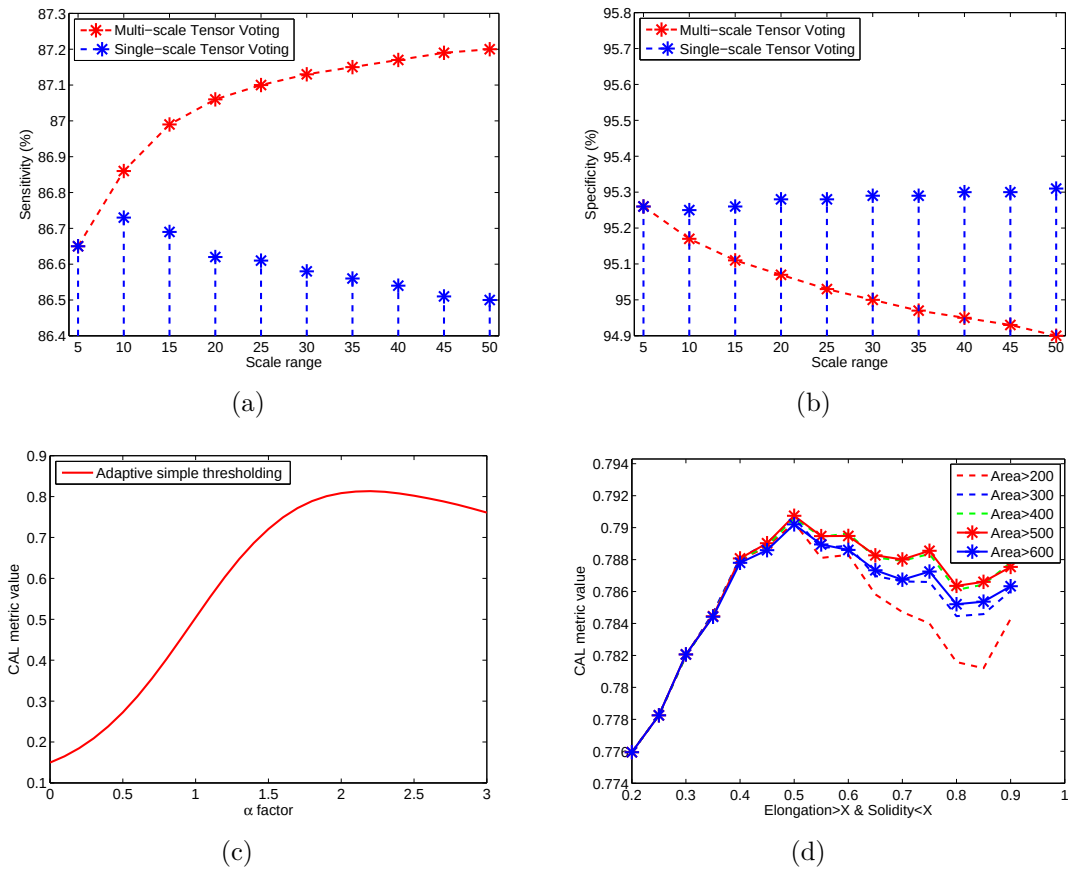

Figure 3.9 Analysis of parameter settings. (a) Sensitivity rates for multi- and single-scale TVF vs. scale range, (b) specificity rates of multi- and single-scale TVF vs. scale range, (c) CAL metric vs. adaptive thresholding factor, and (d) CAL metric vs. postprocessing parameters.

3.3 Vessel segmentation performance

In our experiments we compared two segmentation methods : (1) the MSLD approach [80], and (2) our proposed approach. This was done by applying each of the methods on the test set composed of the healthy (H) and diabetic retinopathy (DR) groups of images from the HRF database.

3.3.1 Full vasculature performance

The standard discrepancy metrics of sensitivity, specificity and accuracy were employed. The methods were also assessed using a perceptual evaluation metric proposed by M. Gegúndez-Arias *et al.* [239] that is tailored to retinal applications.

For the MSLD approach [80], we first determined that a thresholding value ($T > 0.671$) gave the same specificity level as our approach ; then we compared their sensitivities. We were

interested to see if we had an improvement with respect to the rate of successfully identified vessels, or true positives (TPs), at the same background noise level (specificity). Given the same level of background noise, we can easily examine which method identifies more vessel pixels. Our method can be represented as a single operating point on the ROC curve and not as a complete curve because the final segmentation depends on many parameters that must be optimized at the same time.

Table 3.2 shows the results across the test set. In the following discussion, the mean and standard deviation of a given performance measure are abbreviated as M and SD. Also, we tested the statistical significance of the results using T-test analysis; when relevant, this is presented as $t-value$(degrees of freedom), $p-value$. For the sensitivity, our approach ($M = 85.06, SD = 4.03$) segmented significantly more vessels than the original MSLD method [80] ($M = 81.06, SD = 3.65$), $t(58) = 4.0344, p < 0.05$. The specificity was equivalent in both methods, while the accuracy was slightly better with our method. However, the metric used here is global in the sense that it cannot distinguish between the smaller and larger vessels in the segmentation results.

Table 3.2 Full vasculature performance evaluation on test set in terms of sensitivity specificity accuracy

Method	Sensitivity ± SD	Specificity ± SD	Accuracy ± SD
MSLD [80]	81.06% ± 3.65%	95.82% ± 2.14%	94.35% ± 1.72%
Proposed approach	85.06% ± 4.03%	95.82% ± 1.15%	94.79% ± 1.06%

Figure 3.10 shows examples of the two segmentation methods for two images, one from the (H) group and another from the (DR) group. For the top image, more small peripheral vessels were identified by our approach (Sensitivity : 82.07% vs. 73.12%). Additionally, less noise originating from the nerve fiber layer, which is adjacent to the major arcades, was segmented. The major arcades are defined as the largest vessel branches, i.e. the first order vessel branches that are superior and inferior to the optic disc. In both our approach and MSLD [80], the border of the optic disc was wrongly segmented. For the bottom image, the vessel segmentation performance is similar in both methods (sensitivity : 80.82% vs. 80.89%). However, our approach identifies considerably fewer background lesions than MSLD, which is reflected in the specificity rates (96.27% vs. 92.13%).

Generally, our approach relies on the connectivity criterion in the postprocessing step to exclude background noise that is not connected to the main vasculature. In DR images, it succeeds in eliminating much of the background noise, including lesions, and this contributes to lowering the false positive rate. Consequently, a higher T value must be used to threshold

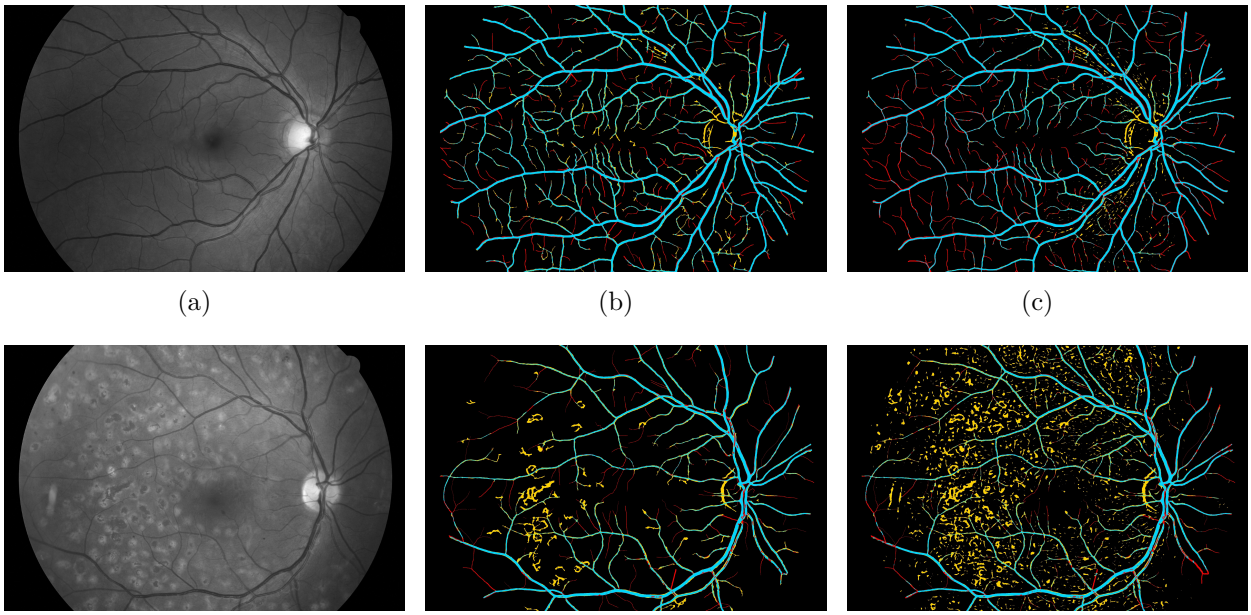

(a) (b) (c)

(d) (e) (f)

Figure 3.10 Full vessel segmentation examples in Image_01_healthy (first row) and Image_04_diabetic (second row). (a) and (d) original image, (b) and (e) segmentation result of our approach, (c) and (f) segmentation result of MSLD method. In the segmentation maps (b, c and e, f), blue pixels represent the true positives, red pixels are the false negatives, yellow pixels are the false positives, and black pixels are the true negatives.

the MSLD response to achieve the same specificity rate as our approach for pathological cases. For healthy cases, the difference in sensitivity between the two methods is even greater, as exemplified in Figure 3.10.

Table 3.3 shows the results in terms of the perceptual performance metric (CAL, or Connectivity Area Length). This measure is the product of three individual metrics : connectivity, area and length. The connectivity criterion penalizes any deviation from the number of connected components in the reference image. Meanwhile, the length (resp. area) criterion measures the degree of coincidence, in terms of total skeleton length (resp. vessel area), between the groundtruth and tested segmentations (239). Length is an important individual metric because it shows to what extend each method can identify vessels. This criterion evaluates the skeletonized vasculature, thereby disregarding the influence of the pixel areas of the different categories of vessels.

Our approach ($M = 0.779, SD = 0.060$) achieves significantly higher CAL performance than the original MSLD method [80] ($M = 0.701, SD = 0.127$), $t(58) = 3.0203, p < 0.05$. The proposed method seeks to maximize resulting vascular connectivity, thus that particular criterion is very close to 1 (or perfectly preserved connectivity compared to the reference

Table 3.3 Full vasculature performance evaluation on test set in terms of CAL metric

Method	Connectivity ± SD	Area ± SD	Length ± SD	CAL ± SD
MSLD [80]	0.997 ± 0.002	0.867 ± 0.074	0.804 ± 0.084	0.701 ± 0.127
Proposed approach	0.999 ± 0.000	0.902 ± 0.036	0.862 ± 0.034	0.779 ± 0.060

image) in our approach. However, the CAL metric penalizes false positives, which explains the lower results for the area and length criteria for both segmentation methods. Nonetheless, our approach achieves area and length results that are more than 3% higher than MSLD.

Table 3.4 and Figure 3.11 gives the performances of different methods proposed in the literature in terms of the standard discrepancy metrics. The segmentation methods of R. Annunziata *et al.* [259], J. Hannink *et al.* [260], J. Odstrcilik *et al.* [63], A. Budai *et al.* [261], H. Yu *et al.* [262] and A.F. Frangi *et al.* [260] were considered. The methods are sorted chronologically. The proposed approach achieves considerably higher sensitivity than all the other methods for all categories of images, which translates to the segmentation of more vessels. Specificity-wise, our method obtains 95.82% which, aside from the MSLD [80], is the lowest result, with the next closest being for J. Odstrcilik *et al.* [63], at 96.84%. When the accuracy metric is considered, our approach ranks in the lower half of the methods, just ahead of the MSLD [80], and very close to J. Odstrcilik *et al.* [63].

Table 3.4 Performance comparison of different methods on test set in terms of sensitivity specificity accuracy

Method	Sensitivity	Specificity	Accuracy
A.F. Frangi *et al.* [260]	60.55%	98.05%	95.05%
H. Yu *et al.* [262]	77.89%	96.96%	95.13%
A. Budai *et al.* [261]	66.00%	98.45%	95.80%
J. Odstrcilik *et al.* [63]	76.62%	96.84%	94.92%
MSLD [80]	81.06%	95.82%	94.35%
J. Hannink *et al.* [260]	79.85%	97.55%	96.10%
R. Annunziata *et al.* [259]	69.08%	98.61%	95.70%
Proposed approach	85.06%	95.82%	94.79%

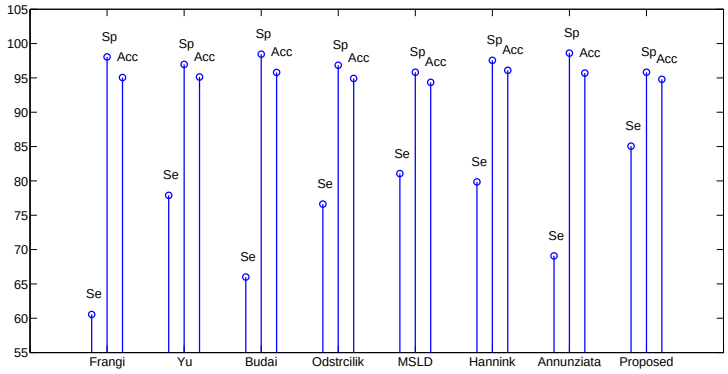

Figure 3.11 Differences in the discrepancy metrics across the available segmentation methods.

3.3.2 Small vessels analysis

The standard discrepancy measures cannot account for the heterogeneity in the pixel areas of vessel segments of different diameters [175]. Thus, we confined the following part of our analysis to the smallest vessels. The smallest vessels of the groundtruth images were first isolated from the rest of the vessel network. To achieve this, the minimization of a rotating line on the pixels belonging to the skeletonized reference image was applied as in Section 3.1.5.3. Next, the diameter value at each skeleton point is assigned to all vessel pixels along the normal direction at that point. Then, the pixels belonging to vessels of diameter less than 8 pixels were isolated, and the final result of this operation was subtracted from the rest of the reference image. The segmentation algorithms were assessed by computing the same discrepancy measures as those used for the full vasculature analysis (Section 3.3.1), and by assigning the large vessel pixels from the reference to the true negative class. The segmentation maps of A.F. Frangi [260] and J. Hannink [260] were also available, so our analysis included these methods.

Table 3.5 shows the performance of the four methods on the smallest vessels when the pixel-based discrepancy measures were considered. Our approach ($M = 68.64, SD = 6.78$) achieved significantly higher sensitivity than MSLD [80] ($M = 62.17, SD = 8.51, t(58) = 3.225, p < 0.05$), J. Hannink [260] ($M = 54.08, SD = 12.36, t(58) = 5.6580, p < 0.05$), and A.F. Frangi [260] ($M = 49.01, SD = 11.11, t(58) = 8.2576, p < 0.05$) methods. In fact, the difference between our method and the available ones is greater than when all the vessels were considered. Our approach detected approximately 6% more small vessels than the MSLD [80]. Moreover, this increase doubles and triples when our approach is compared with the J. Hannink [260] and A.F. Frangi methods [260], respectively. In our analysis we remove the detected medium to large-sized vessels, however the oversegmentation of the vessels boundary is not taken into account which explains the differences in the specificity and accuracy metrics

between the MSLD and the proposed approach.

Table 3.5 Smallest vessel ($D < 8$) segmentation evaluation on test set in terms of sensitivity specificity and accuracy

Method	Sensitivity ± SD	Specificity ± SD	Accuracy ± SD
A.F. Frangi [260]	49.01% ± 11.11%	95.82% ± 2.29%	94.58% ± 2.09%
MSLD [80]	62.17% ± 8.51%	96.84% ± 2.44%	95.91% ± 2.24%
J. Hannink [260]	54.08% ± 12.36%	97.99% ± 2.05%	96.82% ± 1.80%
Proposed approach	68.64% ± 6.78%	96.54% ± 1.33%	95.80% ± 1.32%

Table 3.6 shows the performance of the four methods on the smallest vessels when the perceptual-based discrepancy measure is considered. Even though our approach ($M = 0.363, SD = 0.064$) achieved a higher overall CAL performance than the original MSLD [80] ($M = 0.334, SD = 0.085, t(58) = 1.4487, p > 0.05$) and J. Hannink [260] ($M = 0.313, SD = 0.089, t(58) = 2.4551, p > 0.05$) methods, the difference is not statistically significant. The A. F. Frangi method [260] obtained the lowest performance of all ; this poor performance can be explained by the excessive amount of disconnected background noise produced by that method. The individual criteria of the CAL metric heavily penalize false positives, so the net effect is that when all three criteria are multiplied, the final CAL metric ranges from around 1% to a maximum of 36%.

Table 3.6 Smallest vessel ($D < 8$) segmentation evaluation on test set in terms of CAL metric

Method	Connectivity ± SD	Area ± SD	Length ± SD	CAL ± SD
A.F. Frangi [260]	0.741 ± 0.148	0.548 ± 0.087	0.402 ± 0.077	0.177 ± 0.079
MSLD [80]	0.980 ± 0.006	0.594 ± 0.091	0.563 ± 0.070	0.334 ± 0.085
J. Hannink [260]	0.991 ± 0.005	0.569 ± 0.090	0.544 ± 0.075	0.313 ± 0.089
Proposed approach	0.991 ± 0.004	0.624 ± 0.060	0.582 ± 0.053	0.363 ± 0.064

Figures 3.12, 3.13, and 3.14 provide examples where the analysis focuses on the smallest vessels. Each figure illustrates the segmentation results of the four methods under comparison (A.F. Frangi [260], MSLD [80], J. Hannink [260], and Proposed) for the square region corresponding to the green inset superimposed on the small vessel groundtruth image. The segmentation results of each algorithm are colorized to reflect the confusion matrix : blue pixels represent the true positives, red pixels are the false negatives, yellow pixels are the false positives, and black pixels are the true negatives.

Figure 3.12 (Image_15_healthy), presents the best performance of the proposed approach for both the large and small vessel categories. Qualitatively, our approach segments most of the vessels without retaining any disconnected background noise, however the terminal vessels and the boundary of the large vessels are overestimated in terms of length and width. Also, some false positive vessels are reconnected to the main vasculature. Quantitatively, our approach achieves the highest sensitivity but the lowest specificity.

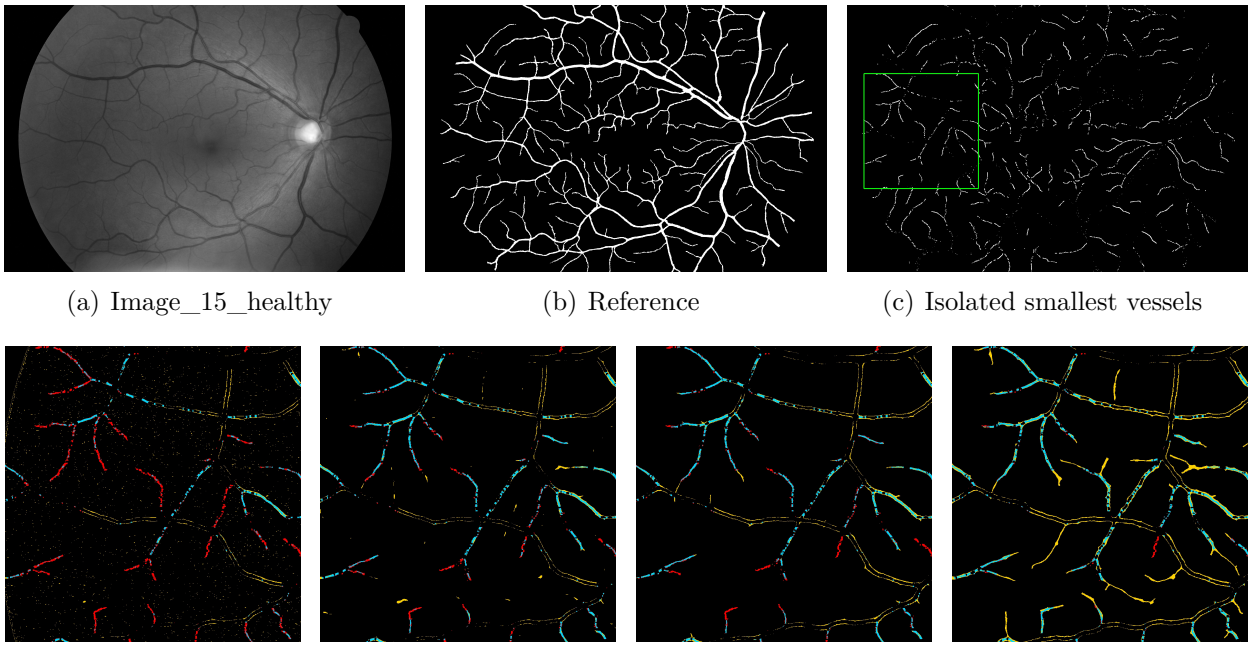

(a) Image_15_healthy (b) Reference (c) Isolated smallest vessels

(d) A. F. Frangi (e) MSLD (f) J. Hannink (g) Proposed approach

Figure 3.12 Small vessel segmentation example in Image_15_healthy. (a) Grayscale input image, (b) manual segmentation of the whole vasculature, (c) isolated smallest vessels, (d) A. F. Frangi [260] segmentation result :($Sens._{full} = 70.97\%, Specif._{full} = 98.44\%, Sens._{smallest} = 40.36\%, Specif._{smallest} = 99.34\%$), (e) MSLD [80] segmentation result :($Sens._{full} = 87.28\%, Specif._{full} = 97.14\%, Sens._{smallest} = 72.41\%, Specif._{smallest} = 97.85\%$), (f) J. Hannink [260] segmentation result :($Sens._{full} = 86.27\%, Specif._{full} = 97.80\%, Sens._{smallest} = 66.30\%, Specif._{smallest} = 98.47\%$), and (g) Proposed approach segmentation result :($Sens._{full} = 92.91\%, Specif._{full} = 95.99\%, Sens._{smallest} = 83.83\%, Specif._{smallest} = 96.36\%$)

Figure 3.13 (Image_10_healthy), presents the worst performance of the proposed approach for the small vessel category. Our method has the same qualitative behavior as in the best case ; it segments most of the vessels without retaining any disconnected background noise. But this is achieved at the expense of overestimating the vessel diameters/endpoints and reconnecting vessel-like false positives components. Even though this image represents the worst-case performance, our method still reaches the highest sensitivity rate among the

considered methods.

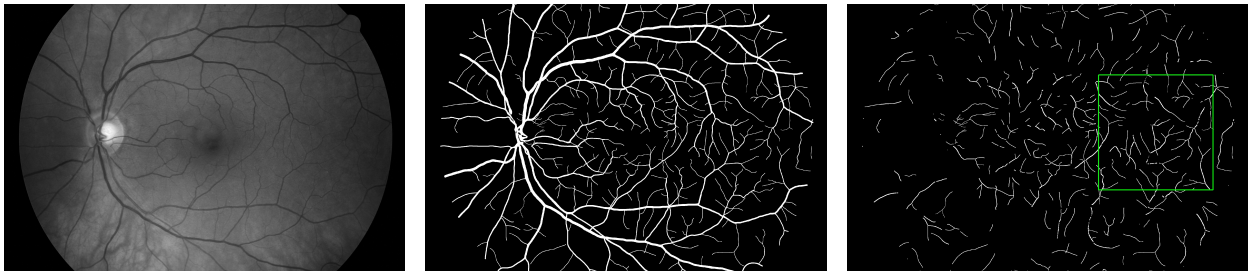

(a) Image_10_healthy (b) Reference (c) Isolated smallest vessels

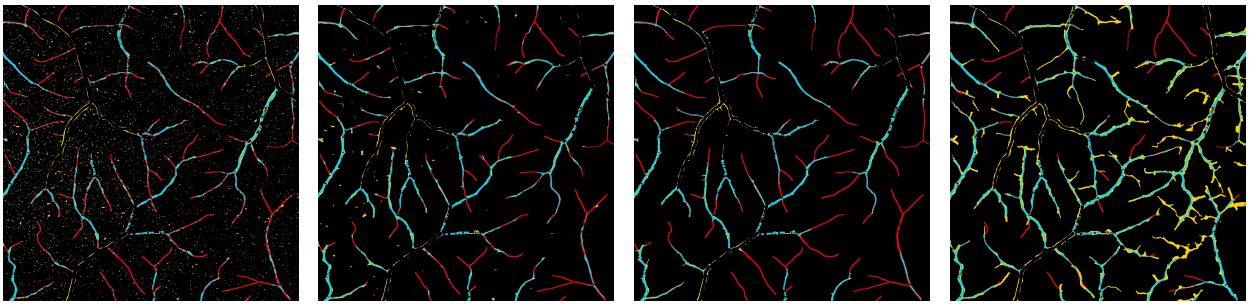

(d) A. F. Frangi (e) MSLD (f) J. Hannink (g) Proposed approach

Figure 3.13 Small vessel segmentation example in Image_10_healthy. (a) grayscale input image, (b) manual segmentation of the whole vasculature, (c) isolated smallest vessels ($D < 8$), (d) A. F. Frangi [260] segmentation result :($Sens._{full} = 70.97\%, Specif._{full} = 98.44\%, Sens._{smallest} = 39.47\%, Specif._{smallest} = 97.58\%$), (e) MSLD [80] segmentation result :($Sens._{full} = 79.37\%, Specif._{full} = 97.58\%, Sens._{smallest} = 53.15\%, Specif._{smallest} = 98.45\%$), (f) J. Hannink [260] segmentation result :($Sens._{full} = 74.94\%, Specif._{full} = 98.53\%, Sens._{smallest} = 35.01\%, Specif._{smallest} = 99.32\%$), and (g) Proposed approach segmentation result :($Sens._{full} = 82.54\%, Specif._{full} = 96.96\%, Sens._{smallest} = 57.08\%, Specif._{smallest} = 97.59\%$)

Finally, Figure 3.14 (Image_06_diabetic) presents the worst performance of the proposed approach in terms of full vascular network segmentation. An interesting feature of this image is that it includes many convoluted vessels that could be neovessels. Our approach managed to segment most of these vessels. The majority of them were segmented earlier in our pipeline (at the adaptive thresholding stage), while the MTVF partially completed the network (Figure 3.15). We note as well that the the vessel widths were over-estimated. At the same time, the other three methods failed to segment many vessels in this region of interest. This is reflected in their sensitivity rates, which are lower than for our approach.

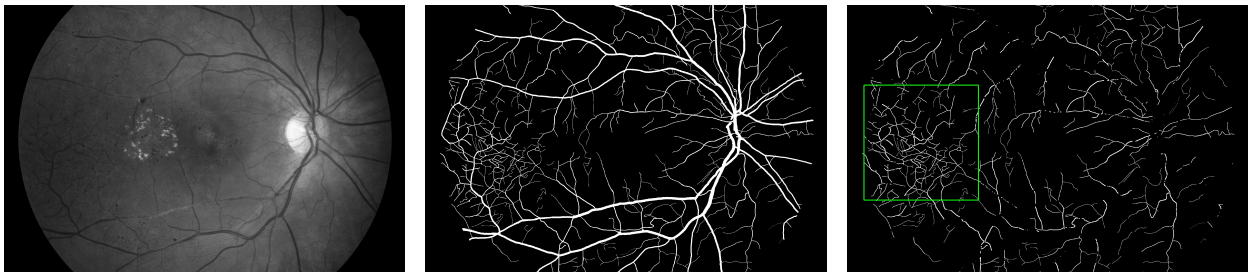

(a) Image_06_diabetic (b) Reference (c) Isolated smallest vessels

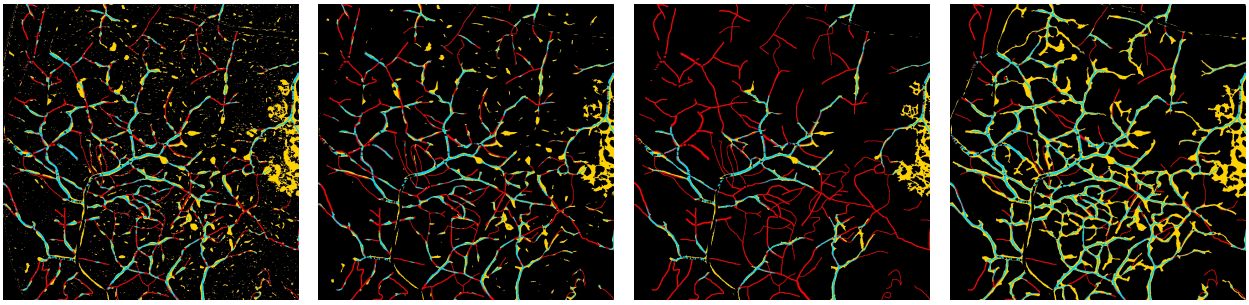

(d) A. F. Frangi (e) MSLD (f) J. Hannink (g) Proposed approach

Figure 3.14 Small vessel segmentation example in Image_06_diabetic. (a) grayscale input image, (b) manual segmentation of the whole vasculature, (c) isolated smallest vessels ($D < 8$), (d) A. F. Frangi [260] segmentation result :($Sens._{full} = 71.26\%, Specif._{full} = 92.94\%, Sens._{smallest} = 54.19\%, Specif._{smallest} = 92.44\%$), (e) MSLD [80] segmentation result :($Sens._{full} = 72.59\%, Specif._{full} = 93.90\%, Sens._{smallest} = 55.35\%, Specif._{smallest} = 94.79\%$), (f) J. Hannink [260] segmentation result :($Sens._{full} = 68.25\%, Specif._{full} = 95.85\%, Sens._{smallest} = 42.56\%, Specif._{smallest} = 96.66\%$), and (g) Proposed approach segmentation result :($Sens._{full} = 74.43\%, Specif._{full} = 93.62\%, Sens._{smallest} = 58.62\%, Specif._{smallest} = 94.47\%$)

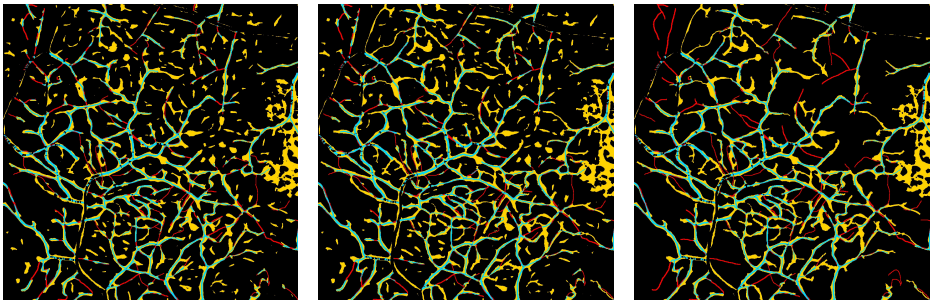

(a) (b) (c)

Figure 3.15 Small vessel segmentation at different stages in proposed pipeline, for Image_06_diabetic. (a) adaptive thresholding result, (b) small vessel reconnection result, and (c) postprocessed result.

3.3.2.1 Group differences between healthy and diabetic performance

We divided the entire test set into the healthy (H) and diabetic (DR) images in order to assess how the proposed method performed on the separate groups as compared to the overall case. For the healthy group, the improvement in sensitivity over the original MSLD method [80] widened : our method detected 11% more small vessels than MSLD. However, this was accomplished at the expense of more false positives, probably due to overestimation of the vessel endpoints and widths or from false positive reconnections. The opposite trend was observed for the DR group. The gain in sensitivity over MSLD [80] dropped, but in terms of specificity the proposed method segmented less noise. This can be accounted for by the inherent connectivity criterion that removes isolated background noise and artifacts. When the two image groups are merged, the performances are averaged so the specificity is the same across the database and the sensitivity is reduced compared to the healthy case. Tables 3.7 and 3.8 give the results for the standard discrepancy metrics separately in each image group.

Table 3.7 Full Vasculature performance evaluation on test set in terms of sensitivity specificity accuracy

Category	Method	Sensitivity ± SD	Specificity ± SD	Accuracy ± SD
H	MSLD [80]	80.50% ± 4.04%	97.66% ± 0.55%	95.74% ± 0.63%
.	Proposed approach	86.60% ± 3.40%	96.67% ± 0.43%	95.54% ± 0.43%
DR	MSLD [80]	81.62% ± 3.26%	93.99% ± 1.41%	92.95% ± 1.23%
	Proposed approach	83.53% ± 4.13%	94.97% ± 1.02%	94.05% ± 0.98%

Table 3.8 Smallest vessel ($D < 8$) segmentation evaluation on test set in terms of sensitivity specificity accuracy

Category	Method	Sensitivity ± SD	Specificity ± SD	Accuracy ± SD
H	MSLD [80]	58.10% ± 8.64%	97.86% ± 0.51%	96.90% ± 0.46%
.	Proposed approach	69.90% ± 7.15%	96.96% ± 0.42%	96.30% 0.39%
DR	MSLD [80]	66.25% ± 6.31%	94.33% ± 1.36%	93.61% ± 1.21%
	Proposed approach	67.38% ± 6.39%	95.55% ± 1.06%	94.81% ± 1.06%

3.4 Discussion

Segmenting the smallest retinal vessels is still a challenging problem. The MSLD method [80] is based on straight line segments, which is inadequate in this context. Using tensor

voting can help by retaining only the information that is perceptually significant to extending the segmentation to the smallest vessels. In this chapter, we have proposed a novel hybrid approach that combines the two methods. Multi-scale information from the TVF is combined in a new way that allows us to reconnect vessels at greater distances than single scale tensor voting. Besides, our approach can fully reconstruct the vessels, which enables the use of the framework for lesion detection in CAD systems.

Even though the proposed method achieved higher performance than MSLD [80] in the majority of full and small vessel experiments, several challenges remain to be addressed. In the final result, the segmented small vessels can be slightly translated from their groundtruth counterparts. Similarly, their reconstructed widths do not exactly coincide in some locations with the corresponding vessels in the manually segmented image. Moreover, small vessel terminal points are over-estimated. Additionally, the TVF can reconnect vessel-like false positive structures to the main vasculature, while conversely it can miss real vessels lying after junctions.

The errors in the reconstructed width of a small vessel can be attributed to the pixel painting process. The diameter obtained from the larger vessel is used without taking into account local information such as the local saliency from TVF. This gives rise to false positives and to an equivalent reduction in the true positive counts. The issue of vessel over-extension was also raised by Z. Leng *et al.* [209], however their solution was based on simple post-processing, taking into account the information from an initial centerline map extracted by a Canny edge detector. The vessel over-extension problem, together with the false positive reconnection problem, is related to the quality of the available reference. Precise manual segmentation of the smallest vessels is not obvious in high resolution images, even for an expert. Therefore, the use of multiple experts who manually segment the same images would allow a consensus groundtruth to be constructed. With such a reference, there would be higher confidence about the smallest vessels' positions and extents. In our case, there were instances where the expert did not identify small vessels or did not extend them until their endpoints. Figure 3.16 highlights examples where small vessels of weaker contrast are missing or they were not completed in the manual segmentation. Our approach, on the other hand, managed to identify and/or complete these vessels.

Furthermore, there is significant difficulty in reconnecting vessel segments that are located beyond junctions. As was highlighted in Section 3.1.6, the high level of orientation uncertainty causes the TVF to fragment the vessels at junctions, even if these structures are well defined. In the proposed method, we try to retain branched vessels via morphological processing, but alternatives could be considered. The ballness measure (λ_2) reaches local maxima at junctions. Using it directly via concurrent tracking and searching for branched

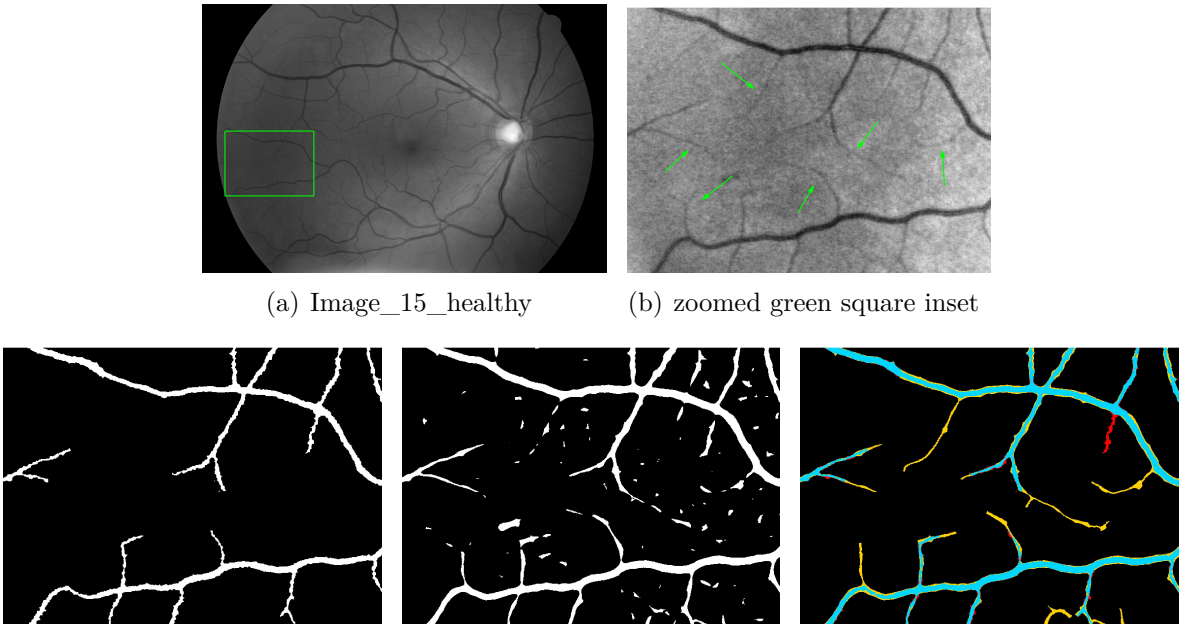

(a) Image_15_healthy (b) zoomed green square inset

(c) zoomed reference (d) adaptive simple thresholded MSLD (e) Proposed approach

Figure 3.16 Missing small vessels in the reference segmentation of Image_15_healthy. (a) Grayscale input image, (b) zoomed region corresponding to inset in (a) ; green arrows indicate faint vessels, (c) corresponding reference region, (d) adaptive thresholded MSLD, (e) final segmentation result of the proposed method.

vessels to reconnect could be advantageous. Alternatively, the use of higher than second-order tensors [217] could resolve the inability of the TVF to infer the information at junctions. Finally, new metrics should be proposed that will be tailored to the analysis of the smallest vessels by removing the influence of the larger vessels.

3.5 Conclusion

A novel approach was proposed to segment small vessels in high resolution retinal images. Simple thresholding the MSLD [80] response leads to the fragmentation of the low contrasted smallest vessels. Instead, this work proposes the combination of an adaptively thresholded MSLD with a perceptual organization approach (TVF) to reconnect the small fragmented vessels. Multiple scales for the TVF are considered which promote the reconnection in a greater distance than single scale. The method was applied in high resolution fundus images. According to the available data, our approach can segment more vessels than MSLD [80], both when all the vessel diameters are considered and when the analysis is confined to the smallest vessels. In addition, our method can further extend the detected vasculature and produce a more connected result than previous works ; both these advantages translate to better

perceptual performance. Compared to other published methods, our approach segments more vessels at the expense of slightly higher background noise. However, the proposed algorithm should be validated in datasets containing images with different pixel resolutions.

Methods relying on a connectivity criterion for segmenting the vessels are well suited for preprocessing the retinal vasculature in CAD systems. On the other hand, simple thresholding does not set any restriction on the background responses, which can result in false negatives at a subsequent lesion detection step, i.e. failure to detect potentially vision-threatening lesions.

Future work will focus on utilizing the ballness measure (λ_2) computed in the tensor voting framework for neovascularization detection. This category of vessels is even more challenging to detect because neovessels are very fine and tortuous structures with low contrast that form chaotic networks around the optic disc or in other areas of the retina. Their presence in the fundus image signals the transition to the final stage of diabetic retinopathy and thus their accurate detection is essential.

CHAPTER 4 SMALL RETINAL VESSEL CHARACTERIZATION

This chapter will present the developed method for the characterization problem of healthy or proliferative diabetic retinopathy regions (PDR). Besides, it will provide the experimental results.

4.1 Methodology

The methodology consists of three steps, each one separated in individual basic steps : (1) the junction center detection step, (2) the feature extraction step, and (3) the classification step. Diagram in Figure 4.1 demonstrates the proposed pipeline for the junction center detection stage. Vessels are firstly extracted based on the method presented in Chapter 4. Postprocessing is then applied to remove backgroun noise. Next, the TVF is applied at a single scale to detect the junctions. Finally, noisy or very close junctions are suppressed. Following the junction center detection steps, features are selected from manually identified regions, while classification is applied to examine the performance of the selected features.

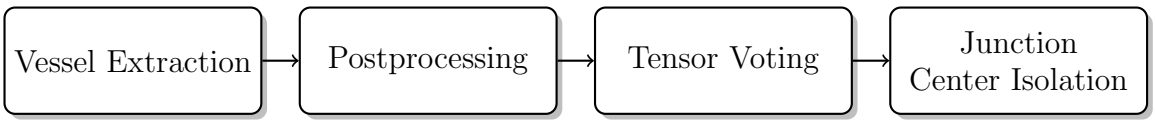

Figure 4.1 Junction center detection pipeline.

4.1.1 Junction center detection

4.1.1.1 Vessel extraction

We apply the MSLD [80] on the green channel of the retinal images whose illumination is corrected and background noise is filtered, as in Chapter 3. We apply the line detector, adjusting the line length parameter W according to the image resolution. The overall distribution of line response values varies according to the considered image and database, so we determine the simple threshold value adaptively by fitting a Gaussian function on the distribution of each image. We use the same threshold value $T = \lfloor \mu_{\text{Gaussian}} \rfloor + \lfloor \sigma_{\text{Gaussian}} \rfloor$ for all the available images, where μ_{Gaussian} is the mean value and σ_{Gaussian} is the standard deviation of the fitted function, respectively.

4.1.1.2 Postprocessing

Simple thresholding the line response leads to the retention of disconnected background structures that are either small in size or irregular in shape. In order to remove this type of noise we perform a conservative morphological analysis. We suppress all the disconnected components that have $400 < \text{Area}_{CC} < 1000$ and that are not elongated enough ($\text{Elongation}_{CC} < 0.99$). Smaller components are completely removed, while larger components are kept regardless of their shape. The values of these parameters are chosen empirically aiming for background noise suppression, and at the same time retention of NV regions that are identified as PDR.

4.1.1.3 Tensor voting

We detect the junctions by decomposing the second order tensor $\mathbf{T}$ into its eigenvalues (λ_1, λ_2), and measuring the ballness measure (λ_2) there :

$$\mathbf{T} = \lambda_1 \widehat{\mathbf{e}}_1 \widehat{\mathbf{e}}_1^T + \lambda_2 \widehat{\mathbf{e}}_2 \widehat{\mathbf{e}}_2^T = (\lambda_1 - \lambda_2)\, \widehat{\mathbf{e}}_1 \widehat{\mathbf{e}}_1^T + \lambda_2 \left(\widehat{\mathbf{e}}_1 \widehat{\mathbf{e}}_1^T + \widehat{\mathbf{e}}_2 \widehat{\mathbf{e}}_2^T \right),$$

where $\widehat{\mathbf{e}}_{1,2}$ are orthogonal eigenvectors that hold the direction of the inferred lines at each pixel location. Furthermore, scale parameter σ_{TVF} defines the extend of the voting field and subsequently controls the distance in which the neighbor information is taken into account. The ballness measure of the tensor quantifies the local orientation uncertainty of the segmented vessels and it exhibits local maximum there. Since we are interested in extracting information from cluttered vessels low scale value should be used ($\sigma_{\text{TVF}} = 20$). One advantage of using TVF for junction detection is that it can infer the information based on the perceptual organization of the neighbor structures. Morphological processing, on the other hand, is inadequate to detect the junctions if the information is missing.

4.1.1.4 Junction centers isolation

The result of the previous step is a map with junctions as the local maxima on the image. Directly thresholding the map might be efficient, but not as effective as morphological processing. The orientation uncertainty for junctions varies significantly across the image because its value depends on how clutter the neighbor structures of a junction are. Figure 4.2 shows an example where the orientation uncertainty is computed across junctions with ascending clutterness. Thresholding can suppress junctions that have low values. In our method, we first identify the regional maxima by applying the height-domes [263] algorithm. We then isolate the maximum values inside these domes. We morphologically reconstruct the original grayscale image I from $I - h_1$, and then we subtract the result from the input image. This way, whole regions, unlike single pixels that demonstrate local maxima, can be identified.

Additionally, we select the most prominent domes, namely the regions that have height over h_2. The values for the parameters are empirically set to $h_1 = 2600$ and $h_2 = 1400$ and depend on the value of the scale σ_{TVF}. Finally, we merge closely identified junctions that belong to the same region by finding the barycenter in an 11x11 window. Figure 4.3 shows an example of the previous algorithmic steps in an image with NVDs.

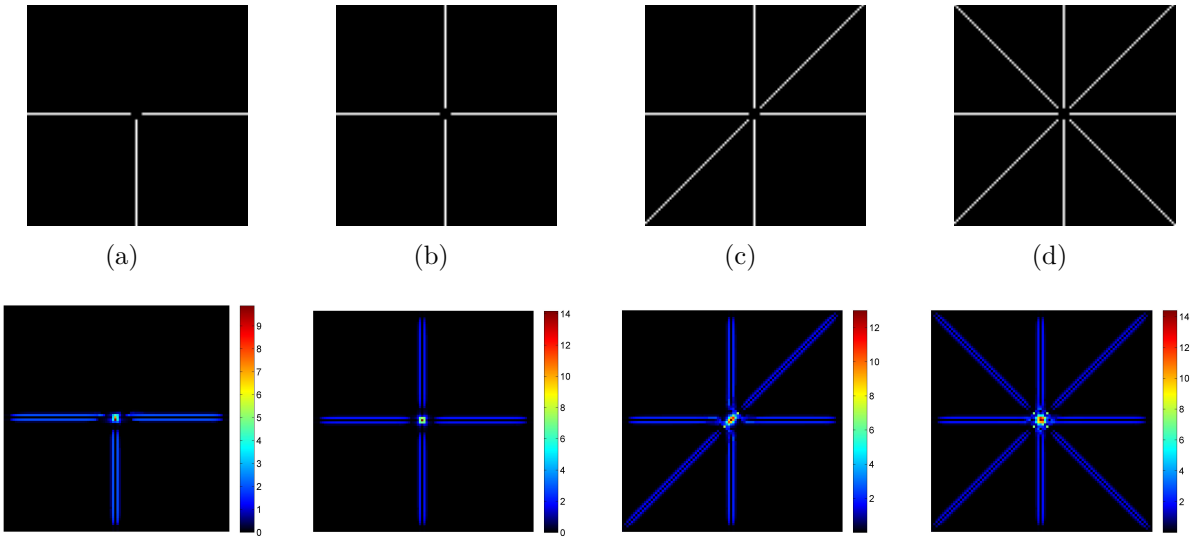

Figure 4.2 The orientation uncertainty in junctions of varying degrees of complexity. The first row (a-d) shows input junctions to TVF that have three (a), four (b), six (c), or eight (d) branches. The second row (e-h) shows the orientation uncertainty value for each junction. Generally, higher order junctions have higher uncertainty.

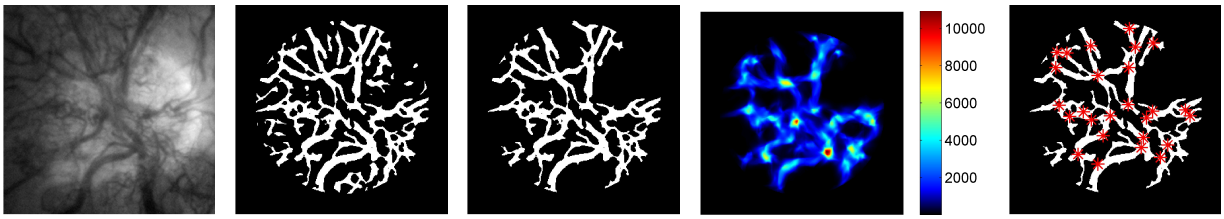

Figure 4.3 Algorithmic steps for the junction center isolation. (a) PDR region, (b) vessel extraction after MSLD, (c) postprocessed result, (d) tensor voting ballness measure, and (e) final detected junction centers.

4.1.2 Features extraction

4.1.2.1 Spatial distribution measures

We compute the following spatial statistics. Two versions of the **dispersion index** defined as : i) the variance over the mean number of junctions (VMR) across the healthy and the PDR group of images, and ii) the mean distance from the center of mass of junctions (VMR (μ_d)). Additionally, we compute two versions of the **Kth-Nearest Neighbor index**. The first is the index described in [264], that in turn is based on the aggregation index R proposed by P.J. Clark [265], and defined as :

$$\text{K}^{\text{th}}\text{-NN}\,(K) = \frac{\text{D(observed)}\,(K)}{\text{D(random)}\,(K)} = \frac{\frac{\sum_{i=1}^{K}\mu(d_i)}{N}}{\frac{K(2K)!}{(2^K!)^2\sqrt{\rho}}},$$

where $\mu\,(d_i)$ is the mean nearest Kth-order neighbor distance between all the junctions, N is the number of points, and ρ is the density. The second version of the measure is just the numerator of the index, without the comparison against the random distribution which is also a second-order statistic that can quantify the spatial arrangement.

The first measure can quantify if the arrangement of points, or the area pattern, is more clustered or ordered than if it have been randomly arranged in the same region. The second measure summarizes, in pixels, the inter-junction distances. Both measures are straightforward to compute, and in contrast with the first-order measures they take into account distances. By applying these measures we can study the relative aggregation of the patterns in the two considered cases, the healthy and the PDR. Therefore, we can investigate if the assumption that the vessel junctions are denser in PDR holds. It also allow us to study the spatial interactions between the junctions that give rise to the formation of the specific pattern in each case. Finally, Kth-order neighbor index is a second-order characteristic.

4.1.3 Classification Protocol

We assess the benefit of "incorporating" the newly proposed measures for classifying regions to PDR. For that reason, we extract 21 features from each region, that were first proposed in the literature [220, 230]. Furthermore, we include the following that were also proposed in [229] : local entropy, measurements on the gray-level co-occurrence matrix (GLCM), and the proposed spatial distribution measures up to the 20th order for the Kth-NN case. Additionally, we compute the mean, median, minimum, maximum values of the new measures, as well as the slope of a linear function fitted on the proposed measures in Section 4.1.2.1. In total, 88 features thus are considered. We use a wrapper method for forward feature selection using a

support vector machine (SVM) with an RBF kernel, as in [220, 230]. We dedicate 2/3 of the whole set for training and validation, and the rest for testing.

4.2 Results and Discussion

We perform our analysis in images collected from 5 databases (Diaretdb [266], HRF [63], Messidor [251], Kaggle [267], and a private one). In order to compare the healthy and the abnormal junctions we confine our analysis at a region-level.

4.2.1 Anatomically Corresponding Regions

We apply the spatial point pattern analysis in anatomically corresponding circular regions. Confining the analysis on anatomically corresponding regions removes the user influence from the healthy region selection process. It also allows, up to a degree, an introduction of natural variance in the collected data. Generally, two regions from different images are corresponding if they are in approximately similar locations in the available field of view (FOV). A trained member isolated 114 regions with NVs from the 5 databases, each region originating from a single image. Then we transform the NV center into polar coordinates (R, ϕ). With R being the distance, in optic disc (OD) radius, between the OD center and the NV center, while ϕ is the angle. In the healthy images we select the regions that are at R distance and ϕ angle with respect to the OD, manually adjusting if the center is found outside of the FOV. Thus, each NV region is compared to a set of healthy regions. The area of the selected regions was set to one fifth of the total FOV area of each image. The healthy group of images contained 99 images. Overall, 5688 regions from the healthy group are compared with 114 abnormal regions. We perform the spatial analysis using the measures described in Section 4.1.3. Figure 4.4 shows an isolated region with NVDs along with the corresponding regions from the healthy cases. For each region we provide the segmented vessels with superimposed the junctions.

4.2.2 Result on First-order Measure

The boxplot in Figure 4.5(a) shows the results on the number of junctions for the two cases. Generally, there is an overlap between the healthy and the diabetic groups. Even though we have a denser pattern in the PDR cases, just counting the number of junctions is not enough to highlight any differences between the healthy and the PDR group.

4.2.3 Dispersion Indices

The value for the dispersion is different for the two groups for both measures (Table 4.1). Both the healthy and the PDR regions are over-dispersed with respect to the mean number

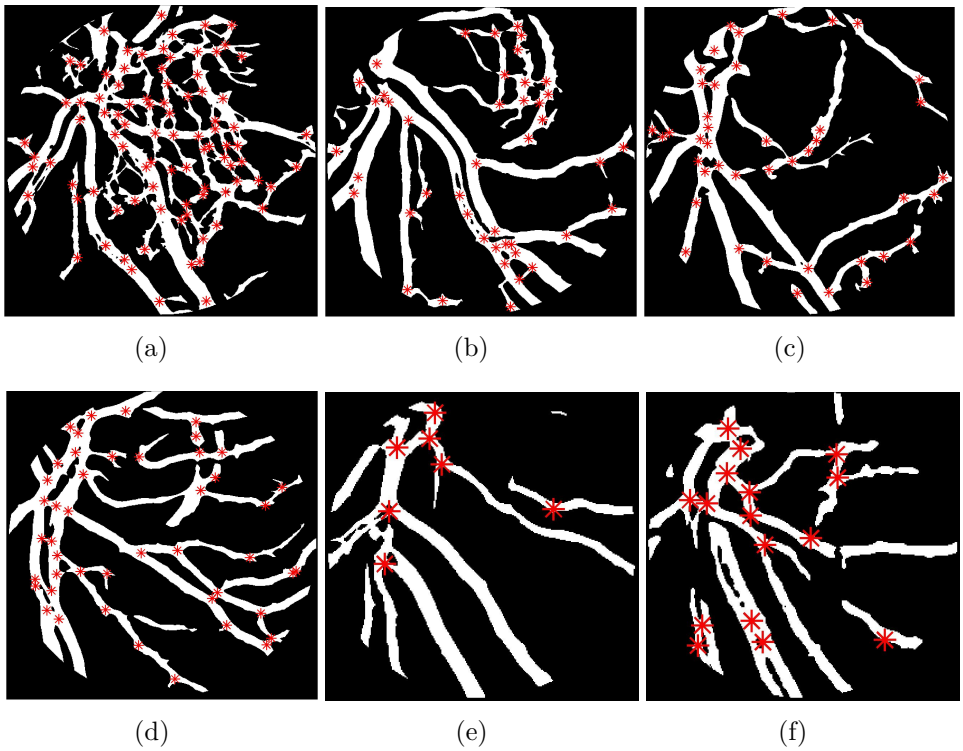

Figure 4.4 Isolated areas and junctions for analysis in HRF and Messidor database. (a) PDR region, (b-f) anatomically corresponding healthy areas together with superimposed their isolated junctions (red stars).

of junctions. According to this measure, there are many instances where the count of junctions is higher or lower than the mean value of the corresponding group. Furthermore, the junctions are approximately 3 pixels closer to the center of mass of junctions, an artificially generated reference point, when a PDR case is encountered. These measure are not sensitive to the spatial arrangement of junctions in each region so they are invariant to changes in the underlying pattern, namely they cannot distinguish between a dense or a scattered pattern.

4.2.4 Kth-Order Nearest Neighbor Indices

The two measures based on Kth-NN (K) take into account the inter-junction distances. The Kth-order index includes the $K = 1$ case which only examines the nearest neighbor. Higher order nearest neighbors better highlight the differences between the two considered groups. The graphs in Figures 4.5(b) and 4.5(c) show the results. For the first case, values under one show that the arrangement of points, or the area pattern, is more clustered than the random distribution. In PDR, we have a generally more clustered pattern than the healthy regions (20th-order Mann-Whitney U-test : $p<0.05$). Furthermore, we show that the mean inter-junction distance, when it is not compared against the random distribution, is considerable

lower for the diabetic than the healthy group (20th-order Mann-Whitney U-test : p<0.05).

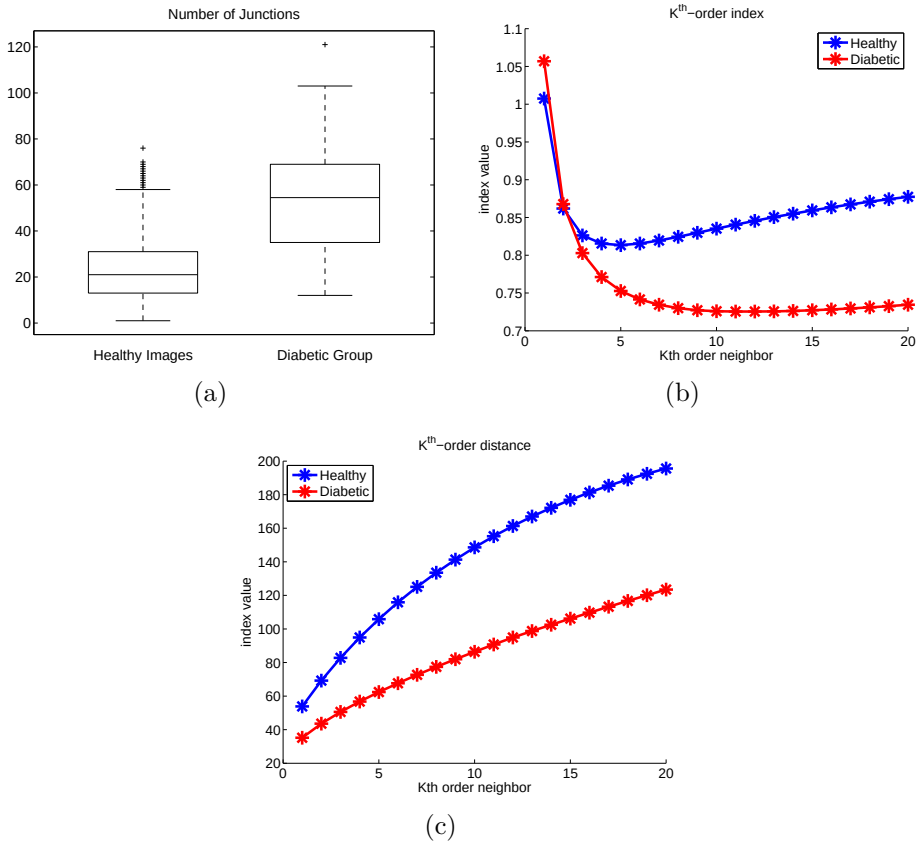

Figure 4.5 (a) Boxplot of junction counts. (b) Kth-order index measurements over the expected random distribution of the junctions. (c) Kth-order distance of the junctions for each group.

4.2.5 Classification

We apply a 10-fold feature selection process on two different feature sets : (a) including 39 features proposed in the literature, and (b) including 88 features, with 49 newly proposed. In both cases the following features are selected : mean vessel wall gradient (Wall (μ_{∇})), number of junctions obtained by skeletonizing the segmented vessels (Skel (J)), mean gray level $(Seg\,(\mu_I))$, mean local gray level (μ_I), and local entropy (E). Additionally, in the (a) case the number of vessel orientations (Dir_N) is included, while in the (b) case the Kth-NN (2) without the random comparison is added. Replacing the number of vessel orientations with the proposed second-order feature improves the classification sensitivity by approximately 9%, and slightly the accuracy (Table 4.2).

Table 4.1 Dispersion indices across the different cases

Category	VMR	VMR (μ_d)
$Healthy$	8.95	11.13
PDR	7.14	8.26

Table 4.2 Classification performance per feature set case

Selected Features	Sensitivity	Specificity	Accuracy	Precision
(a) feature set	75.76%	99.94%	99.48%	96.15%
(b) feature set	84.85%	99.94%	99.66%	96.55%

4.3 Conclusion

In this chapter we proposed a new method for the characterization of the retinal blood vessels. This is important in the direction of assisting the physician in the effective detection of this category of vessels. For the first time, TVF is applied for the vessel characterization problem as well as the distribution analysis of junctions with measures that originate from the spatial point pattern analysis theory. We observe significant differences between healthy and regions with PDR when we apply our analysis. Finally, including the $\mathrm{K^{th}}$-NN (K) distance measure improves the classification performance.

Accurate a priori information about the vessel location is crucial for the junction detection step. TVF infers the information from the neighborhood so it can partially compensate for missed segmentation at junctions which is not the case for junction detection from the skeleton. In parallel, the postprocessing and the center isolation step ensure the suppression of irrelevant junctions. However, their parameter values are empirically set. Future work will focus towards the application of the proposed methodology for accomplishing the detection task. This could be achieved by training the features on non-proliferative diabetic retinopathy cases and then testing on whole images. Moreover, higher order tensors could be used to resolve the orientation uncertainty problem, and thus distinguish junctions from crossings. This could allow to further study the differences in the distribution of different kinds of vessel junctions under healthy or abnormal cases.

CHAPTER 5 GENERAL DISCUSSION

This chapter will summarize the scientific contributions with respect to the state-of-the art. It will also highlight the limits of the methodology, and discuss possible future developments.

5.1 Work summary

The main objective of the research was to propose and validate a method targeted towards the realization of a CAD system for diabetic retinopathy. This system could, in turn, assist the physician in the detection and diagnosis of sight-threatening diabetic retinopathy under different scenarios. This thesis focused on the earliest stages of the pipeline of a potentially usable system, namely the segmentation and the characterization step of the vessels. Both steps are crucial for the success of most of the systems. The previous chapters presented two contributions to the scientific community.

Firstly, we proposed a new methodology for the retinal vessel segmentation problem. A local linearity criterion is considered for the vessels by several existing methods, including the multi-scale line detector. We eliminated the assumption that the vessels have to be piecewise straight to be detected by combining the MSLD with the tensor voting framework. Tensor voting works as an inference engine, propagating structural, directional, and orientation uncertainty information. Moreover, the method models the visual perception and not directly the vessels. Therefore it offers better generalization than other methods that try to model a specific object of interest. For the first objective, we utilized the structural and directional information provided by tensor voting to reconnect fragmented small vessels. While tensor voting scale parameter can reconnect curves at a specific distance, vessels appear fragmented at variable distances closer or more distant than the response from a specific value of the parameter. Therefore, we proposed multiple scales for the structural reconnection. In our method, we use all the centerlines from the scales to better support the existence of a centerline at a specific location. Then, we fuse the multiple centerlines into a single more representative one using local tracking, and the direction information provided by TVF. The existing algorithms stop when the centerline is segmented, however, subsequent steps in CAD systems require full vasculature to perform detection. Therefore, in parallel to the local tracking small vessels' width is reconstructed by pixel painting perpendicularly to the curve direction. Finally, the multi-scale line detector threshold value is computed using a globally adaptive method which is faster than if a more locally adaptive method has been used. The result of our method is a fully connected vasculature without fragmented vessels, and with reduced background noise.

The existing methods are validated globally using the standard discrepancy measures, however the major vessels contribute more than the minor to the performance results. Instead, the validation of the new methodology was tested not only globally, but also on isolated small vessels from high-resolution fundus images. Therefore, our protocol is more comprehensive on validating new retinal vessel segmentation methods.

The second contribution concerns the characterization of regions to healthy or proliferative. Building on the multi-scale line segmentor, and relying on the orientation uncertainty information provided by TVF we extract features that facilitate the characterization of vessels to healthy or proliferative. The existing methods detect junctions using mathematical morphology, which is an unreliable way when information is missing. Instead, we use a perceptual way, via single-scale TVF, to compensate for the missed segmentation information, and detect the junctions. Then, a new category of features is applied that measure second-order information. Computing the inter-junction distances is a reliable way to incorporate second-order information, as junctions is a more stable anatomical landmark than other vascular features like the center of the vessels. Employing the new features into a standard classification protocol improves the recognition performance of neovascularizations, compared to the case when already existing features are used.

5.2 Limitations of the proposed solution and future perspectives

This thesis introduced two main contributions to the scientific community, however the work is far from complete. Based on the presented developments, we will highlight the limitations of our method, and possible directions of research to further advance the retinal imaging field.

5.2.1 Vessel segmentation limits

The most important shortcoming is that the segmentation methodology developed for the first contribution is not extended to the neovascularization segmentation problem. The proposed segmentation method does not actively exploit all the available information provided by the tensor voting framework. Finally, it is not fully automatic and demonstrates high computational cost.

The local tracking process stops or tracks a single branch if it encounters a junction. This is caused by the high orientation uncertainty at junctions that is not actively taken into account, and thus centerline fragments under non-maximal suppression, consequently stopping the tracking process. Neovascularizations are lesions with an increased number of junctions, so the current approach does not improve the segmentation of the MSLD step there. During tracking, we do not consider the high orientation uncertainty, or λ_2, to track

multiple branches, the framework is also limited by the utilization of second-order tensors that are insufficient at directly detecting junctions. Moreover, the small vessel reconstruction from the local tracking step is not optimal. The propagated width is just the diameter of the preceding large vessel bounded by the definition of the small vessels, which is not adaptive enough to compensate for different caliber of small vessels. Initially, we were using a more adaptive approach where Gaussian fitting on the saliency profile along all the TVF scales, averaging the acquired estimation of vessel diameter. However, this was abandoned because it was approximately 200 times slower than the current approach, and hard to motivate the steps. Finally, advanced pathology can affect the large vessels, so an unreliable medium-to-large vessel segmentation result could be obtained from MSLD, further hampering the small vessel reconnection and tracking steps.

The vessel tracking method is not fully automatic. It requires the detection of the optic disc and the initiation of the tracking step from there. Additionally, the whole pipeline is not free of tunable parameters. For the first two steps, the preprocessing and the MSLD, the values depend on the utilized acquisition of the data. In the second contribution, we manage to automate the adaptive thresholding stage. Still, many more steps have to be optimized in order for our algorithm to become fully automatic. The vessel segmentation method was validated only on high-resolution images. Even though high-resolution data are more relevant, as more advanced cameras are common in the clinical setting, we have to validate the method on standard lower resolution databases (DRIVE, STARE) to have a better comparison against other available methods. However, in order to achieve that we have to first tune the parameter of the method for the specifications of these databases.

The proposed approach could be deployed into a comprehensive CAD system where vessels are firstly segmented, and then lesion analysis is performed to detect diabetic retinopathy at different stages. However, the required computational resources are very high for the utilized tensor voting framework, in term of execution speed, and this limits its applicability. Even though the execution is done on the graphical processing unit the expended time is high, in the order of hundreds of seconds per scale, and not constant. Namely, it depends on the size of the voting field (σ_{TVF}). Additionally, other components of the algorithm further hinder the execution time.

5.2.2 Vessel characterization limits

For the second contribution, our method heavily relies on the vessels segmentation performance. The proposed segmentation approach inherits the non-robusteness of the MSLD method to lesions. The postprocessing step partially compensates this. Then the method proceeds to the feature extraction from the extracted vessels. Besides all the problems related to

the segmentation, there are additional parameters for the junction center detection, some of which are tuned empirically. Finally, we do not examine the robustness of the classification method to non-proliferative diabetic retinopathy cases.

Another limitation that is not covered by the current as well as the existing studies is the discrimination between similar categories of abnormal vessels. As diabetic retinopathy progresses from non-proliferative to proliferative stage two categories of tortuous vessels can exist : 1) Intra-retinal microvascular abnormalities (IRMAs) and 2) neovascularizations (NVs). Although both have similar appearance, their similarities are limited, up to some degree, only to their morphological characteristics. Each one has different functional characteristics, visible under angiography, and their appearance reflects the different severity of the disease. As far as we are concerned, the issue of distinguishing between IRMAs, NVs, and healthy vessels has not been investigated in the literature.

5.2.3 Future developments

The aforementioned limitations can lead to new developments that are necessary for the direction of realizing a comprehensive CAD system for sight-threatening diabetic retinopathy. We could further exploit the utilized information provided by the tensor voting framework, modify certain algorithmic as well as computational aspects at the MTVF, the local tracking, and the vessel reconnection steps. Finally, improve the vessel characterization step.

For example, a possible extension of the method would be to actively search for high orientation uncertainty, or λ_2, during tracking to reconnect fragmented branches. However, there are two main issues that should be first addressed. Firstly, the maximum response of orientation uncertainty is not located on an exact vessel location, and thus a large searching area is needed, potentially risking tracking noise. Secondly, the local tracking has to examine what is reconnected not only from the segmented structures point of view, e.g. linear structures that gave high MSLD responses, but also from another feature perspective to avoid reconnecting lesions, or irrelevant background noise. A different approach is to use higher than second order tensors that can compensate for the orientation uncertainty, and therefore minimize the centerline fragmentation around junctions. For the computational resources issue, another possible direction is to use the tensor voting implemented via steerable filtering as it was proposed in [211]. This method is an approximation of the original TVF that has a very low constant execution time of 8 seconds regardless of the scale for images of the HRF database. However, the alternative implementation is an approximation to the original TVF [217], and thus a comprehensive assessment of the centerline extraction performance should be first performed before it is being applied to our problem. Finally, for the small vessel reconstruction, a different approach is to infer the small vessel diameter information from

the neighborhood of already segmented vessels, namely to reconstruct the width using the binary information before and/or after possible gaps.

The second stage is the characterization stage. We could incorporate regions with NPDR into the characterization step and perform the classification protocol to measure the robustness of the newly proposed features of this thesis. Then, based on the learned descriptors and assuming that the features are robust we could construct a proliferative diabetic retinopathy detector that could work at the region level.

CHAPTER 6 CONCLUSION

This thesis proposed and validated a new algorithm for the segmentation of the smallest retinal vessels. The method combines a standard retinal vessel segmentation method (Section 3.1.2) with a new method adopted from the computer vision field, into a hybrid scheme, for the perceptual reconnection of curves. Besides the combination, which is novel, important algorithmic aspects were incorporated into the method. Firstly, to achieve better initial segmentation for the vessels global adaptive thresholding is applied (Section 3.1.3). The perceptual reconnection of curves at variable distances is achieved by multiple scales (Section 3.1.4). Finally, for the width reconstruction of the small vessels pixel painting is applied (Section 3.1.5).

The new algorithm was compared against the standard vessel segmentation method improving the sensitivity by 4%. Moreover, we confined the analysis on the small vessels, which is a new way to examine the limits of the segmentation algorithms. The new method improved the sensitivity difference even further to a difference of 6.47%.

This thesis also proposed a new approach for characterizing regions with already segmented vessels to healthy or proliferative. The method achieves the junction extraction in a perceptual way by exploiting the TVF orientation uncertainty (Section 4.1.1). Then, we extracted new features that when they are incorporated into existing one can improve the classification of regions to healthy or proliferative by approximately 9%. The new features are adopted from the spatial statistics field. They measure second-order information by incorporating the inter-junction distance information (Section 4.1.2).

6.1 Future research work

6.1.1 Tensor voting

There are several directions for future work. In the tensor voting framework, and consequently in our work, second order tensors are used for curve segmentation and orientation uncertainty estimation. Three research directions could be investigated.

Higher order tensor can be used to resolve the orientation uncertainty at junctions, distinguish between junctions and crossings, or even facilitate the local tracking. The study in [268] applied higher order tensor voting for resolving fiber crossings in brain MRI data. Figure 6.1 shows an example, in 3D, of how second-order tensors are unable to give direction information, instead sixth-order tensors can resolve the different directions.

In connection to the previous, several important concepts are introduced and applied in the TVF method, such as second-order tensors for data representation, tensor addition for

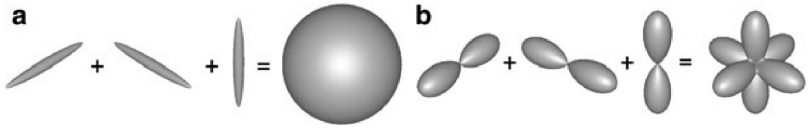

Figure 6.1 Second order versus higher order tensors on resolving a 3D crossing. (a) Second-order tensors have no directional information. (b) Instead, sixth-order tensors can give high local values perpendicularly to their direction [19].

vote accumulation, and spectral analysis for saliency and orientation uncertainty extraction. These concepts are part of a recent branch of mathematics, the tensor calculus that could inspire us to use new tools to analyze even further the vector field data with different formalized ways adopted from this branch of mathematics. In the same direction, R. Duits et al. [218] defined tensor voting as part of the Lie group, a mathematical set theory. Figure 6.2 shows an example of their method for extracting curves. Tensors are also used to represent the data in machine learning, and more particularly deep learning, so probably there might be a link between tensor voting and machine learning.

Tensor voting is an effort to model the human visual perception by formalizing the Gestalt theory. Currently, the framework incorporates three basic rules for the perceptual grouping, namely the proximity, the similarity, and the good continuation criteria. Therefore, another direction of research is to incorporate into the model the rest of the rules as well as global gestalt principles such as their interactions, conflicts, and masking effects between the laws [269]. These will lead to a more complete model for visual perception. Figure 6.3 shows examples of series where gestalt principles for grouping are applied.

6.1.2 Discrepancy measures

The segmentation algorithms are assessed using standard discrepancy measures. New better measures could be proposed that take into account the differences between the large, the small, as well as other categories of lesions (neovascularizations). These new measures could weight a pixel, from the reference image, according to the vessel caliber. Another direction is to develop perceptual measures that utilize special psychometric functions [236] for different kind of lesions or artifacts.

19. New Developments in the Visualization and Processing of Tensor Fields, Towards resolving fiber crossings with higher order tensor inpainting, 2012, page 253-265, T. Schultz, With permission of Springer, [268]

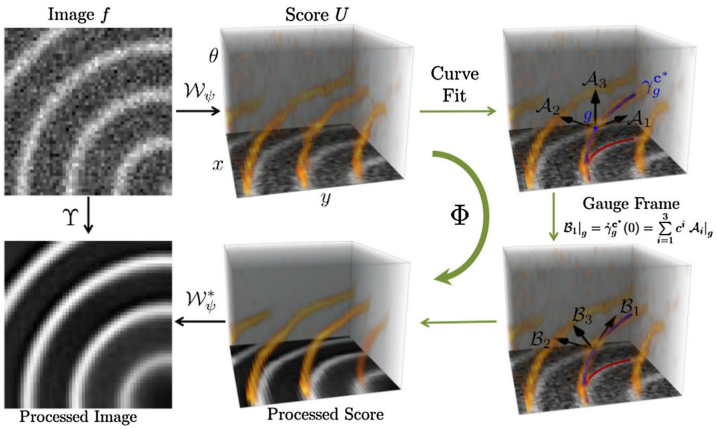

Figure 6.2 Duits et al. pipeline for curve extraction. The curves are described in a new domain, the roto-translation frame, where curves are defined as series of simpler functions [218] ((c) R. Duits et al., 2016).

Figure 6.3 Example of the Gestalt principles for grouping. From top left to right : color constancy and proximity, similarity of shape and texture, good continuation, closure, convexity, parallelism, amodal completion, color constancy, good continuation, closure and continuation, and modal completion [20].

6.1.3 Spatial point processes and neovascularizations

The second-order metrics applied in this thesis are adopted from the spatial point process field, a recognized scientific field for the statistical investigation of spatial patterns. There are many more features that could be investigated that have been proposed for other applications [270, 271]. Besides measuring second order information, we can infer the process that gives rise to an examined spatial pattern, and even model it. For example, it has been observed that the healthy angiogenesis, as well as the unhealthy neovascularization, is guided by interactions

20. From gestalt theory to image analysis : a probabilistic approach, 2007, vol. 34, A. Desolneux et al., With permission of Springer [269]

between neurons and vessels that are biochemically regulated [15]. In our experiments in Chapter 4 we proved that the process that gives rise to the junctions not only is not random for the healthy and proliferative regions, but it is also different for the two process, which is supported by the literature [272]. Therefore, we can use the tools from the spatial point process field to analyze the data from a different perspective.

There is a lack of proliferative diabetic retinopathy data because the sign is at the latest stage and therefore rare. We can try to overcome this problem by simulating the neovascularization. Even though there has been a study [249] where the authors generated artificial neovascularizations based on random walk, the developed model is very simple incorporating only a single parameter. However, we can be inspired by other studies where they try to model the growth of neovascularizations in other systems and diseases [273] by taking into account more parameters, such as the remodelling of the diameters, the ageing of the network, the chemical response to the VEGF, and the branching/bifurcations. The artificial neovascularization generation method could also be combined with a learned spatial point process model constructed on real data, to select only the NVs that satisfy some conditions. Another completely different approach is to utilize deep learning to simulate more data [274].

6.1.4 Other applications

The work described in this thesis can lay the foundations for new CAD systems for the detection of sight-threatening diabetic retinopathy. The segmentation of smaller vessels can eventually lead to a reduction of false positives, as misrecognized vessels can be falsely detected as lesions in the latest stages of a CAD pipeline. Other retinopathies, equally significant to diabetic complications like hypertension, glaucoma, or cataract that might affect the acquisition as well as the appearance of the vessels co-exist. An effective CAD system should take into account these too. Finally, our approach is tailored to fundus images, and diabetic retinopathy pathologies. The proposed methods could be tested to other 2D/3D imaging modalities (e.g. MRI/X-ray/CT angiography), pathologies, as well as ocular OCT, interventional OCT for retinal microsurgery, hyperspectral imaging, retinal fluoroscopy, and for the detection of other similar to the vessels anatomical structures like neurons from microscopy.

REFERENCES

[1] World Health Organisation, "Prevention of blindness from diabetes mellitus : report of who consulation in gevena, switzerland 9-11 november 2005," November 2005.

[2] C. Keeler, "The ophthalmoscope in the lifetime of hermann von helmholtz," *Archives of Ophthalmology*, vol. 120, no. 2, pp. 194–201, 2002. [Online]. Available : +http://dx.doi.org/10.1001/archopht.120.2.194

[3] T. Duane, W. Tasman, and E. Jaeger, *Duane's Ophthalmology 2006*. Lippincott Williams & Wilkins, 2006.

[4] G. A. Williams, I. U. Scott, J. A. Haller, A. M. Maguire, D. Marcus, and H. McDonald, "Single-field fundus photography for diabetic retinopathy screening : A report by the american academy of ophthalmology," *Ophthalmology*, vol. 111, no. 5, pp. 1055–1062, 2004.

[5] R. L. Drake, A. Wayne, and A. W. Mitchell, *Gray's anatomy for students*, 3rd ed. Churchill Livingstone, February 2013.

[6] E. D. Hilton, *Retina*, 5th ed. Elsevier, 2012.

[7] D. Hubel, *Eye, Brain, and Vision*, ser. Scientific American Library Series. Henry Holt and Company, 1995. [Online]. Available : http://books.google.ca/books?id=2Id9QgAACAAJ

[8] H. Kolb, "How the retina works," *Amer. Scientist*, vol. 91, no. 1, pp. 28–35, 2003.

[9] J. Werner and L. Chalupa, *The Visual Neurosciences*. MIT Press, 2004.

[10] D. Huang, E. Swanson, C. Lin, J. Schuman, W. Stinson, W. Chang, M. Hee, T. Flotte, K. Gregory, C. A. Puliafito *et al.*, "Optical coherence tomography," *Science*, vol. 254, no. 5035, pp. 1178–1181, 1991.

[11] E. A. Kimbrel and R. Lanza, "Current status of pluripotent stem cells : moving the first therapies to the clinic," *Nature Reviews Drug Discovery*, 2015.

[12] C. V. Network, "Developmental anatomy of the retinal and choroidal vasculature," *The Retina and Its Disorders*, p. 179, 2011.

[13] S. S. Hayreh, M. Zimmerman, A. Kimura, and A. Sanon, "Central retinal artery occlusion. : Retinal survival time," *Experimental Eye Research*, vol. 78, no. 3, pp. 723–736, 2004.

[14] M. D. Abràmoff, M. K. Garvin, and M. Sonka, "Retinal imaging and image analysis," *Biomedical Engineering, IEEE Reviews in*, vol. 3, pp. 169–208, 2010.

[15] R. F. Gariano and T. W. Gardner, "Retinal angiogenesis in development and disease," *Nature*, vol. 438, no. 7070, pp. 960–966, 2004.

[16] D. B. Archer, "Diabetic retinopathy : some cellular, molecular and therapeutic considerations," *Eye*, vol. 13, no. 4, pp. 497–523, 1999.

[17] H. F. Jelinek and M. J. Cree, *Automated image detection of retinal pathology.* CRC Press, 2010.

[18] S. Melmed, K. S. Polonsky, P. R. Larsen, and H. M. Kronenberg, *Williams Textbook of Endocrinology : Expert Consult.* Elsevier Health Sciences, 2011.

[19] J. W. Miller, A. P. Adamis, and L. P. Aiello, "Vascular endothelial growth factor in ocular neovascularization and proliferative diabetic retinopathy," *Diabetes/metabolism reviews*, vol. 13, no. 1, pp. 37–50, 1997.

[20] M. D. Davis, M. R. Fisher, R. E. Gangnon, F. Barton, L. M. Aiello, E. Y. Chew, F. Ferris, G. L. Knatterud *et al.*, "Risk factors for high-risk proliferative diabetic retinopathy and severe visual loss : Early treatment diabetic retinopathy study report# 18." *Investigative ophthalmology & visual science*, vol. 39, no. 2, pp. 233–252, 1998.

[21] *Diabetic Retinopathy Guidelines.* Royal College of Ophthalmologists, December 2012.

[22] T. Y. Wong, M. Mwamburi, R. Klein, M. Larsen, H. Flynn, M. Hernandez-Medina, G. Ranganathan, B. Wirostko, A. Pleil, and P. Mitchell, "Rates of progression in diabetic retinopathy during different time periods a systematic review and meta-analysis," *Diabetes Care*, vol. 32, no. 12, pp. 2307–2313, 2009.

[23] J. Wilson and G. Jungner, "Principles and practice of screening," *WHO : Geneva*, 1968.

[24] P. Scanlon, "The english national screening programme for sight-threatening diabetic retinopathy," *Journal of Medical Screening*, vol. 15, no. 1, pp. 1–4, 2008.

[25] D. Y. Lin, M. S. Blumenkranz, R. J. Brothers, and D. M. Grosvenor, "The sensitivity and specificity of single-field nonmydriatic monochromatic digital fundus photography with remote image interpretation for diabetic retinopathy screening : a comparison with ophthalmoscopy and standardized mydriatic color photography," *American journal of ophthalmology*, vol. 134, no. 2, pp. 204–213, 2002.

[26] D. Maberley, H. Walker, A. Koushik, and A. Cruess, "Screening for diabetic retinopathy in James Bay, Ontario : a cost-effectiveness analysis," *Canadian Medical Association Journal*, vol. 168, no. 2, pp. 160–164, 2003.

[27] DRSSW, "Diabetic Retinopathy Screening Service for Wales," http://www.cardiffandvaleuhb.wales.nhs.uk/page/42582, 2013, [Online ; accessed 17-March-2013].

[28] D. A. Askew, L. Crossland, R. S. Ware, S. Begg, P. Cranstoun, P. Mitchell, and C. L. Jackson, "Diabetic retinopathy screening and monitoring of early stage disease in general practice : Design and methods," *Contemporary Clinical Trials*, vol. 33, pp. 969–975, 2012.

[29] M. Philip Hooper, M. C. Boucher, M. Alan Cruess, K. G. Dawson, M. Walter Delpero, M. Mark Greve, M. Vladimir Kozousek, M. Wai-Ching Lam, and D. A. Maberley, "Canadian ophthalmological society evidence-based clinical practice guidelines for the management of diabetic retinopathy," *Can J Ophthalmol*, vol. 47, pp. 1–30, 2012.

[30] M. D. Abramoff, M. Niemeijer, and S. R. Russell, "Automated detection of diabetic retinopathy : barriers to translation into clinical practice," *Expert review of medical devices*, vol. 7, no. 2, pp. 287–296, 2010.

[31] Retinacheck project. Accessed : 2016-11-10. [Online]. Available : http://www.retinacheck.org/research

[32] P. Hooper, M.-C. Boucher, K. Colleaux, A. Cruess, M. Greve, W.-C. Lam, S. Shortt, and E. Tourville, "Contemporary management of diabetic retinopathy in Canada : from guidelines to algorithms guidance," *Opthalmologica*, vol. 231, no. 1, pp. 1–14, 2013.

[33] C. A. Glasbey and G. W. Horgan, *Image analysis for the biological sciences*. John Wiley & Sons New York, 1995.

[34] M. R. K. Mookiah, U. R. Acharya, C. K. Chua, C. M. Lim, E. Ng, and A. Laude, "Computer-aided diagnosis of diabetic retinopathy : A review," *Computers in biology and medicine*, vol. 43, no. 12, pp. 2136–2155, 2013.

[35] M. M. Fraz, P. Remagnino, A. Hoppe, B. Uyyanonvara, A. R. Rudnicka, C. G. Owen, and S. A. Barman, "Blood vessel segmentation methodologies in retinal images–a survey," *Computer methods and programs in biomedicine*, vol. 108, no. 1, pp. 407–433, 2012.

[36] D. Lesage, E. D. Angelini, I. Bloch, and G. Funka-Lea, "A review of 3d vessel lumen segmentation techniques : Models, features and extraction schemes," *Medical image analysis*, vol. 13, no. 6, pp. 819–845, 2009.

[37] K. Bühler, P. Felkel, and A. La Cruz, *Geometric methods for vessel visualization and quantification-a survey*. Springer, 2004.

[38] W. K. Pratt, *Digital image processing*. New York, London : John Wiley & Sons, Inc., 2001.

[39] S. Chaudhuri, S. Chatterjee, N. Katz, M. Nelson, and M. Goldbaum, "Detection of blood vessels in retinal images using two-dimensional matched filters," *Medical Imaging, IEEE Transactions on*, vol. 8, no. 3, pp. 263–269, 1989.

[40] C.-Y. Lin and Y.-T. Ching, "Extraction of coronary arterial tree using cine x-ray angiograms," *Biomedical Engineering : Applications, Basis and Communications*, vol. 17, no. 03, pp. 111–120, 2005.

[41] K. A. Al-Kofahi, S. Lasek, D. H. Szarowski, C. J. Pace, G. Nagy, J. N. Turner, and B. Roysam, "Rapid automated three-dimensional tracing of neurons from confocal image stacks," *Information Technology in Biomedicine, IEEE Transactions on*, vol. 6, no. 2, pp. 171–187, 2002.

[42] J. Jan, J. Odstrcilik, J. Gazarek, and R. Kolár, "Retinal image analysis aimed at blood vessel tree segmentation and early detection of neural-layer deterioration," *Computerized Medical Imaging and Graphics*, vol. 36, no. 6, pp. 431–441, 2012.

[43] R. Annunziata, A. Kheirkhah, S. Aggarwal, P. Hamrah, and E. Trucco, "A fully automated tortuosity quantification system with application to corneal nerve fibres in confocal microscopy images," *Medical image analysis*, vol. 32, pp. 216–232, 2016.

[44] B. Zhang, L. Zhang, L. Zhang, and F. Karray, "Retinal vessel extraction by matched filter with first-order derivative of Gaussian," *Computers in biology and medicine*, vol. 40, no. 4, pp. 438–445, 2010.

[45] A. Hoover, V. Kouznetsova, and M. Goldbaum, "Locating blood vessels in retinal images by piecewise threshold probing of a matched filter response," *Medical Imaging, IEEE Transactions on*, vol. 19, no. 3, pp. 203–210, 2000.

[46] N.-X. Lion, V. Zagorodnov, and Y.-P. Tan, "Retinal vessel detection using self-matched filtering," in *Image Processing, 2007. ICIP 2007. IEEE International Conference on*, vol. 6. IEEE, 2007, pp. VI–33.

[47] M. Al-Rawi, M. Qutaishat, and M. Arrar, "An improved matched filter for blood vessel detection of digital retinal images," *Computers in Biology and Medicine*, vol. 37, no. 2, pp. 262–267, 2007.

[48] D. A. Roberts, "Analysis of vessel absorption profiles in retinal oximetry," *Medical physics*, vol. 14, p. 124, 1987.

[49] L. Gang, O. Chutatape, and S. M. Krishnan, "Detection and measurement of retinal vessels in fundus images using amplitude modified second-order Gaussian filter," *Biomedical Engineering, IEEE Transactions on*, vol. 49, no. 2, pp. 168–172, 2002.

[50] H. Narasimha-Iyer, J. M. Beach, B. Khoobehi, and B. Roysam, "Automatic identification of retinal arteries and veins from dual-wavelength images using structural and functional features," *Biomedical Engineering, IEEE Transactions on*, vol. 54, no. 8, pp. 1427–1435, 2007.

[51] J. Lowell, A. Hunter, D. Steel, A. Basu, R. Ryder, and R. L. Kennedy, "Measurement of retinal vessel widths from fundus images based on 2-d modeling," *Medical Imaging, IEEE Transactions on*, vol. 23, no. 10, pp. 1196–1204, 2004.

[52] K. A. Vermeer, F. M. Vos, H. Lemij, and A. M. Vossepoel, "A model based method for retinal blood vessel detection," *Computers in Biology and Medicine*, vol. 34, no. 3, pp. 209–219, 2004.

[53] L. Wang, A. Bhalerao, and R. Wilson, "Analysis of retinal vasculature using a multiresolution hermite model," *Medical Imaging, IEEE Transactions on*, vol. 26, no. 2, pp. 137–152, 2007.

[54] L. Wang and A. Bhalerao, "Detecting branching structures using local gaussian models," in *Biomedical Imaging, 2002. Proceedings. 2002 IEEE International Symposium on.* IEEE, 2002, pp. 161–164.

[55] N. P. Singh and R. Srivastava, "Retinal blood vessels segmentation by using gumbel probability distribution function based matched filter," *Computer methods and programs in biomedicine*, vol. 129, pp. 40–50, 2016.

[56] D. Zhang, Q. Li, and J. You, "A modified matched filter with double-sided thresholding for screening proliferative diabetic retinopathy," *Information Technology in Biomedicine, IEEE Transactions on*, vol. 13, no. 4, pp. 528–534, 2009.

[57] T. Zhu, "Fourier cross-sectional profile for vessel detection on retinal images," *Computerized Medical Imaging and Graphics*, vol. 34, no. 3, pp. 203–212, 2010.

[58] B. S. Lam, Y. Gao, and A.-C. Liew, "General retinal vessel segmentation using regularization-based multiconcavity modeling," *Medical Imaging, IEEE Transactions on*, vol. 29, no. 7, pp. 1369–1381, 2010.

[59] B. S. Lam and H. Yan, "A novel vessel segmentation algorithm for pathological retina images based on the divergence of vector fields," *Medical Imaging, IEEE Transactions on*, vol. 27, no. 2, pp. 237–246, 2008.

[60] R. M. Haralick, S. R. Sternberg, and X. Zhuang, "Image analysis using mathematical morphology," *Pattern Analysis and Machine Intelligence, IEEE Transactions on*, no. 4, pp. 532–550, 1987.

[61] G. G. Matheron, *Random sets and integral geometry.* New York, London : Wiley, 1975. [Online]. Available : http://opac.inria.fr/record=b1086458

[62] J. Serra, *Image Analysis and Mathematical Morphology*, 1st ed. Academic Press, 1982.

[63] J. Odstrcilik, R. Kolar, A. Budai, J. Hornegger, J. Jan, J. Gazarek, T. Kubena, P. Cernosek, O. Svoboda, and E. Angelopoulou, "Retinal vessel segmentation by improved

matched filtering : evaluation on a new high-resolution fundus image database," *IET Image Processing*, vol. 7, no. 4, pp. 373–383, 2013.

[64] M. E. Martínez-Pérez, A. D. Hughes, A. V. Stanton, S. A. Thom, N. Chapman, A. A. Bharath, and K. H. Parker, "Geometrical and morphological analysis of vascular branches from fundus retinal images," in *Medical Image Computing and Computer-Assisted Intervention–MICCAI 2000*. Springer, 2000, pp. 756–765.

[65] B. D. Thackray and A. C. Nelson, "Semi-automatic segmentation of vascular network images using a rotating structuring element (ROSE) with mathematical morphology and dual feature thresholding," *Medical Imaging, IEEE Transactions on*, vol. 12, no. 3, pp. 385–392, 1993.

[66] A. M. Mendonca and A. Campilho, "Segmentation of retinal blood vessels by combining the detection of centerlines and morphological reconstruction," *Medical Imaging, IEEE Transactions on*, vol. 25, no. 9, pp. 1200–1213, 2006.

[67] M. S. Miri and A. Mahloojifar, "Retinal image analysis using curvelet transform and multistructure elements morphology by reconstruction," *Biomedical Engineering, IEEE Transactions on*, vol. 58, no. 5, pp. 1183–1192, 2011.

[68] F. Zana and J.-C. Klein, "A multimodal registration algorithm of eye fundus images using vessels detection and hough transform," *Medical Imaging, IEEE Transactions on*, vol. 18, no. 5, pp. 419–428, 1999.

[69] ——, "Segmentation of vessel-like patterns using mathematical morphology and curvature evaluation," *Image Processing, IEEE Transactions on*, vol. 10, no. 7, pp. 1010–1019, 2001.

[70] C. Heneghan, J. Flynn, M. Ó Keefe, and M. Cahill, "Characterization of changes in blood vessel width and tortuosity in retinopathy of prematurity using image analysis," *Medical Image Analysis*, vol. 6, no. 4, pp. 407–429, 2002.

[71] T. Walter and J.-C. Klein, "Segmentation of color fundus images of the human retina : Detection of the optic disc and the vascular tree using morphological techniques," in *Medical Data Analysis*. Springer, 2001, pp. 282–287.

[72] E. M. Sigurðsson, S. Valero, J. A. Benediktsson, J. Chanussot, H. Talbot, and E. Stefánsson, "Automatic retinal vessel extraction based on directional mathematical morphology and fuzzy classification," *Pattern Recognition Letters*, vol. 47, pp. 164–171, 2014.

[73] B. Yin, H. Li, B. Sheng, X. Hou, Y. Chen, W. Wu, P. Li, R. Shen, Y. Bao, and W. Jia, "Vessel extraction from non-fluorescein fundus images using orientation-aware detector," *Medical image analysis*, vol. 26, no. 1, pp. 232–242, 2015.

[74] A. Dufour, O. Tankyevych, B. Naegel, H. Talbot, C. Ronse, J. Baruthio, P. Dokládal, and N. Passat, "Filtering and segmentation of 3d angiographic data : Advances based on mathematical morphology," *Medical Image Analysis*, vol. 17, no. 2, pp. 147–164, 2013.

[75] S. R. Deans, "Hough transform from the radon transform," *Pattern Analysis and Machine Intelligence, IEEE Transactions on*, no. 2, pp. 185–188, 1981.

[76] Mathworks documentation : Inverse radon transform definition. Accessed : 2017-02-17. [Online]. Available : https://www.mathworks.com/help/images/the-inverse-radon-transformation.html

[77] R. Zwiggelaar, S. M. Astley, C. R. Boggis, and C. J. Taylor, "Linear structures in mammographic images : detection and classification," *Medical Imaging, IEEE Transactions on*, vol. 23, no. 9, pp. 1077–1086, 2004.

[78] R. N. Czerwinski, D. L. Jones, and W. D. O'Brien Jr, "Detection of lines and boundaries in speckle images-application to medical ultrasound," *Medical Imaging, IEEE Transactions on*, vol. 18, no. 2, pp. 126–136, 1999.

[79] E. Ricci and R. Perfetti, "Retinal blood vessel segmentation using line operators and support vector classification," *Medical Imaging, IEEE Transactions on*, vol. 26, no. 10, pp. 1357–1365, 2007.

[80] U. T. Nguyen, A. Bhuiyan, L. A. Park, and K. Ramamohanarao, "An effective retinal blood vessel segmentation method using multi-scale line detection," *Pattern Recognition*, 2013.

[81] I. Lazar and A. Hajdu, "Retinal microaneurysm detection through local rotating cross-section profile analysis," *Medical Imaging, IEEE Transactions on*, 2013.

[82] L. Giancardo, F. Meriaudeau, T. Karnowski, Y. Li, K. Tobin, and E. Chaum, "Microaneurysm detection with radon transform-based classification on retina images," in *Engineering in Medicine and Biology Society, EMBC, 2011 Annual International Conference of the IEEE*. IEEE, 2011, pp. 5939–5942.

[83] X. You, Q. Peng, Y. Yuan, Y.-m. Cheung, and J. Lei, "Segmentation of retinal blood vessels using the radial projection and semi-supervised approach," *Pattern Recognition*, vol. 44, no. 10, pp. 2314–2324, 2011.

[84] J. Chen, Y. Sato, and S. Tamura, "Orientation space filtering for multiple orientation line segmentation," *Pattern Analysis and Machine Intelligence, IEEE Transactions on*, vol. 22, no. 5, pp. 417–429, 2000.

[85] S. Lu and J. H. Lim, "Automatic optic disc detection from retinal images by a line operator," *Biomedical Engineering, IEEE Transactions on*, vol. 58, no. 1, pp. 88–94, 2011.

[86] M. M. Orkisz, C. Bresson, I. E. Magnin, O. Champin, and P. C. Douek, "Improved vessel visualization in MR angiography by nonlinear anisotropic filtering," *Magnetic Resonance in Medicine*, vol. 37, no. 6, pp. 914–919, 1997.

[87] K. Allen, N. Joshi, and J. A. Noble, "Tramline and np windows estimation for enhanced unsupervised retinal vessel segmentation," in *Biomedical Imaging : From Nano to Macro, 2011 IEEE International Symposium on*. IEEE, 2011, pp. 1387–1390.

[88] M. Zhang and J.-C. Liu, "Directional local contrast based blood vessel detection in retinal images," in *Image Processing, 2007. ICIP 2007. IEEE International Conference on*, vol. 4. IEEE, 2007, pp. IV–317.

[89] P. T. Truc, M. A. Khan, Y.-K. Lee, S. Lee, and T.-S. Kim, "Vessel enhancement filter using directional filter bank," *Computer Vision and Image Understanding*, vol. 113, no. 1, pp. 101–112, 2009.

[90] C. Steger, "An unbiased detector of curvilinear structures," *Pattern Analysis and Machine Intelligence, IEEE Transactions on*, vol. 20, no. 2, pp. 113–125, 1998.

[91] Y.-J. Jeong, S. Ley, R. Dillmann, and R. Unterhinninghofen, "Vessel centerline extraction in phase-contrast MR images using vector flow information," in *SPIE Medical Imaging*. International Society for Optics and Photonics, 2012, pp. 83 143H–83 143H.

[92] L. Sukkaew, B. Uyyanonvara, and S. Barman, "Comparison of edge detection techniques on vessel detection of infant's retinal image," *Proceeding of ICIM2005*, pp. 6–1, 2005.

[93] F. Oloumi, R. M. Rangayyan, P. Casti, and A. L. Ells, "Computer-aided diagnosis of plus disease via measurement of vessel thickness in retinal fundus images of preterm infants," *Computers in biology and medicine*, vol. 66, pp. 316–329, 2015.

[94] G. Agam, S. G. Armato III, and C. Wu, "Vessel tree reconstruction in thoracic CT scans with application to nodule detection," *Medical Imaging, IEEE Transactions on*, vol. 24, no. 4, pp. 486–499, 2005.

[95] M. Fraz, S. Barman, P. Remagnino, A. Hoppe, A. Basit, B. Uyyanonvara, A. R. Rudnicka, and C. G. Owen, "An approach to localize the retinal blood vessels using bit planes and centerline detection," *Computer methods and programs in biomedicine*, 2011.

[96] V. Mahadevan, H. Narasimha-Iyer, B. Roysam, and H. L. Tanenbaum, "Robust model-based vasculature detection in noisy biomedical images," *Information Technology in Biomedicine, IEEE Transactions on*, vol. 8, no. 3, pp. 360–376, 2004.

[97] P. Perona and J. Malik, "Scale-space and edge detection using anisotropic diffusion," *Pattern Analysis and Machine Intelligence, IEEE Transactions on*, vol. 12, no. 7, pp. 629–639, 1990.

[98] H. L. Manh, A. Moelker, C. Klink, A. Mendrik, W. Niessen, and T. van Walsum, "Evaluation of diffusion filters for 3D CTA liver vessel enhancement," in *Medical Image Computing and Computer-Assisted Intervention–MICCAI 2012*. Springer, 2012, pp. 168–172.

[99] M. Ben Abdallah, J. Malek, R. Tourki, and K. Krissian, "Restoration of retinal images using anisotropic diffusion like algorithms," in *Computer Vision in Remote Sensing (CVRS), 2012 International Conference on*. IEEE, 2012, pp. 116–121.

[100] C. Bauer and H. Bischof, "A novel approach for detection of tubular objects and its application to medical image analysis," in *Pattern Recognition*. Springer, 2008, pp. 163–172.

[101] F. Benmansour and L. D. Cohen, "Tubular structure segmentation based on minimal path method and anisotropic enhancement," *International Journal of Computer Vision*, vol. 92, no. 2, pp. 192–210, 2011.

[102] C. Lorenz, I.-C. Carlsen, T. M. Buzug, C. Fassnacht, and J. Weese, "Multi-scale line segmentation with automatic estimation of width, contrast and tangential direction in 2D and 3D medical images," in *CVRMed-MRCAS'97*. Springer, 1997, pp. 233–242.

[103] Y. Sato, S. Nakajima, H. Atsumi, T. Koller, G. Gerig, S. Yoshida, and R. Kikinis, "3D multi-scale line filter for segmentation and visualization of curvilinear structures in medical images," in *CVRMed-MRCAS'97*. Springer, 1997, pp. 213–222.

[104] A. F. Frangi, W. J. Niessen, K. L. Vincken, and M. A. Viergever, "Multiscale vessel enhancement filtering," in *Medical Image Computing and Computer-Assisted Interventation-MICCAI-98*. Springer, 1998, pp. 130–137.

[105] W. Zhang, J. Liu, J. Yao, A. Louie, T. Nguyen, S. Wank, W. Nowinski, and R. Summers, "Mesenteric vasculature-guided small bowel segmentation on 3-D CT," *Medical Imaging, IEEE Transactions on*, vol. 32, no. 11, pp. 2006–2021, 2013.

[106] R. D. Rudyanto, S. Kerkstra, E. M. Van Rikxoort, C. Fetita, P.-Y. Brillet, C. Lefevre, W. Xue, X. Zhu, J. Liang, İ. Öksüz *et al.*, "Comparing algorithms for automated vessel segmentation in computed tomography scans of the lung : the vessel12 study," *Medical image analysis*, vol. 18, no. 7, pp. 1217–1232, 2014.

[107] T. Lindeberg, "Edge detection and ridge detection with automatic scale selection," *International Journal of Computer Vision*, vol. 30, no. 2, pp. 117–156, 1998.

[108] M. E. Martinez-Perez, A. D. Hughes, S. A. Thom, A. A. Bharath, and K. H. Parker, "Segmentation of blood vessels from red-free and fluorescein retinal images," *Medical Image Analysis*, vol. 11, no. 1, pp. 47–61, 2007.

[109] C. Xiao, M. Staring, Y. Wang, D. Shamonin, and B. Stoel, "A multiscale bi-Gaussian filter for adjacent curvilinear structures detection with application to vasculature images," *Image Processing, IEEE Transactions on*, vol. 22, no. 1, pp. 174–188, 2013.

[110] M. Sofka and C. V. Stewart, "Retinal vessel centerline extraction using multiscale matched filters, confidence and edge measures," *Medical Imaging, IEEE Transactions on*, vol. 25, no. 12, pp. 1531–1546, 2006.

[111] F. Isikdogan, A. Bovik, and P. Passalacqua, "Automatic channel network extraction from remotely sensed images by singularity analysis," *IEEE Geoscience and Remote Sensing Letters*, vol. 12, no. 11, pp. 2218–2221, 2015.

[112] T. Jerman, F. Pernus, B. Likar, and Z. Spiclin, "Enhancement of vascular structures in 3d and 2d angiographic images," *Medical Imaging, IEEE Transactions on*, vol. 35, no. 9, pp. 2107–2118, 2016.

[113] J. Zhang, B. Dashtbozorg, E. Bekkers, J. Pluim, R. Duits, and B. ter Haar Romeny, "Robust retinal vessel segmentation via locally adaptive derivative frames in orientation scores," *Medical Imaging, IEEE Transactions on*, 2016.

[114] M. Kass, A. Witkin, and D. Terzopoulos, "Snakes : Active contour models," *International journal of computer vision*, vol. 1, no. 4, pp. 321–331, 1988.

[115] V. Uhlmann, J. Fageot, and M. Unser, "Hermite snakes with control of tangents," *IEEE Transactions on Image Processing*, vol. 25, no. 6, pp. 2803–2816, 2016.

[116] H. Tek and B. B. Kimia, "Image segmentation by reaction-diffusion bubbles," in *Computer Vision, 1995. Proceedings., Fifth International Conference on.* IEEE, 1995, pp. 156–162.

[117] C. Xu and J. L. Prince, "Snakes, shapes, and gradient vector flow," *Image Processing, IEEE Transactions on*, vol. 7, no. 3, pp. 359–369, 1998.

[118] B. Li and S. T. Acton, "Active contour external force using vector field convolution for image segmentation," *Image Processing, IEEE Transactions on*, vol. 16, no. 8, pp. 2096–2106, 2007.

[119] R. Toledo, X. Orriols, P. Radeva, X. Binefa, J. Vitria, C. Canero, and J. Villanuev, "Eigensnakes for vessel segmentation in angiography," in *Pattern Recognition, 2000. Proceedings. 15th International Conference on*, vol. 4. IEEE, 2000, pp. 340–343.

[120] H. Mayer, I. Laptev, and A. Baumgartner, "Multi-scale and snakes for automatic road extraction," in *Computer Vision-ECCV'98*. Springer, 1998, pp. 720–733.

[121] B. Al-Diri, A. Hunter *et al.*, "A ribbon of twins for extracting vessel boundaries," in *Medical and Biological Engineering, 2000. Proceedings. The 3rd European Conference on.* Society for the organization of the european medical and biological engineering conference, 2005.

[122] B. Al-Diri, A. Hunter, and D. Steel, "An active contour model for segmenting and measuring retinal vessels," *Medical Imaging, IEEE Transactions on*, vol. 28, no. 9, pp. 1488–1497, 2009.

[123] T. McInerney and D. Terzopoulos, "T-snakes : Topology adaptive snakes," *Medical image analysis*, vol. 4, no. 2, pp. 73–91, 2000.

[124] N. Bova, Ó. Ibáñez, and Ó. Cordón, "Extended topological active nets," *Image and Vision Computing*, vol. 31, no. 12, pp. 905–920, 2013.

[125] S. Osher and J. A. Sethian, "Fronts propagating with curvature-dependent speed : algorithms based on Hamilton-Jacobi formulations," *Journal of computational physics*, vol. 79, no. 1, pp. 12–49, 1988.

[126] J. A. Sethian, "Fast marching methods and level set methods for propagating interfaces," in *von Karman Institute Lecture Series, Computational Fluid Mechanics*, 1998.

[127] R. Malladi, J. A. Sethian, and B. C. Vemuri, "Shape modeling with front propagation : A level set approach," *Pattern Analysis and Machine Intelligence, IEEE Transactions on*, vol. 17, no. 2, pp. 158–175, 1995.

[128] V. Caselles, "Geometric models for active contours," in *Image Processing, 1995. Proceedings., International Conference on*, vol. 3. IEEE, 1995, pp. 9–12.

[129] N. Paragios, O. Mellina-Gottardo, and V. Ramesh, "Gradient vector flow fast geodesic active contours," in *Computer Vision, 2001. ICCV 2001. Proceedings. Eighth IEEE International Conference on*, vol. 1. IEEE, 2001, pp. 67–73.

[130] M. Descoteaux, D. L. Collins, and K. Siddiqi, "A geometric flow for segmenting vasculature in proton-density weighted mri," *Medical image analysis*, vol. 12, no. 4, pp. 497–513, 2008.

[131] Y. Zhao, L. Rada, K. Chen, S. P. Harding, and Y. Zheng, "Automated vessel segmentation using infinite perimeter active contour model with hybrid region information with application to retinal images," *IEEE transactions on medical imaging*, vol. 34, no. 9, pp. 1797–1807, 2015.

[132] T. F. Chan and L. A. Vese, "Active contours without edges," *Image Processing, IEEE Transactions on*, vol. 10, no. 2, pp. 266–277, 2001.

[133] D. Mumford and J. Shah, "Optimal approximations by piecewise smooth functions and associated variational problems," *Communications on pure and applied mathematics*, vol. 42, no. 5, pp. 577–685, 1989.

[134] K. Sum and P. Y. Cheung, "Vessel extraction under non-uniform illumination : a level set approach," *Biomedical Engineering, IEEE Transactions on*, vol. 55, no. 1, pp. 358–360, 2008.

[135] X. Du and T. D. Bui, "Retinal image segmentation based on mumford-shah model and gabor wavelet filter," in *Pattern Recognition (ICPR), 2010 20th International Conference on*. IEEE, 2010, pp. 3384–3387.

[136] D. Rivest-Heénault, M. Cheriet, S. Descheñes, and C. Lapierre, "Length increasing active contour for the segmentation of small blood vessels," in *Pattern Recognition (ICPR), 2010 20th International Conference on*. IEEE, 2010, pp. 2796–2799.

[137] G. Sundaramoorthi, A. Yezzi, A. C. Mennucci, and G. Sapiro, "New possibilities with Sobolev active contours," *International Journal of Computer Vision*, vol. 84, no. 2, pp. 113–129, 2009.

[138] D. Nain, A. Yezzi, and G. Turk, "Vessel segmentation using a shape driven flow," in *Medical Image Computing and Computer-Assisted Intervention–MICCAI 2004*. Springer, 2004, pp. 51–59.

[139] P. Yan and A. A. Kassim, "MRA image segmentation with capillary active contour," in *Medical Image Computing and Computer-Assisted Intervention–MICCAI 2005*. Springer, 2005, pp. 51–58.

[140] O. Wink, W. J. Niessen, and M. A. Viergever, "Fast delineation and visualization of vessels in 3-d angiographic images," *Medical Imaging, IEEE Transactions on*, vol. 19, no. 4, pp. 337–346, 2000.

[141] S. R. Rao, S. E. Shelton, and P. A. Dayton, "The "fingerprint" of cancer extends beyond solid tumor boundaries : Assessment with a novel ultrasound imaging approach," *IEEE Transactions on Biomedical Engineering*, vol. 63, no. 5, pp. 1082–1086, 2016.

[142] O. Chutatape, L. Zheng, and S. Krishnan, "Retinal blood vessel detection and tracking by matched Gaussian and Kalman filters," in *Engineering in Medicine and Biology Society, 1998. Proceedings of the 20th Annual International Conference of the IEEE*, vol. 6. IEEE, 1998, pp. 3144–3149.

[143] A. La Cruz, M. Straka, A. Kochl, M. Sramek, E. Groller, and D. Fleischmann, "Non-linear model fitting to parameterize diseased blood vessels," in *Proceedings of the conference on Visualization'04*. IEEE Computer Society, 2004, pp. 393–400.

[144] O. Friman, M. Hindennach, C. Kühnel, and H.-O. Peitgen, "Multiple hypothesis template tracking of small 3D vessel structures," *Medical Image Analysis*, vol. 14, no. 2, pp. 160–171, 2010.

[145] H. Shim, D. Kwon, I. D. Yun, and S. U. Lee, "Robust segmentation of cerebral arterial segments by a sequential monte carlo method : Particle filtering," *Computer methods and programs in biomedicine*, vol. 84, no. 2, pp. 135–145, 2006.

[146] B. Whited, J. Rossignac, G. Slabaugh, T. Fang, and G. Unal, "Pearling : 3D interactive extraction of tubular structures from volumetric images," *Interaction in Medical Image Analysis and Visualization, held in conjunction with MICCAI*, 2007.

[147] J. A. Tyrrell, E. di Tomaso, D. Fuja, R. Tong, K. Kozak, R. K. Jain, and B. Roysam, "Robust 3-D modeling of vasculature imagery using superellipsoids," *Medical Imaging, IEEE Transactions on*, vol. 26, no. 2, pp. 223–237, 2007.

[148] Y. A. Tolias and S. M. Panas, "A fuzzy vessel tracking algorithm for retinal images based on fuzzy clustering," *IEEE Transactions on Medical Imaging*, vol. 17, no. 2, pp. 263–273, 1998.

[149] S. Worz and K. Rohr, "Segmentation and quantification of human vessels using a 3-d cylindrical intensity model," *Image Processing, IEEE Transactions on*, vol. 16, no. 8, pp. 1994–2004, 2007.

[150] K.-S. Lin, C.-L. Tsai, C.-H. Tsai, M. Sofka, S.-J. Chen, and W.-Y. Lin, "Retinal vascular tree reconstruction with anatomical realism," *IEEE Transactions on Biomedical Engineering*, vol. 59, no. 12, pp. 3337–3347, 2012.

[151] B. Nayebifar and H. Abrishami Moghaddam, "A novel method for retinal vessel tracking using particle filtering," *Computers in Biology and Medicine*, vol. 43, pp. 541–548, 2013.

[152] D. Lesage, E. D. Angelini, G. Funka-Lea, and I. Bloch, "Adaptive particle filtering for coronary artery segmentation from 3d ct angiograms," *Computer Vision and Image Understanding*, vol. 151, pp. 29–46, 2016.

[153] J. Zhang, H. Li, Q. Nie, and L. Cheng, "A retinal vessel boundary tracking method based on bayesian theory and multi-scale line detection," *Computerized Medical Imaging and Graphics*, vol. 38, no. 6, pp. 517–525, 2014.

[154] C. Bołdak, Y. Rolland, C. Toumoulin, and J. Coatrieux, "An improved model-based vessel tracking algorithm with application to computed tomography angiography," *Journal of Biocybernetics and Biomedical Engineering*, vol. 3, no. 1, pp. 41–64, 2003.

[155] D. Rueckert, P. Burger, S. Forbat, R. Mohiaddin, and G.-Z. Yang, "Automatic tracking of the aorta in cardiovascular MR images using deformable models," *Medical Imaging, IEEE Transactions on*, vol. 16, no. 5, pp. 581–590, 1997.

[156] N. H. Solouma, A. Youssef, Y. A. Badr, and Y. M. Kadah, "A new real-time retinal tracking system for image-guided laser treatment," *Biomedical Engineering, IEEE Transactions on*, vol. 49, no. 9, pp. 1059–1067, 2002.

[157] K. K. Delibasis, A. I. Kechriniotis, C. Tsonos, and N. Assimakis, "Automatic model-based tracing algorithm for vessel segmentation and diameter estimation," *Computer methods and programs in biomedicine*, vol. 100, no. 2, pp. 108–122, 2010.

[158] A. Can, H. Shen, J. N. Turner, H. L. Tanenbaum, and B. Roysam, "Rapid automated tracing and feature extraction from retinal fundus images using direct exploratory algorithms," *Information Technology in Biomedicine, IEEE Transactions on*, vol. 3, no. 2, pp. 125–138, 1999.

[159] E. Dijkstra, "A note on two problems in connexion with graphs," *Numerische Mathematik*, vol. 11, pp. 269–271, 1959.

[160] L. D. Cohen and R. Kimmel, "Global minimum for active contour models : A minimal path approach," *International journal of computer vision*, vol. 24, no. 1, pp. 57–78, 1997.

[161] V. S. Joshi, M. K. Garvin, J. M. Reinhardt, and M. D. Abràmoff, "Identification and reconnection of interrupted vessels in retinal vessel segmentation," in *Biomedical Imaging : From Nano to Macro, 2011 IEEE International Symposium on*. IEEE, 2011, pp. 1416–1420.

[162] O. Wink, A. F. Frangi, B. Verdonck, M. A. Viergever, and W. J. Niessen, "3d mra coronary axis determination using a minimum cost path approach," *Magnetic Resonance in Medicine*, vol. 47, no. 6, pp. 1169–1175, 2002.

[163] L. Pedersen, M. Grunkin, B. Ersbøll, K. Madsen, M. Larsen, N. Christoffersen, and U. Skands, "Quantitative measurement of changes in retinal vessel diameter in ocular fundus images," *Pattern Recognition Letters*, vol. 21, no. 13, pp. 1215–1223, 2000.

[164] W. Liao, K. Rohr, and S. Wörz, "Globally optimal curvature-regularized fast marching for vessel segmentation," in *Medical Image Computing and Computer-Assisted Intervention–MICCAI 2013*. Springer, 2013, pp. 550–557.

[165] D. Chen, J.-M. Mirebeau, and L. D. Cohen, "A new finsler minimal path model with curvature penalization for image segmentation and closed contour detection," in *Proceedings of the IEEE Conference on Computer Vision and Pattern Recognition*, 2016, pp. 355–363.

[166] O. Wink, W. J. Niessen, and M. A. Viergever, "Minimum cost path determination using a simple heuristic function," in *Pattern Recognition, 2000. Proceedings. 15th International Conference on*, vol. 3. IEEE, 2000, pp. 998–1001.

[167] T. Deschamps and L. D. Cohen, "Fast extraction of tubular and tree 3D surfaces with front propagation methods," in *Pattern Recognition, 2002. Proceedings. 16th International Conference on*, vol. 1. IEEE, 2002, pp. 731–734.

[168] H. Li and A. Yezzi, "Vessels as 4-D curves : Global minimal 4-D paths to extract 3-D tubular surfaces and centerlines," *Medical Imaging, IEEE Transactions on*, vol. 26, no. 9, pp. 1213–1223, 2007.

[169] R. Estrada, C. Tomasi, M. T. Cabrera, D. K. Wallace, S. F. Freedman, and S. Farsiu, "Exploratory dijkstra forest based automatic vessel segmentation : applications in video indirect ophthalmoscopy (vio)," *Biomedical optics express*, vol. 3, no. 2, pp. 327–339, 2012.

[170] D. Chen, J.-M. Mirebeau, and L. D. Cohen, "Vessel tree extraction using radius-lifted keypoints searching scheme and anisotropic fast marching method," *Journal of Algorithms & Computational Technology*, p. 1748301816656289, 2016.

[171] G. G. Gardner, D. Keating, T. H. Williamson, and A. T. Elliott, "Automatic detection of diabetic retinopathy using an artificial neural network : a screening tool," *British Journal of Opthalomology*, vol. 80, no. 11, pp. 940–944, 1996.

[172] D. Marín, A. Aquino, M. E. Gegúndez-Arias, and J. M. Bravo, "A new supervised method for blood vessel segmentation in retinal images by using gray-level and moment invariants-based features," *Medical Imaging, IEEE Transactions on*, vol. 30, no. 1, pp. 146–158, 2011.

[173] S. W. Franklin and S. E. Rajan, "Retinal vessel segmentation employing ann technique by gabor and moment invariants-based features," *Applied Soft Computing*, vol. 22, pp. 94–100, 2014.

[174] C. Zhu, B. Zou, R. Zhao, J. Cui, X. Duan, Z. Chen, and Y. Liang, "Retinal vessel segmentation in colour fundus images using extreme learning machine," *Computerized Medical Imaging and Graphics*, 2016.

[175] M. Niemeijer, J. Staal, B. van Ginneken, M. Loog, and M. D. Abramoff, "Comparative study of retinal vessel segmentation methods on a new publicly available database," in *Medical Imaging 2004*. International Society for Optics and Photonics, 2004, pp. 648–656.

[176] J. Staal, M. D. Abràmoff, M. Niemeijer, M. A. Viergever, and B. van Ginneken, "Ridge-based vessel segmentation in color images of the retina," *Medical Imaging, IEEE Transactions on*, vol. 23, no. 4, pp. 501–509, 2004.

[177] A. Osareh and B. Shadgar, "Automatic blood vessel segmentation in color images of retina," *Iran. J. Sci. Technol. Trans. B : Engineering*, vol. 33, no. B2, pp. 191–206, 2009.

[178] L. Xu and S. Luo, "A novel method for blood vessel detection from retinal images," *Biomedical engineering online*, vol. 9, no. 1, p. 14, 2010.

[179] A. Simó and E. de Ves, "Segmentation of macular fluorescein angiographies. a statistical approach," *Pattern Recognition*, vol. 34, no. 4, pp. 795–809, 2001.

[180] J. V. Soares, J. J. Leandro, R. M. Cesar, H. F. Jelinek, and M. J. Cree, "Retinal vessel segmentation using the 2-D Gabor wavelet and supervised classification," *Medical Imaging, IEEE Transactions on*, vol. 25, no. 9, pp. 1214–1222, 2006.

[181] A. Pourmorteza, S. H. R. Tofighi, A. Roodaki, A. Yazdani, and H. Soltanian-Zadeh, "Context-dependent segmentation of retinal blood vessels using hidden markov models," in *Advances in Computer Science and Engineering*. Springer, 2009, pp. 348–355.

[182] K. Basak, G. Dey, D. Sheet, M. Mahadevappa, M. Mandal, and P. K. Dutta, "Probabilistic graphical modeling of speckle statistics in laser speckle contrast imaging for noninvasive and label-free retinal angiography," in *2015 37th Annual International Conference of the IEEE Engineering in Medicine and Biology Society (EMBC)*. IEEE, 2015, pp. 6244–6247.

[183] M. M. Fraz, P. Remagnino, A. Hoppe, B. Uyyanonvara, A. R. Rudnicka, C. G. Owen, and S. A. Barman, "An ensemble classification-based approach applied to retinal blood vessel segmentation," *Biomedical Engineering, IEEE Transactions on*, vol. 59, no. 9, pp. 2538–2548, 2012.

[184] M. M. Fraz, A. R. Rudnicka, C. G. Owen, and S. A. Barman, "Delineation of blood vessels in pediatric retinal images using decision trees-based ensemble classification," *International journal of computer assisted radiology and surgery*, vol. 9, no. 5, pp. 795–811, 2014.

[185] C. Lupaşcu, D. Tegolo, and E. Trucco, "FABC : Retinal vessel segmentation using adaboost," *Information Technology in Biomedicine, IEEE Transactions on*, vol. 14, no. 5, pp. 1267–1274, 2010.

[186] F. Sahba, H. R. Tizhoosh, and M. M. Salama, "Increasing object recognition rate using reinforced segmentation," in *Image Processing, 2006 IEEE International Conference on*. IEEE, 2006, pp. 781–784.

[187] L. Wang, K. Lekadir, S.-L. Lee, R. Merrifield, and G.-Z. Yang, "A general framework for context-specific image segmentation using reinforcement learning," *IEEE transactions on medical imaging*, vol. 32, no. 5, pp. 943–956, 2013.

[188] P. Komarek, "Logistic regression for data mining and high-dimensional classification," *Robotics Institute*, p. 222, 2004.

[189] A. Sironi, E. Türetken, V. Lepetit, and P. Fua, "Multiscale centerline detection," *IEEE Transactions on Pattern Analysis and Machine Intelligence*, vol. 38, no. 7, pp. 1327–1341, 2016.

[190] R. Rigamonti and V. Lepetit, "Accurate and efficient linear structure segmentation by leveraging ad hoc features with learned filters," in *Medical Image Computing and Computer-Assisted Intervention–MICCAI 2012*. Springer, 2012, pp. 189–197.

[191] V. Estivill-Castro, "Why so many clustering algorithms : a position paper," *ACM SIGKDD Explorations Newsletter*, vol. 4, no. 1, pp. 65–75, 2002.

[192] A. K. Jain, M. N. Murty, and P. J. Flynn, "Data clustering : a review," *ACM computing surveys (CSUR)*, vol. 31, no. 3, pp. 264–323, 1999.

[193] M. Niemeijer, X. Xu, A. V. Dumitrescu, P. Gupta, B. van Ginneken, J. C. Folk, and M. D. Abramoff, "Automated measurement of the arteriolar-to-venular width ratio in digital color fundus photographs," *IEEE Transactions on medical imaging*, vol. 30, no. 11, pp. 1941–1950, 2011.

[194] E. Emary, H. M. Zawbaa, A. E. Hassanien, G. Schaefer, and A. T. Azar, "Retinal vessel segmentation based on possibilistic fuzzy c-means clustering optimised with cuckoo search," in *2014 International Joint Conference on Neural Networks (IJCNN)*. IEEE, 2014, pp. 1792–1796.

[195] S. S. Kar and S. P. Maity, "Blood vessel extraction and optic disc removal using curvelet transform and kernel fuzzy c-means," *Computers in biology and medicine*, vol. 70, pp. 174–189, 2016.

[196] D. Relan, T. MacGillivray, L. Ballerini, and E. Trucco, "Retinal vessel classification : sorting arteries and veins," in *35th Annual International Conference of the IEEE EMBS Engineering in Medicine and Biology Society (EMBC), Osaka, Japan*, 2013, pp. 7396–7399.

[197] D. Kaba, A. G. Salazar-Gonzalez, Y. Li, X. Liu, and A. Serag, "Segmentation of retinal blood vessels using Gaussian mixture models and expectation maximisation," in *Health Information Science*. Springer, 2013, pp. 105–112.

[198] M. Tagore, G. B. Kande, E. Rao, and B. P. Rao, "Segmentation of retinal vasculature using phase congruency and hierarchical clustering," in *Advances in Computing, Communications and Informatics (ICACCI), 2013 International Conference on*. IEEE, 2013, pp. 361–366.

[199] S. Xie and H. Nie, "Retinal vascular image segmentation using genetic algorithm plus FCM clustering," in *Intelligent System Design and Engineering Applications (ISDEA), 2013 Third International Conference on*. IEEE, 2013, pp. 1225–1228.

[200] T. Kohonen, "Self-organization and associative memory," *Self-Organization and Associative Memory, 100 figs. XV, 312 pages.. Springer-Verlag Berlin Heidelberg New York. Also Springer Series in Information Sciences, volume 8*, vol. 1, 1988.

[201] H. Yin, "The self-organizing maps : Background, theories, extensions and applications," in *Computational intelligence : a compendium*. Springer, 2008, pp. 715–762.

[202] J. Zhang, Y. Cui, W. Jiang, and L. Wang, "Blood vessel segmentation of retinal images based on neural network," in *International Conference on Image and Graphics*. Springer, 2015, pp. 11–17.

[203] Q. Li, B. Feng, L. Xie, P. Liang, H. Zhang, and T. Wang, "A cross-modality learning approach for vessel segmentation in retinal images," *IEEE transactions on medical imaging*, vol. 35, no. 1, pp. 109–118, 2016.

[204] Y. LeCun, Y. Bengio, and G. Hinton, "Deep learning," *Nature*, vol. 521, no. 7553, pp. 436–444, 2015.

[205] R. Annunziata and E. Trucco, "Accelerating convolutional sparse coding for curvilinear structures segmentation by refining scird-ts filter banks," *IEEE transactions on medical imaging*, 2016.

[206] P. Liskowski and K. Krawiec, "Segmenting retinal blood vessels with deep neural networks," *IEEE transactions on medical imaging*, 2016.

[207] G. Medioni and S. B. Kang, *Emerging topics in computer vision*. Prentice Hall PTR, 2004.

[208] G. Medioni, M.-S. Lee, and C.-K. Tang, *A computational framework for segmentation and grouping*. Elsevier, 2000.

[209] Z. Leng, J. R. Korenberg, B. Roysam, and T. Tasdizen, "A rapid 2-d centerline extraction method based on tensor voting," in *2011 IEEE international symposium on biomedical imaging : From nano to macro*. IEEE, 2011, pp. 1000–1003.

[210] L. R. Williams and K. K. Thornber, "A comparison of measures for detecting natural shapes in cluttered backgrounds," *International Journal of Computer Vision*, vol. 34, no. 2-3, pp. 81–96, 1999.

[211] E. Franken, M. van Almsick, P. Rongen, L. Florack, and B. ter Haar Romeny, "An efficient method for tensor voting using steerable filters," in *European Conference on Computer Vision*. Springer, 2006, pp. 228–240.

[212] E. Franken, P. Rongen, M. van Almsick, and B. ter Haar Romeny, "Detection of electrophysiology catheters in noisy fluoroscopy images," in *International Conference on Medical Image Computing and Computer-Assisted Intervention*. Springer, 2006, pp. 25–32.

[213] L. Risser, F. Plourabouré, and X. Descombes, "Gap filling of 3-d microvascular networks by tensor voting," *IEEE transactions on medical imaging*, vol. 27, no. 5, pp. 674–687, 2008.

[214] L. A. Loss, G. Bebis, and B. Parvin, "Iterative tensor voting for perceptual grouping of ill-defined curvilinear structures," *IEEE transactions on medical imaging*, vol. 30, no. 8, pp. 1503–1513, 2011.

[215] M. Yigitsoy and N. Navab, "Structure propagation for image registration," *IEEE transactions on medical imaging*, vol. 32, no. 9, pp. 1657–1670, 2013.

[216] M. A. Zuluaga, R. Rodionov, M. Nowell, S. Achhala, G. Zombori, A. F. Mendelson, M. J. Cardoso, A. Miserocchi, A. W. McEvoy, J. S. Duncan *et al.*, "Stability, structure and scale : improvements in multi-modal vessel extraction for seeg trajectory planning," *International journal of computer assisted radiology and surgery*, vol. 10, no. 8, pp. 1227–1237, 2015.

[217] E. Maggiori, H. L. Manterola, and M. del Fresno, "Perceptual grouping by tensor voting : a comparative survey of recent approaches," *IET Computer Vision*, vol. 9, no. 2, pp. 259–277, 2014.

[218] R. Duits, M. Janssen, J. Hannink, and G. Sanguinetti, "Locally adaptive frames in the roto-translation group and their applications in medical imaging," *Journal of Mathematical Imaging and Vision*, pp. 1–36, 2016.

[219] J. Park, N. T. Kien, and G. Lee, "Optic disc detection in retinal images using tensor voting and adaptive mean-shift," in *2007 IEEE International Conference on Intelligent Computer Communication and Processing*. IEEE, 2007, pp. 237–241.

[220] K. A. Goatman, A. D. Fleming, S. Philip, G. J. Williams, J. A. Olson, and P. F. Sharp, "Detection of new vessels on the optic disc using retinal photographs," *Medical Imaging, IEEE Transactions on*, vol. 30, no. 4, pp. 972–979, 2011.

[221] C. Agurto, H. Yu, V. Murray, M. Pattichis, S. Barriga, W. Bauman, and P. Soliz, "Detection of neovascularization in the optic disc using an AM-FM representation, granulometry, and vessel segmentation," in *Engineering in Medicine and Biology Society (EMBC), 2012 Annual International Conference of the IEEE*. IEEE, 2012, pp. 4946–4949.

[222] G. Tamil Pavai and S. Tamil Selvi, "Identification of proliferative diabetic retinopathy using texture segmentation," *Journal of Computer Science*, vol. 9, no. 3, 2013.

[223] C. Agurto, H. Yu, V. Murray, M. S. Pattichis, S. Nemeth, S. Barriga, and P. Soliz, "A multiscale decomposition approach to detect abnormal vasculature in the optic disc," *Computerized Medical Imaging and Graphics*, vol. 43, pp. 137–149, 2015.

[224] C. Agurto, V. Murray, E. Barriga, S. Murillo, M. Pattichis, H. Davis, S. Russell, M. Abràmoff, and P. Soliz, "Multiscale am-fm methods for diabetic retinopathy lesion detection," *IEEE Transactions on Medical Imaging*, vol. 29, no. 2, pp. 502–512, 2010.

[225] S. S. A. Hassan, D. B. Bong, and M. Premsenthil, "Detection of neovascularization in diabetic retinopathy," *Journal of digital imaging*, vol. 25, no. 3, pp. 437–444, 2012.

[226] K. Saranya, B. Ramasubramanian, and S. Kaja Mohideen, "A novel approach for the detection of new vessels in the retinal images for screening Diabetic Retinopathy," in *Communications and Signal Processing (ICCSP), 2012 International Conference on*. IEEE, 2012, pp. 57–61.

[227] M. U. Akram, A. Tariq, and S. A. Khan, "Detection of neovascularization for screening of proliferative diabetic retinopathy," in *Image Analysis and Recognition*. Springer, 2012, pp. 372–379.

[228] M. Usman Akram, S. Khalid, A. Tariq, and M. Younus Javed, "Detection of neovascularization in retinal images using multivariate m-Mediods based classifier," *Computerized Medical Imaging and Graphics*, vol. 37, no. 5, pp. 346–357, 2013.

[229] J. Lee, B. C. Y. Zee, and Q. Li, "Detection of neovascularization based on fractal and texture analysis with interaction effects in diabetic retinopathy," *PloS one*, vol. 8, no. 12, p. e75699, 2013.

[230] R. Welikala, M. Fraz, J. Dehmeshki, A. Hoppe, V. Tah, S. Mann, T. Williamson, and S. Barman, "Genetic algorithm based feature selection combined with dual classification for the automated detection of proliferative diabetic retinopathy," *Computerized Medical Imaging and Graphics*, vol. 43, pp. 64–77, 2015.

[231] G. Gupta, S. Kulasekaran, K. Ram, N. Joshi, M. Sivaprakasam, and R. Gandhi, "Local characterization of neovascularization and identification of proliferative diabetic retinopathy in retinal fundus images," *Computerized Medical Imaging and Graphics*, 2016.

[232] M. Vatanparast and A. Harati, "A feasibility study on detection of neovascularization in retinal color images using texture," in *Computer and Knowledge Engineering (ICCKE), 2012 2nd International eConference on*. IEEE, 2012, pp. 221–226.

[233] U. R. Acharya, E. Ng, J.-H. Tan, S. V. Sree, and K.-H. Ng, "An integrated index for the identification of diabetic retinopathy stages using texture parameters," *Journal of medical systems*, vol. 36, no. 3, pp. 2011–2020, 2012.

[234] Y. J. Zhang, "A survey on evaluation methods for image segmentation," *Pattern recognition*, vol. 29, no. 8, pp. 1335–1346, 1996.

[235] P. L. Correia and F. Pereira, "Objective evaluation of video segmentation quality," *Image Processing, IEEE Transactions on*, vol. 12, no. 2, pp. 186–200, 2003.

[236] E. D. Gelasca, "Full-reference objective quality metrics for video watermarking, video segmentation and 3D model watermarking," Ph.D. dissertation, Department of Electical and Electronic Engineering, Ecole Polytechnique Federal de Lausanne, 2005.

[237] T. Fawcett, "An introduction to ROC analysis," *Pattern recognition letters*, vol. 27, no. 8, pp. 861–874, 2006.

[238] U. T. Nguyen, K. Ramamohanarao, L. A. Park, L. Wang, A. Bhuiyan, and I. Ahmed, "A quantitative measure for retinal blood vessel segmentation evaluation," *IJCVSP*, vol. 1, no. 1, pp. 1–8, 2012.

[239] M. E. Gegúndez-Arias, A. Aquino, J. M. Bravo, and D. Marin, "A function for quality evaluation of retinal vessel segmentations," *Medical Imaging, IEEE Transactions on*, vol. 31, no. 2, pp. 231–239, 2012.

[240] E. D. Gelasca and T. Ebrahimi, "On evaluating video object segmentation quality : a perceptually driven objective metric," *Selected Topics in Signal Processing, IEEE Journal of*, vol. 3, no. 2, pp. 319–335, 2009.

[241] M. D. Heath, S. Sarkar, T. Sanocki, and K. W. Bowyer, "A robust visual method for assessing the relative performance of edge-detection algorithms," *Pattern Analysis and Machine Intelligence, IEEE Transactions on*, vol. 19, no. 12, pp. 1338–1359, 1997.

[242] C. W. Shaffrey, I. H. Jermyn, and N. G. Kingsbury, "Psychovisual evaluation of image segmentation algorithms," in *Proc. Advanced Concepts for Intelligent Vision Systems 2002*, 2002.

[243] P. Villegas, X. Marichal, and A. Salcedo, "Objective evaluation of segmentation masks in video sequences," in *Proc. Workshop Image Analysis for Multimedia Interactive Services*, vol. 99, 1999, pp. 85–88.

[244] K. McKoen, R. Navarro-Prieto, B. Duc, E. Durucan, F. Ziliani, and T. Ebrahimi, "Evaluation of video segmentation methods for surveillance applications," in *Proc. European Signal Processing Conference 2000*, 2000.

[245] P. Villegas and X. Marichal, "Perceptually-weighted evaluation criteria for segmentation masks in video sequences," *Image Processing, IEEE Transactions on*, vol. 13, no. 8, pp. 1092–1103, 2004.

[246] T. A. Lampert, A. Stumpf, and P. Gançarski, "An empirical study into annotator agreement, ground truth estimation, and algorithm evaluation," *IEEE Transactions on Image Processing*, vol. 25, no. 6, pp. 2557–2572, 2016.

[247] J. Jomier, V. LeDigarcher, and S. R. Aylward, "Comparison of vessel segmentations using STAPLE," in *Medical Image Computing and Computer-Assisted Intervention–MICCAI 2005*. Springer, 2005, pp. 523–530.

[248] D. W. Paglieroni, "Design considerations for image segmentation quality assessment measures," *Pattern Recognition*, vol. 37, no. 8, pp. 1607–1617, 2004.

[249] X. Xu, B. Li, J. F. Florez, and H. K. Li, "Simulation of diabetic retinopathy neovascularization in color digital fundus images," in *Advances in Visual Computing*. Springer, 2006, pp. 421–433.

[250] T. Kauppi, V. Kalesnykiene, J.-K. Kamarainen, L. Lensu, I. Sorri, H. Uusitalo, H. Kälviäinen, and J. Pietilä, "Diaretdb0 : Evaluation database and methodology for diabetic retinopathy algorithms."

[251] E. Decencière, X. Zhang, G. Cazuguel, B. Laÿ, B. Cochener *et al.*, "Feedback on a publicly distributed image database : the messidor database," *Image Analysis and Stereology*, vol. 33, no. 3, pp. 231–234, 2014.

[252] M. Foracchia, E. Grisan, and A. Ruggeri, "Luminosity and contrast normalization in retinal images," *Medical Image Analysis*, vol. 9, no. 3, pp. 179–190, 2005.

[253] N. G. Kingsbury, "The dual-tree complex wavelet transform : a new technique for shift invariance and directional filters," in *IEEE Digital Signal Processing Workshop*, vol. 86. Citeseer, 1998, pp. 120–131.

[254] D. L. Donoho, "De-noising by soft-thresholding," *IEEE transactions on information theory*, vol. 41, no. 3, pp. 613–627, 1995.

[255] G. van Antwerpen, P. Verbeek, and F. Groen, "Automatic counting of asbestos fibres," in *Signal Processing Conference (EUSIPCO), 1986 Proceedings of the 3rd European*. Elsevier, 1986, pp. 891–896.

[256] P. Berens *et al.*, "Circstat : a matlab toolbox for circular statistics," *J Stat Softw*, vol. 31, no. 10, pp. 1–21, 2009.

[257] R. M. Haralick and L. G. Shapiro, *Computer and robot vision*. Addison-Wesley Longman Publishing Co., Inc., 1991.

[258] A. Budai, J. Odstrcilik, R. Kolar, J. Hornegger, J. Jan, T. Kubena, and G. Michelson, "A public database for the evaluation of fundus image segmentation algorithms," *Investigative Ophthalmology & Visual Science*, vol. 52, no. 14, pp. 1345–1345, 2011.

[259] R. Annunziata, A. Garzelli, L. Ballerini, A. Mecocci, and E. Trucco, "Leveraging multiscale hessian-based enhancement with a novel exudate inpainting technique for retinal vessel segmentation," *Biomedical and Health Informatics, IEEE Journal of*, vol. PP, no. 99, pp. 1–1, 2015.

[260] J. Hannink, R. Duits, and E. Bekkers, "Crossing-preserving multi-scale vesselness," in *Medical Image Computing and Computer-Assisted Intervention–MICCAI 2014*. Springer, 2014, pp. 603–610.

[261] A. Budai, R. Bock, A. Maier, J. Hornegger, and G. Michelson, "Robust vessel segmentation in fundus images," *International journal of biomedical imaging*, vol. 2013, 2013.

[262] H. Yu, S. Barriga, C. Agurto, G. Zamora, W. Bauman, and P. Soliz, "Fast vessel segmentation in retinal images using multiscale enhancement and second-order local entropy," in *SPIE medical imaging*. International Society for Optics and Photonics, 2012, pp. 83 151B–83 151B.

[263] L. Vincent, "Morphological grayscale reconstruction in image analysis : applications and efficient algorithms," *IEEE transactions on image processing*, vol. 2, no. 2, pp. 176–201, 1993.

[264] H. Thompson, "Distribution of distance to nth neighbour in a population of randomly distributed individuals," *Ecology*, vol. 37, no. 2, pp. 391–394, 1956.

[265] P. J. Clark and F. C. Evans, "Distance to nearest neighbor as a measure of spatial relationships in populations," *Ecology*, vol. 35, no. 4, pp. 445–453, 1954.

[266] T. Kauppi, V. Kalesnykiene, J.-K. Kamarainen, L. Lensu, I. Sorri *et al.*, "The diaretdb1 diabetic retinopathy database and evaluation protocol." in *BMVC*, 2007, pp. 1–10.

[267] https ://www.kaggle.com/c/diabetic-retinopathy-detection/data. Accessed : 2016-11-03. [Online]. Available : https://www.kaggle.com/c/diabetic-retinopathy-detection/data

[268] T. Schultz, "Towards resolving fiber crossings with higher order tensor inpainting," in *New Developments in the Visualization and Processing of Tensor Fields*. Springer, 2012, pp. 253–265.

[269] A. Desolneux, L. Moisan, and J.-M. Morel, *From gestalt theory to image analysis : a probabilistic approach*. Springer Science & Business Media, 2007, vol. 34.

[270] E. Velázquez, I. Martínez, S. Getzin, K. A. Moloney, and T. Wiegand, "An evaluation of the state of spatial point pattern analysis in ecology," *Ecography*, 2016.

[271] R. A. Krasnoperov and D. Stoyan, "Spatial correlation analysis of isotropic microvessels : methodology and application to thyroid capillaries," *Annals of biomedical engineering*, vol. 34, no. 5, pp. 810–822, 2006.

[272] A. Weidemann, T. U. Krohne, E. Aguilar, T. Kurihara, N. Takeda, M. I. Dorrell, M. C. Simon, V. H. Haase, M. Friedlander, and R. S. Johnson, "Astrocyte hypoxic response is essential for pathological but not developmental angiogenesis of the retina," *Glia*, vol. 58, no. 10, pp. 1177–1185, 2010.

[273] G. Landini and G. Misson, "Simulation of corneal neovascularization by inverted diffusion limited aggregation." *Investigative ophthalmology & visual science*, vol. 34, no. 5, pp. 1872–1875, 1993.

[274] A. Radford, L. Metz, and S. Chintala, "Unsupervised representation learning with deep convolutional generative adversarial networks," *arXiv preprint arXiv :1511.06434*, 2015.